TACTILE SENSING AND ANALOGIC ALGORITHMS

Ph.D. dissertation

Attila Kis

Scientific adviser:
Ferenc Kovács, D.Sc.
Doctor of the Hungarian Academy of Sciences

Supervisor:
Péter Szolgay, D.Sc.
Doctor of the Hungarian Academy of Sciences

Péter Pázmány Catholic University
Faculty of Information Technology
Multidisciplinary Technical Sciences Doctoral School

Budapest, 2006

For Ádám and Éva

Acknowledgment

First of all I would like to thank Professor Tamás Roska, for his consistent help and support in very many ways, for his unbroken enthusiasm and fatherly guidance during my studies.

I thank Professor Szolgay Péter for taking me under his wings, for his suggestions and our exciting conversations about science.

I thank Professor Kovács Ferenc for his wise ideas and thoughts.

I am grateful to Fodroczi Zoltán and Wagner Róbert for their friendly suggestions and encouragement and for our chats and colloquies.

I thank my older and younger colleagues for their advices and with whom I could discuss all my ideas: Péter Jónás, András Mozsáry, Gaurav Gandhi, Gábor Matyi, Gábor Hodász, Iván Kristóf. For the younger ones I take the oppurtunity to wish success and endurance.

Special thanks go to the 'tactile guys': Vásárhelyi Gábor, Mária Ádám, Éva Vázsonyi, Tibor Mohácsy, István Bársony and Csaba Dücsõ.

I am indebted to Katalin Keserű and Gabi Kékné from MTA-SZTAKI, and Office of the Registrar at PPCU for their practical and official aid.

I had some really great teachers who should be mentioned here; as well I am greatful to Professor László Dávid and Piroska Haller from Petru Major University and to László Bálint, Ferenc Kacsó and Ágota Lakatos from Bolyai Farkas High School.

Parts of my work were supported by the following grants: "Telesense Project" of the National R&D Program (NKFP 2001/2/035) and Hungarian National Research Fund (OTKA) via grants No.T47002 and TS040858.

And last, but certainly not least, I would like to thank my family; my parents, András and Ildikó, and my sister, Annamária. Words simply can not express my gratitude for my family's love and support. They have been with me every step of the way and I could not have done it without them.

TACTILE SENSING AND ANALOGIC ALGORITHMS

by Attila Kis

Abstract

The challenges associated with sensing tactile events are formidable, requiring the ability to sense changing contact geometries, pressure distributions and vibrations at the user's fingertips. Despite years of research, telerobotic consoles provide their operators mainly with visual feedback and overall handling forces. The goal of the research presented herein is to extend the capabilities of current systems by adding tactile sensing and processing.

This thesis presents new methods of tactile sensing and processing for dexterous telemanipulation, i.e., telemanipulation that involves imparting forces and motions with the fingertips. The motivating hypothesis for this work is that sensing and processing forces and torques at the contact location provides essential information for dexterous telemanipulation.

The main topic of this dissertation is a proactive-adaptive, multi-modal sensing-processing-actuating investigation system based on behavior patterns observed in nature. Humans in an unknown, unstructured environment first get global information about surroundings by using vision. If attention is focused on a given object, humans gather additional information in order to complete the visual information with palpation. It is possible to detect new attributes fusing the two modalities. It is impossible to detect them using these two modalities separately.

The most important part of the experimental system is the tactile sensor array. I present a new tactile sensor array that consists of an array of piezo-resistive tactile sensing elements (taxel). This sensor is developed as a collaboration of MTA-MFA, MTA SZTAKI and “Ányos Jedlik” Lab. The spatial distribution of the taxels is comparable to the machanoreceptors in the human fingertips i.e. 1.5 mm. The most important aspect of this new sensor array is that in contrast to the conventional tactile sensors, this sensor can sense the 3D component of the acting forces, and has 6 Degree Of Freedom.

TABLE OF CONTENTS

Chapter One

INTRODUCTION

1. Preface

With the help of telerobotics it has become possible to manipulate an object across the world or even on another planet. But how can the user feel what the remote robot hand is touching?

The challenges associated with sensing tactile events are formidable, requiring the ability to sense changing contact geometries, pressure distributions and vibrations at the user's fingertips. Despite years of research, telerobotic consoles provide their operators mainly with visual feedback and overall handling forces. The goal of the research presented herein is to extend the capabilities of current systems by adding tactile sensing and processing.

This thesis presents new methods of tactile sensing and processing for dexterous telemanipulation, i.e., telemanipulation that involves imparting forces and motions with the fingertips. The motivating hypothesis for this work is that sensing and processing forces and torques at the contact location provides essential information for dexterous telemanipulation.

In most of the cases the vision provides enough information to guide most of the dexterous tasks. The vision helps to focus on the desired target and the tactile investigation is only on that area. The tactile information helps reorient the object grasped and optimize the grasping forces.

The main topic of this dissertation is a proactive-adaptive, multi-modal sensing-processing-actuating investigation system based on behavior patterns observed in nature. Humans in an unknown, unstructured environment first get global information about surroundings by using vision. If attention is focused on a given object, humans gather additional information in order to complete the visual information with palpation. It is possible to detect new attributes fusing the two modalities. It is impossible to detect them using these two modalities separately.

The most important part of the experimental system is the tactile sensor array. I present a new tactile sensor array that consists of an array of piezo-resistive tactile sensing elements (taxel). This sensor is developed as a collaboration of MTA-MFA, MTA

SZTAKI and “Ányos Jedlik” Lab. The spatial distribution of the taxels is comparable to the machanoreceptors in the human fingertips i.e. 1.5 mm. The most important aspect of this new sensor array is that in contrast to the conventional tactile sensors, this sensor can sense the 3D component of the acting forces, and has 6 Degree Of Freedom.

Usually the objects grasped by robotic arms are exposed to various fast, unpredictable forces. The system must respond to these perturbations fast and precise enough in order to maintain the stability. Experimental results show that humans respond to a fast event with a quick, stored movement, where only the direction and the speed is the issue.

2. Framework of the dissertation

The dissertation is organized as follows. Chapter 2 describes tactile event detection algorithms with embedded morphological preprocessing methods within the CNN-UM framework. Chapter 3 presents a real-time surface quality control system based on tactile and visual inspection unit. Chapter 4 summarizes the main results and highlights further potential applications, where the contributions of this dissertation could be efficiently exploited.

A number of appendices illustrate this work and summarize some of the theoretical background. In Appendix A and B a short summary of CNN technology as well as a new mathematical description of continuous machines on flows are given.

The author’s publications and other publications connected to the dissertation can be found at the end of this document.

Chapter Two

SENSING, DETECTING AND ANALYZING TIPICAL TACTILE EVENTS

1. Introduction

In this chapter a fast and efficient technique for detecting and identifying the slippage and twisting motion of touching objects is presented. This kind of action cannot be detected with tactile sensors sensing only the normal (perpendicular) component of the forces acting between surfaces. My approach utilizes an integrated sensing-processing-actuating system comprising: (1) A 2*2 taxel (tactile pixel) array mounted on a two-fingered robot hand, (2) a 64*64 CNN-UM (Cellular Neural Network-Universal machine), and (3) a closed loop controller. This arrangement, along with the proper analogic algorithm, allows detection and the control of the tactile event. It is essential to know and comprehend the forces between contact surfaces and the related 3D pressure.

The benefits of and the need for tactile sensing are demonstrated by using a number of laboratory experiments that include combining vision and tactile sensing, gentle grasping, reorienting objects within the grasp and exploration of unknown structures [1, 2]. The results demonstrate that tactile information improves the performance of robot manipulation.

Certainly, robots perform very useful and repetitive tasks in a controlled industrial environment, but to perform useful tasks in a consumer's home, robots need to be able to sense the unstructured and changing environment. The necessity of vision to guide the robot and the high degrees of freedom required to perform these tasks are obvious. The paper addresses the needs and benefits of tactile sensing for robots to perform useful tasks in an unstructured environment.

Usually, vision is sufficiently accurate to provide an initial set of conditions under which tactile feedback operates accurately [3]. Uncertainties in the angles of the object orientation can be compensated by tactile sensors. Tactile sensors can help to optimize the grasping forces on the object.

Despite the huge amount of work in tactile sensing and haptics, making reliable and accurate tactile sensors has proved to be very hard. Many different designs have been

proposed, and every conceivable transducer technology has been employed, see e.g. [4, 5]. Piezoresistive materials are the oldest and best known transducers for tactile arrays. Pressure on the surface of the sensor results in compressing the material, which changes its electrical resistance [6, 7]. Other successful transducer technologies include capacitive sensors [8], and optical sensors [9, 10]. Some sensors directly measure object shapes by sensing the deflection of a compliant rubber covering [11]. Other sensors measure pressure, usually, by sensing strain.

All of the above mentioned tactile sensors sense only the normal component of the acting force. The importance of sensing the shear force has not been realized for a long time, but in the last decade a lot of papers have been published on the importance of shear stress. [12, 13, 14]

In a previous experiment [15] I used a capacitor based tactile sensor array, Tactilus®, available on the market. This unit makes it possible to monitor precisely how force is dispersed between any two contacting, or mating surfaces in real-time, while the event occurs. The system includes a 50mm x 50mm palm sensor with 2.5 mm spatial resolution (21x21 taxels) and five finger sensors, 13mm x 13mm each, 1.5 mm spatial resolution (9x9 taxels). The query rate of this system is up to 60,000 sensor points/sec. The optimal range of pressure for sensor pads is 0-1 atm, accuracy $\pm 10\%$. The analogic algorithm processed one dimensional pressure field.

In the present experimental setup a Si-based tactile sensor array, developed by our group, is used. Taxel size is 500x500μm2 with wiring. Each individual sensor is composed of a central shuttle plate suspended by four bridges over an etched pit. Embedded in each of the four bridges one-one piezoresistor is built in. The suspension of the structure over the substrate may result in deformation occurring in the bridges, as normal and shear loads are applied to the central plate through an overlying protective elastomer layer.

The size of the “basic” array is 2*2 taxels. Using “these building blocks”, it is possible to put together a larger and configurable array of sensors, in accordance with the requirement of the task.

One of the biggest issues in using sensory arrays is to process the large amount of parallely incoming data. For this task the Cellular Neural/Nonlinear Network – Universal Machine (CNN-UM [16, 17]) is well suited, due to its analog, parallel processing architecture. The CNN-UM processes the 3D pressure maps, and acts as a selector of the action to be performed. The low level control of the robot arm is realized on a PC, as the

graphical user interface, and the communication between the main parts of the system (sensor – processor – actuator).

The sensing elements are mounted on a two-fingered Katana® robot hand. The actuator is controlled in closed loop.

The chapter is organized as follows: In Section 2, biological background and motivation is presented. In Section 3 the state of the art in the tactile sensors is summarized. In Senction 4 the experimental system is presented, in Section 5 the new algorithm is introduced. The theoretical aspects are discussed and a real-life example of the application is described. In Section 6, the forces acting on the contacting surface of the objects are discussed; furthermore, the sensing, detecting, and the analysis of slipping and twisting motions are presented. Finally, the conclusions are drawn in Section 7.

2. Biological Background - Human Tactile Sensing and Perception

Designing hardware meant to convey artificial touch to the human hand is a significant challenge. The primary reason is that our hands are incredibly sensitive to even the slightest vibrations over a range from 10-100 Hz. To help define the design requirements of such hardware, it is crucial to understand underlying tactile sensing mechanisms. Not only will this serve as a source of inspiration for improving tactile sensor designs, it will also help focus on which signals are important to communicate and how to communicate them. Although this is requisite knowledge, there is more to consider than simply the neurophysiology of touch. Our sense of touch is really a fusion of tactile and kinesthetic information [18].

The combination of cutaneous and kinesthetic sensing is referred to as haptic perception. At a high level, it is the perception or interpretation of these signals that ultimately interests us. The remainder of this chapter provides an overview of human mechanoreception and somatosensory information processing.

2.1. Introduction

The basic function of the Somatic Sensory System is to provide the Central Nervous System description about the external world.

Somatic sensibility arises from information provided by a variety of receptors distributed throughout the body. Somatic sensibility has four major modalities: discriminative touch (required to recognize the size, shape, and texture of objects and their movement across the skin), propriocepcion (the sense of static position and

movement of the limbs and body), nocicepcion (the signaling of tissue damage or chemical irritation, typically perceived as pain or itch), and temperature sense (warmth and cold).

Each of these modalities is mediated by a distinct system of receptors and pathways to the brain. However all share a common class of sensory neurons: the dorsal root ganglion neurons. Individual dorsal root ganglion neurons respond selectively to specific types of stimuli because of morphological and molecular specification of their peripheral terminals.

The dorsal root ganglion has two principal functions: stimulus transduction and transmission of encoded stimulus information to the central nervous system. The peripheral terminals of dorsal root ganglion neurons are two types. The terminal may be a bare nerve ending or the nerve ending may be encapsulated by a nonneural structure. Dorsal root ganglion neurons with encapsulated terminals mediate the somatic modalities of touch and proprioreception. They sense stimuli that indent or otherwise physically deform the receptive surface. In contrast, dorsal root ganglion neurons with bare nerve endings mediate painful or thermal sensations. Mechanoreceptors and proprioreceptors are innervated by dorsal root ganglion neurons with large-diameter, myelinated axons that conduct actions potentials rapidly. Thermal receptors and nociceptors have smaller-diameter axons that are either unmyelinated or thinly myelinated; these nerves conduct impulses more slowly.

Neurologists distinguish between two classes of somatic sensation: epicritic and protophatic. Epicritic sensations involve fine aspects of touch and are mediated by encapsulated receptors. These sensations include the ability to:

- detect gentle contact of the skin and localize the position that is touched (topognosis);
- discern vibration and determine its frequency and amplitude;
- resolve by touch spatial detail, such as the texture of surfaces, and the spacing of two points touched simultaneously (two-point discrimination);
- recognize the shape of objects grasped in the hand (stereognosis).

Protophatic sensations involve pain and temperature senses (as well as itch and tickle) and are mediated by receptors with bare nerve endings.

Tactile sensitivity is greatest on the hairless (glabrous) skin on the fingers, the palmar surface of the hand, the sole of the foot, and the lips.

Histological and physiological studies have identified four major types of mechanoreceptors in glabrous skin. Two of these receptors are located in the superficial layers of the skin, and two are situated in the subcutaneous tissue (see Figure 2.1.).

The two principal mechanoreceptors in the superficial layers of the skin are the Meissner's corpuscle and the Merkel disk receptor. The Meissner's corpuscle, a rapidly adapting receptor, is coupled mechanically to the edge of the papillary ridge, a relationship that confers fine mechanical sensitivity. The Merkel disk receptor, a slowly adapting receptor, is a small epithelial cell that surrounds the nerve terminal. The Merkel cell encloses a semirigid structure that transmits compressing strain from the skin to the sensory nerve ending, evoking sustained, slowly adapting responses. Merkel disk receptors are normally found in clusters at the center of the papillary ridge.

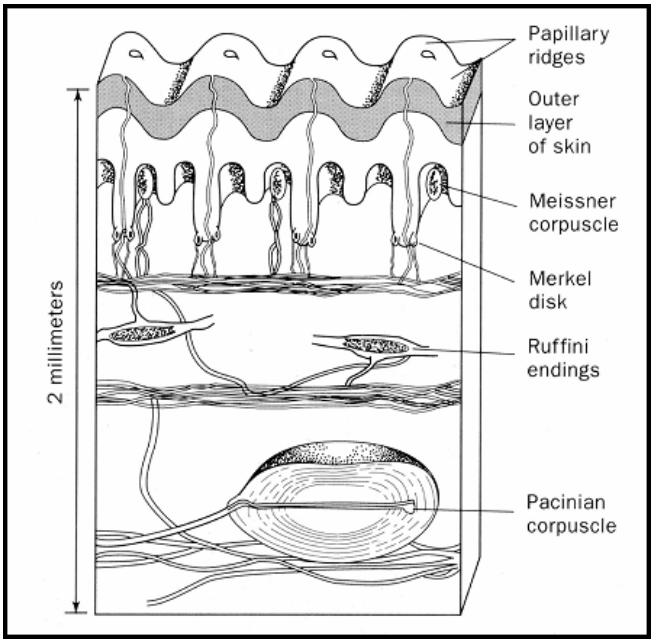

Figure 2.1. Location and morphology of mechanoreceptors in glabrous skin of the human hand

The two mechanoreceptors found in the deep subcutaneous tissue are the Pacinian corpuscle and the Ruffini ending. These receptors are much larger than the Merkel cells and Meissner's corpuscle, and less numerous. The Pacinian corpuscle is physiologically similar to the Meissner's corpuscule. It responds to rapid indentation of the skin but not to steady pressure. The large capsule of this receptor is flexibly attached to the skin, allowing the receptor to sense vibration occurring several centimeters away. Ruffini endings are slowly adapting receptors that link the subcutaneous tissue to folds in the

skin at the joints and in the palm or to the fingernails. These receptors sense stretch of the skin or bending of the fingernails as these stimuli compresses the nerve endings. Mechanical information sensed by Ruffini endings contributes to our perception of the shape of grasped objects.

	SAI	RA	P	SAII monkey?
RF size	1 mm^2	0,82 mm^2	diffuse	diffuse
Aff. denz.	100 cm^{-2}	150 cm^{-2}	350/ ujj	Unknown (low)
Diverg. (RF area)	4-16 (5 mm^2)	4-16 (5 mm^2)	1:1	1:1
Converg.	1:1	2-7	1:1	1:1
Adekv. Ing.	Strain energy density (point, edge, curve)	Slip, load force	High freq. vibration	Skin stretch
Function	Form, texture	Grip control	Distant events	Hand shape

Figure 2.2. Characteristics of mechanoreceptors found in human fingertip skin

2.2. The Receptive Fields of the Mechanoreceptors

The region of skin from which a sensory neuron is exited is called its receptive field. The size and structure of receptive fields differ for receptors in the superficial and deep layers of the skin. A single dorsal root ganglion cell innervating the superficial layers receives input from a cluster of 10-25 Meissner's corpuscles or Merkel disk receptors. The afferent fiber has a receptive field that spans a small circular area with a diameter ranging from 2 to 10 mm. These receptive fields are at least an order of magnitude greater than that of an individual receptor. Therefore, nerve fibers innervating the superficial layers of the skin sample the activity of many different sensory receptors of one particular sort. In contrast, each nerve fiber innervating the deep layers of skin innervates a single Pacinian corpuscle or Ruffini ending. Consequently, the receptive fields of these receptors cover large areas of skin, and their borders are indistinct.

Usually, these receptive fields have a single “hot spot” where sensitivity to touch is greatest.

The difference in size of the receptive fields of receptors in the superficial and deep layers of the skin plays an important role in the functions of the receptors. Meissner’s corpuscle and Merkle disk receptors in the superficial layers resolve fine spatial differences because they transmit information from a restricted area of skin. This very fine spatial resolution allows humans to perform fine tactile discrimination of surface texture and to read Braille. Pacinian corpuscles and Ruffini endings in the deep layers resolve only coarse spatial differences. Mechanoreceptors in the deep layers of the skin sense more global properties of objects and detect displacements from a wide area of skin.

2.3. The distribution of receptor types in the human hand

Meissner’s corpuscles (RA = rapidly adapting) and Merkel disk receptors (SA I = slowly adapting) are the most numerous receptors; they are distributed preferentially on the distal half of the fingertip. Pacinian corpuscles (PC) and Ruffini endings (SA II) are much less common; they are distributed more uniformly on the hand, showing little differentiation of the distal and proximal regions. The fingertips are the most densely innervated region of skin in the human body, receiving approximately 300 mechanoreceptive nerve fibers per square centimeter. The number of mechanoreceptive fibers is reduced to 120/cm^2 in the proximal phalanges, and to 50/cm^2 in the palm. (Adapted from Vallbo and Johansson 1978.)

2.4. Vibration Sense

Spike trains in mechanoreceptors in the skin code the vibration sense. Vibration is the sensation produced by sinusoidal oscillation of objects placed against the skin. Mechanoreceptors in the skin respond to these oscillations by a pulse code in which each action potential signals one cycle of the sinusoidal wave.

Individual mechanoreceptors differ in their threshold sensitivity to vibration (Figure 2.3.). Merkel disk receptors are most responsive to extremely low frequencies (5-15 Hz);

Meissner's corpuscles are most sensitive to midrange stimuli (20-50 Hz). The Pacinian corpuscles have the lowest thresholds for high frequencies (60-400 Hz); at 250 Hz they detect vibrations as small as 1 μm but at 30 Hz require stimuli with much larger amplitudes.

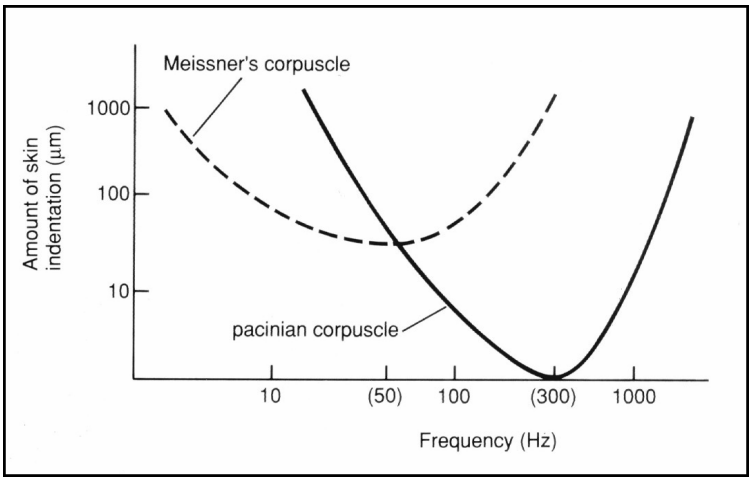

Figure 2.3. The threshold for detecting vibration

The receptor tuning thresholds determine the ability to sense vibration. Humans are most sensitive to vibration at frequencies of 200-250 Hz. To be felt, lower and higher frequencies must have proportionately larger amplitude vibrations. The intensity of vibration is signaled by the total number of sensory nerve fibers that are active rather then the frequency of firing, which codes the vibratory frequency.

2.5. The Spatial Resolution of Stimuli on the Skin

The size of the receptive fields in a particular region of skin delimits the capacity to determine whether one or more points are stimulated. A sensory neuron innervating Meissner's corpuscles and Merkel disk receptors transmits information about the largest skin indentation within its receptive field. If two points within the same receptive field are stimulated, the neuron will signal only the larger indentation. But if the points are located in the receptive fields of two different nerve fibers, then information about both points of stimulation will be signaled. The farther apart the points lie on the surface, the greater the likelihood that the two active nerves will be separated by silent nerve fibers.

The contrast between active and inactive nerve fibers seems to be necessary for resolving spatial detail. The minimum distance between two detectable stimuli is called the two-point threshold.

The Adaptation Properties and Sensory Threshold

Although all four types of mechanoreceptor are exited by indentation of the skin, they signal different information. The slowly adapting receptors signal the pressure and shape of objects by their average firing rate. The total number of action potentials evoked per second is proportional to the indentation force applied to the receptor. Rapidly adapting receptors sense motion of objects on the skin. These receptors respond during the period when the position of a stimulus changes, and they stop firing when it comes to rest. Their firing rates are proportional to the speed of motion, and the duration of activity signals the duration of the motion (Figure 2.4). They sense vertical impact and lateral motion such as stroking, rubbing, or palpation.

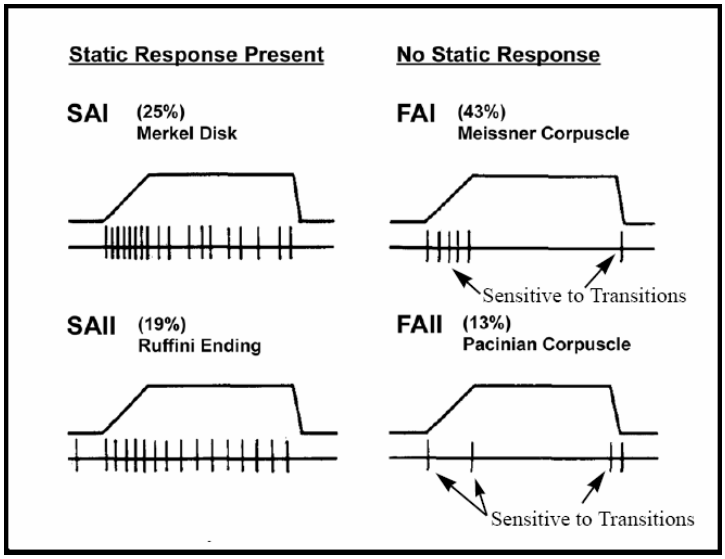

Figure 2.4 Responses of four types of mechanoreceptors to normal indentation of the skin

Mechanoreceptors also differ in sensory thresholds, the minimum intensity of stimulation required to generate an action potential in the nerve. Rapidly adapting receptors have lower touch thresholds than slowly adapting receptors. The Pacinian

corpuscle is the most sensitive mechanoreceptor. Pacinian corpuscles also sense the frictional displacement of the skin when the hand moves across an object, regardless of whether the surface is smooth or rough. The Meissner's corpuscle is particularly sensitive to abrupt changes in the shape of objects that occur at the edges or corners and to small irregularities on the surface sensed during palpation by the hand. Meissner's corpuscles are used to detect and localize small bumps or ridges on an otherwise smooth surface. More salient bumps or edges are required to activate the slowly adapting Merkel disk receptors. However, once stimulated, the Merkel receptors provide a clearer image or contours by changes in the frequency of firing. Responses are proportional to the surface curvature. The strongest responses occur when sharp edges or punctate probes contact the receptive field.

2.6. The Spatial Characteristics of Objects

Information about size and shape is signaled by populations of receptors that are stimulated by different portions of object. Information about texture is also mediated by populations of mechanoreceptors. Humans are able to sense the roughness of surfaces as well as the spacing and orientation of texture patterns, such as gratings or arrays of Braille dots.

Each receptor axon is stimulated by only a small portion of the pattern. The overall picture is not contained in the firing patterns of any one individual nerve fiber but in the total ensemble of inputs provided by the active and inactive sensory nerves. The spatial resolution of detail within a pattern depends on the total area of skin innervated by each sensory nerve. The Merkel disk receptor provides the sharpest resolution of spatial pattern, as each receptor axon monitors a single dot. Meissner's corpuscles also resolve individual dots but the image of the pattern that they provide is not as sharp because they have slightly larger receptive fields. Pacinian corpuscles do not signal changes in surface contour because their large receptive fields encompass several dots in the textured surface. Instead they fire continuosly, measuring the speed at which the hand moves across the surface. The activity of Pacinian corpuscles provides timing information that allows the brain to convert the number of bursts per second fired by Meissner's corpuscles and Merkel disk receptors into spatial information about the number of dots per centimeter on the textured surface.

Natural stimuli rarely activate a single type of receptor; rather they activate different combinations of mechanoreceptors that act synergistically.

2.7. Strereognosis

Neurologists call the ability to perceive form through touch stereognosis. Stereognosis not only tests the ability of dorsal column-medial lemniscal system to transmit sensations from the hand but also measures the ability of cognitive processes in the brain to integrate that information.

Spatial properties are processed by populations of receptors that form many parallel pathways to the brain. It is the job of the central nervous system to construct a coherent image of an object from fragmented information conveyed in multiple pathways.

Mechanoreceptors in the skin send their axons to the caudal medulla, where they terminate in the gracile or cuneate nuclei. These second-order neurons project directly to the contralateral thalamus, terminating in the ventral posterior lateral nucleus. A parallel pathway from the principal trigeminal nucleus, wich represents the face, ascends to the ventral posterior medial nucleus. The third-order neurons in the thalamus send axons to the primary somatic sensory cortex (S-I), located in the postcentral gyrus of the parietal lobe.

The primary somatic cortex S-I contains four cytoarhitectural areas: Brodmann's areas 3a, 3b, 1, and 2. These four regions of the cortex differ functionally. Areas 3b and 1 receive information from receptors in the skin, whereas areas 3a and 2 receive proprioreceptive information from receptors in muscles and joints. However, the four areas of the cortex are extensively interconnected, so that both serial and parallel processing are involved in higher-order elaboration of sensory information.

The secondary somatic sensory cortex (S-I), located on the superior bank of the lateral fissure, is innervated by neurons from each of the four areas of S-I. The S-II cortex projects to the insular cortex, which in turn innervates regions of the temporal lobe believed to be important for tactile memory.

Other important somatosensory cortical areas are located in the posterior parietal cortex (Brodmann's areas 5 and 7). These areas receive input from S-I as well as input from the pulvinar and thus have an associational function. They are also connected bilaterally through the corpus callosum. Area 5 integrates tactile information from

mechanoreceptors in the skin with proprioreceptive inputs from the underlying muscles and joints. This region integrates information from the two hands. Area 7 receives visual as well as tactile and proprioceptive inputs, allowing integration of stereognostic and visual information. The posterior parietal cortex projects to the motor areas of the frontal lobe and plays an important role in sensory initiation and guidance of movement.

2.8. The Receptive Fields and the Modality of the Cortical Neurons

Like mechanoreceptors, the cortical neurons receiving sensory information from the skin are either slowly adapting or rapidly adapting neurons, signaling either the amplitude or rate of the peripheral skin indentation. Moreover, since each cortical neuron receives inputs from receptors in a specific area of the skin, central neurons also have receptive fields. Thus, each cortical neuron is defined by its receptive field as well as by its sensory modality. Any point on the skin is represented in the cortex by a population of cortical cells connected to the afferent fibers that innervate that point on the skin.

The receptive fields of cortical neurons are much larger than those of dorsal root ganglion neurons. The receptive field of a neuron in area 3b represents a composite of inputs from about 300-400 mechanoreceptive afferents. Receptive fields in higher cortical areas are even larger. In the posterior parietal cortex, receptive fields are often bilateral, located at symmetric positions on the contralateral and ipsilateral hands.

2.9. Convergent and Divergent Connections in the Relay Nuclei

Relay nuclei, such as the dorsal column or thalamic nuclei, are composed of projection (or relay) neurons that send their axons to the next nucleus in the pathway inhibitory interneurons that terminate upon relay neurons. Sensory inputs to the relay nucleus are characterized by extensive convergence and divergence. Each sensory afferent has a branched terminal that innervates several postsynaptic neurons, so that each projection neuron receives synaptic input from many sensory axons. This pattern of divergent pre-synaptic connections and convergent postsynaptic connections is repeated at each relay in the pathway.

2.10. The Columnar Organization of the Somatic Sensory Cortex

The cortex is organized into vertical columns or slabs, 300-600 μm wide, spanning all six layers from the cortical surface to the white mater. All of the neurons within a column receive inputs from the same local area of skin and respond to a single class of receptors. Although the receptive fields of the neurons comprising a column are not precisely congruent, they do share a common center.

In addition to sharing a common focal location on the skin, all of the neurons in a column usually respond to only one modality: touch, pressure, temperature, or pain.

Although each of four areas of the primary somatic sensory cortex receives input from all areas of the body surface, one modality tends to dominate each area. In area 3a the dominant input is from proprioreceptors signaling muscle stretch. Area 3b receives input primarily from cutaneous mechanoreceptors. Here the inputs from a discrete site on the skin are divided into two sets of columns, one each for inputs from rapidly adapting and slowly adapting receptors (Figure 2.3.). The receptive fields and response proprieties of neurons in areas 1 and 2 represent convergent input from regions of the hand and fingers that are represented separately in areas 3a and 3b.

2.11. Spatial Resolution in the Cortex

The somatotopic arrangement of somatosensory inputs in the human cortex is called homunculus. Each part of the body is represented in the brain in proportion to its relative importance to sensory perception. The map represents the innervation density of the skin rather than its total surface area. In humans a large number of cortical columns receive input from the hands, particularly from fingers. Similarly, large numbers of cortical neurons receive input from the foot and face.

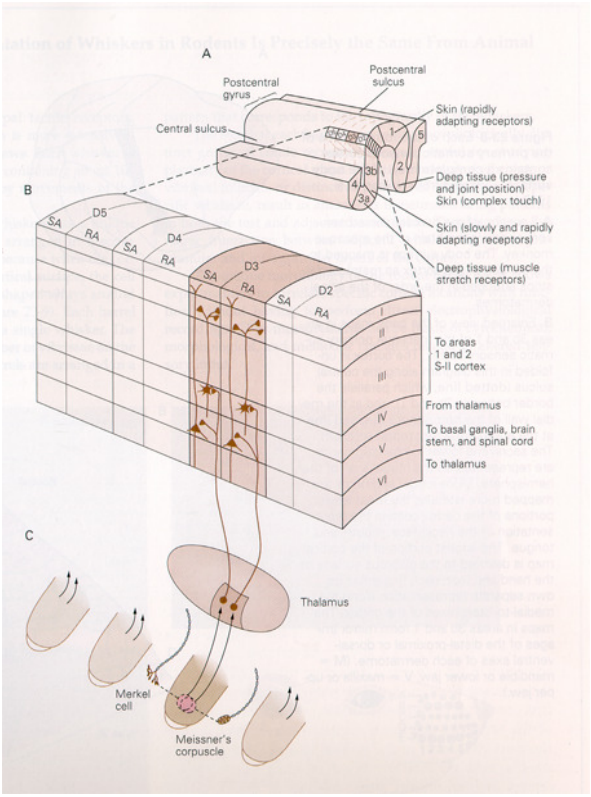

Figure 2.3. a) The Brodmenn's areas; b) Detail of the columnar organization;

c) Overlapping RA and SA receptive fields

2.12. Inhibitory Networks

The receptive fields of individual neurons are identified by touching the skin with a small probe. A more complex receptive field structure emerges when the skin is touched at two or more points simultaneously. Stimulation of regions of skin surrounding the excitatory region of the receptive field of a cortical neuron may reduce the responsiveness of the neuron to an excitatory stimulus because afferent inputs surrounding the excitatory region are inhibitory. These regions of the receptive field of a cortical neuron are called the inhibitory surround. This spatial distribution of excitatory and inhibitory activity serves to sharpen the peak of activity within the brain.

The inhibitory responses observed in the cortex are generated by interneurons in the dorsal column nuclei, the ventral posterior lateral nucleus of the thalamus, and the cortex itself. Inhibitory interneurons in relay nuclei form circuits that tend to limit the spatial

spread of excitation through divergent connections. Peripheral receptors in the somatic sensory system are not themselves inhibited (Figure 2.4.A.). At the first relay point in the somatic sensory system the afferent fibers inhibit the activity of cells in the dorsal column nuclei that surround the cells they excite (Figure 2.4.B.). Inhibition generated by activity of the most intensely activated receptors reduces the output of projection neurons that are less strongly excited. It permits a winner-take-all strategy, which ensures that the strongest of two or more competing responses is expressed. In addition, the most active output neurons use recurrent collateral fibers to limit the activity of adjacent neurons. This lateral inhibition further sharpens the contrast between the active cells and their neighbours (Figure 2.4.C.).

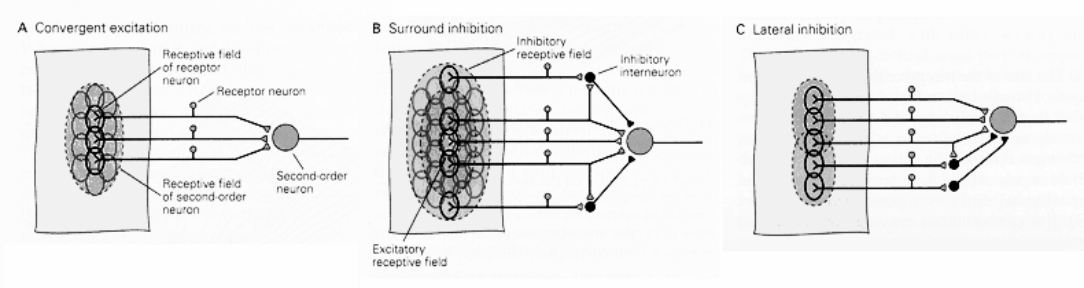

Figure 2.4. Excitation and inhibition in the receptive field of a higher order neuron in the dorsal column nuclei

Inhibitory interactions are particularly important for fine tactile discrimination. We are able to perceive two points rather one because two distinct populations of neurons are activated. If the two stimuli are brought close together, the activity in the two populations tends to overlap, and the distinction between the two peaks might become blurred.

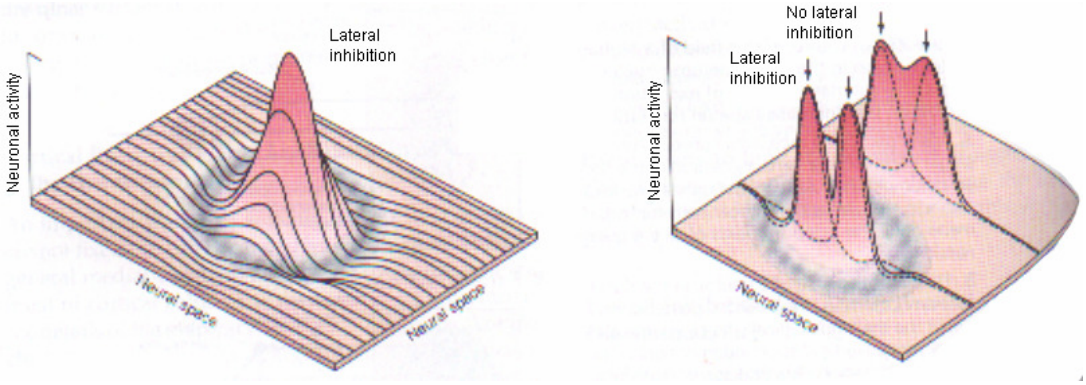

Figure 2.5. a) Stimulation of a single point; b) Stimulation of two adjacent points

However, the inhibition produced by each stimulus also summates in the zone of overlap. As a result of this more effective inhibition, the peaks of activity in the two responding populations become sharpened, thereby separating the two active populations spatially (Figure 2.5.B). This sculpturing role of the inhibition thus preserves the spatial distinction between two stimuli.

2.13. The Representation of Spatial Detail in the Cortex

The sharp sensory images provided by mechanoreceptors are preserved up to the first stage of cortical processing in area 3b of the somatic sensory cortex. Neurons in area 3b fire bursts as each line segment of a texture is scanned across the receptive field and together faithfully signal its shape. The cortical representation of the texture is further sharpened by a pause in firing as the moving edges exit the excitatory receptive field and enter its inhibitory surround.

2.14. The Complex Feature-Detecting Properties of the Higher Cortical Areas

The nervous system integrates information from a large number and variety of receptors as well as the modalities of touch, proprioception, and temperature.

The following factors are involved: (1) The size of the receptive field becomes larger at each level of processing, so that eventually the entire object rather than a single edge is sensed by a neuron. (2) The profile of activity in the active population of neurons changes through the action of inhibitory networks. (3) At successive levels of sensory processing in the cortex individual neurons respond to more complex inputs. (4) The submodalities converge on individual neurons in association cortical areas.

Neurons in areas 1 and 2 are concerned with more abstract properties of tactile stimuli than simply the site of stimulation. These cells ignore many of the myriad details of a stimulus and instead detect regularities amid the confusion. Their firing patterns signal features such as the orientation of edges, the direction of motion across the skin, the surface curvature of objects, or the spatial arrangement of repeated patterns that form

textures. Feature detection is a basic principle of cortical processing that allows the brain to find patterns common to stimuli of a particular class.

Some cortical neurons in area 2 respond preferentially to specific combinations of simultaneously stimulated receptors. Such orientation-sensitive neurons sense the angle of edges contacted by the skin. This information is extremely important in reconstructing the shapes of objects. Other cells are direction sensitive.

The convergent projections from areas 3a and 3b onto areas 1 and 2 permit neurons in area 2 to respond to other complex features, such as the shape of objects. Whereas neurons in 3b and 1 respond only to touch, and neurons in areas 3a respond only to position sense, certain neurons in area 2 have both inputs. These neurons respond best when an object of a specific shape is grasped by the hand.

In the posterior parietal cortex (areas 5 and 7) the somatosensory responses are even more complex and are often integrated with other sensory modalities. These association cortical areas play an important role in the sensory guidance of movement and are consequently organized functionally rather than topographically. Many neurons in area 5 receive inputs from several adjacent joints or groups of muscles that provide information about the posture of the entire hand or arm. Other cells integrate tactile and postural information.

Neurons in area 7 of the posterior parietal cortex integrate tactile and visual stimuli that overlap in space and play an important role in eye-hand coordination. Such neurons are used to monitor visually guided hand movements rather than to convey detailed sensory information concerning the exact position or intensity of touch.

2.15. Parallel Processing in Distinct Areas of Cortex

The somatosensory information necessary for stereognosis is processed in parallel in these areas because palpation involves repetitive touching of the object for several seconds. Such information is not simply relayed from point to point in the brain, as are the somatosensory evoked potentials after a brief shock to the nerve. Instead, tactile sensory information transmitted to higher cortical areas must be compared with more recent information being processed at the early stages. Thus, the activity that occurs simultaneously in different cortical areas is produced by events that happen at different moments in time. Responses in areas 3a and 3b occur 20ms after touch or movement and

therefore reflect stimuli in the immediate past. The more posterior cortical areas receive sensory information at longer latencies, processing stimuli presented 30-100 ms earlier.

The brain is binding together the various stimulus features by synchronizing firing in different cortical areas.

Parallel processing in the brain is a form of processing that we shall encounter repeatedly in the sensory systems. It is designed not to achieve multiplication of identical circuitry but to allow different neuronal pathways and brain relays to deal with sensory information in slightly different ways.

3. Prehension and the Mechanics of Grasp

Firstly, literature concerned with the general concepts of prehension is reviewed (§3.1). Mechanics of grasp is reviewed next (§3.2)

3.1. Prehension

Prehension, the act of seizing or grasping, is a frequent activity in daily life. It usually involves the holding of an object for a purpose of manipulating, restraining, or feeling it. This section consists of six parts:

(1) classification of prehensile actions,

(2) the concepts of virtual finger and opposition space,

(3) muscle activity in prehension,

(4) role of tactile sensing,

(5) forces in prehension and

(6) prehension synergies.

3.1.1. Classifications of prehensile actions

Many attempts have been made to classify hand postures from various perspectives such as medicine, biomechanics, robotics, and occupational therapy (Table 3.1). Schlesinger (1919) [19] was the first to provide a classic taxonomy depicting the versatility of the human hand; the classification was aimed to facilitate designing functionally effective prosthetic hands.

Napier (1992) [20] proposed that power and precision requirements of tasks should be met by the power and precision capabilities of the human hand. Power grasps are characterized by large areas of contact on the fingers and the palm; these grasps are useful where stability, security, or high forces are important. When the sensitivity and dexterity are pursued precision grasps are used. In this case, the object is held with the tips of the fingers and thumb. In robotics literature, the power grasps —the grasps in which the object is contacted by the palm and proximal phalanges—are sometimes called the enveloping grasps, while the precision grasps are called fingertip grasps (Trinkle et al. 1987) [21].

Cutkosky and Howe (1990) [22] extended the Napier precision/power dichotomy by further breaking down each category into sub-categories. For instance, based on the

object shape they proposed two subcategories of precision grasp. For long objects the 10 prismatic precision grasps are used; there are four potential configurations to choose: 2-, 3-, 4- or 5-finger precision grasps. For compact objects the circular precision grasps are commonly chosen; in addition, disk, sphere or tripod grasps are used depending on the corresponding object shapes.

Jacobson and Sperling (1976) [23] proposed a detailed coding system which describes the grips of healthy and injured hands. The authors encoded the grasps in terms of configurations of the fingers and palm, contact surfaces of the fingers and palm with objects.

Some prehension classifications are very detailed and include many classes. For instance, Kamakura et al (1980) [24] photographed the finger positions and contact areas while the subjects grasped 98 different objects. Fourteen identical patterns were identified: five patterns of power grip, four of intermediate grip, four of precision grip, and one other. The subjects grasped 31 of 98 objects in an identical pattern and the rest of the objects, 67, in two or more patterns.

The posture chosen for the grasp is affected by multiple factors including object shape, size, weight, surface characteristics and human motivations (Mamassian 1997; Paulignan et al. 1997a; Churchill et al. 2000; Marotta et al. 2001) [25-26-27-28]. Among these factors the goal of the task or the intended activity seems to be the most important.

TABLE 1. CLASSIFICATIONS OF PREHENSION FROM THE LITERATURE

Researchers	Postures names	
Cooney et al. 1977	Grasp	Tip pinch
[29]	Palmar pinch	Lateral pinch
Cutkosky 1989	Large diameter heavy wrap	4-finger precision grasp
[30]	Small diameter heavy wrap	3-finger precision grasp
	Medium warp	2-finger precision grasp
	Adducted thumb wrap	Disk precision grasp
	Light tool wrap	Spherical precision grasp
	Disk power grasp	Tripod precision grasp
	Spherical power grasp	Lateral pinch
	5-finger precision grasp	Hook, platform, push
Griffiths 1943	Cylinder grip	Ball grip

Iberall 1986 [31]	Palm opposition	Side opposition
	Pad opposition	
Jacobson et al. 1976 [32]	A coding system for fingers, finger positions, finger joint positions, contact surfaces, and orientation of object's longitudinal axis with respect to the hand	
Kroemer 1986 [33]	Disk grip	Lateral grip
	Collect enclosure	Precision or writing grip
	Power grasp	Hook grip
	Pinch or pliers grip	Finger touch
	Tip grip	Palm touch
Landsmeer '62 [34]	Power grasp	Precision handling
Lister 1977 [35]	Span	Chuck grip
	Power grasp	Key pinch
	Precision pinch	Hook grip
	Pulp pinch	Flat hand
Napier 1956 [36]	Power grip	Combined grip
	Precision grip	Hook grip
Schlesinger 1919	Open fisted cylindrical grasp	Cylindrical w/add. thumb
	Close fisted cylindrical grasp	Flat/thin(2 finger)pincer
	Spherical prehension	Large(5 finger)pincer
	Palmar prehension (pincer)	Three-jaw chuck
	Tip prehension	Nippers prehension
	Lateral prehension	
	Hook prehension	
Skerick et al. 1971 [37]	Power grip	Tip pinch
	Two point palmar pinch	Link grip(lateral pinch)
	Three point palmar pinch	Hook grip

3.1.2. Virtual finger and opposition space

Arbib et al.(1985) [38] recorded the way subjects grasped mugs of different size and based on these experiments proposed the *virtual finger* concept. Although—depending on the size of the mug handle—different fingers were involved in the grasp, the underlying generalized pattern was the same: a finger was placed on the top of the handle while one or more fingers were placed inside the handle, against the top of the handle. It was shown that the action of two or more fingers can be reduced to the action of one imaginary finger that was called the virtual finger. In addition to two virtual fingers, an extra finger can apply a force to counteract a task-related force or torque; the latter finger was called a *virtual finger three*. During the prehensile actions, regardless of the grasping type used, an opposition between the virtual fingers and the thumb was always observed.

A concept of *opposition space* was used as a basis of classification (Iberall and MacKenzie 1990) [39]; the concept provided a set of state variables that quantify a posture both in physical terms (magnitude and orientation of force vectors) and abstract terms (types of oppositions, virtual finger mapping). Several state variables were used to characterize the opposition space: a) the type of oppositions (pad, palm, and/or side); b) the virtual to real finger mapping; c) virtual finger state variables that are determined for each virtual finger in each opposition being used. Iberall et al. (1986) [40] proposed three basic opposition types:

• Pad opposition: between thumb pad and finger pad, e.g. holding a needle.

• Palm opposition: between palm and digits, e.g. grasping a large hammer.

• Side opposition: either between thumb pad and side of index finger or between the sides of fingers, e.g. holding a key.

Three-finger grasp tasks (tripods) are examined much more often than other grasping combinations, probably due to their broad applications and simple experimental setup. Baud-Bovy and Soechting (2001) [41] showed that in tripod grasping two finger forces act as a single functional unit even if the fingers are not located closely together. A three virtual-finger grasp for the tripod grasp was also proposed (Cutkosky and Howe 1990) [42].

By studying the reach and grasp of sphere-shaped objects, Gentilucci et al. (2003) demonstrated that grasp is accomplished by using two virtual fingers formed by the thumb and one or more other fingers that synchronously open and close on the object along the opposition space.

Multi-finger prismatic grasps have also been studied (Flanagan et al. 1999 [43]; Santello and Soechting 2000 [44]; Zatsiorsky et al. 2002ab; Zatsiorsky et al. 2003 [46]; Shim et al. 2003 [47], Zatsiorsky and Latash 2004 [48]). In this configuration, the four fingers function as one functional unit (virtual finger) opposing the thumb.

3.1.3. Muscle activity in prehension

The muscles serving the fingers are grouped according to function and location. Based on the location the muscles are classified as extrinsic muscles (the muscles that originate outside the hand and insert within it) and intrinsic muscles (the muscles that originate inside the hand and insert within it too). It is widely accepted that the extrinsic muscles produce the powerful but crude movements of the digits while the intrinsic muscles in the palm produce the weak but intricate and precise digits movements that characterize the human hand (Long et al. 1970 [49]; An 1983; Jacobson et. al. 1992 [50]; Darling et. al. 1994 [51]; Maier and Hepp-Reymond 1995ab [52]; Mahaffey 1999 [53]; Kozin et. al. 1999 [54]; Huesler et. al. 2000 [55]; Milner and Dhaliwal 2002 [56]).

Architectural features of hand muscles, such as muscle length, mass, fiber pennation angle, fiber length, and sarcomere length and physiological cross-sectional area (PCA), determine their functional capacities . Intrinsic muscle lengths are relatively similar to one another. Lumbrical muscles have a high fiber length/muscle length ratio, implying a high excursion. The first dorsal interosseous and adductor pollicis have larger PCAs than other intrinsics. This feature highlights their major contribution to strength production. The interosseous muscles have relatively high PCAs with low fiber length/muscle length ratios, suggesting their adaptation for high force production and low excursion.

Intrinsic muscles play an important role in the function of prehension. According to the EMG studies (Basmajian 1978) [57], the abductor pollicis brevis is significantly activated during opposition and flexion of the thumb as well as in the thumb abduction. The opponens pollicis shows strong activity in abduction and flexion of the metacarpal joint as it does in opposition. The flexor pollicis brevis shows considerable activity in opposition as well as in flexion and adduction. The adductor pollicis is active in adduction and opposition and only to a slight extent in flexion of the thumb. The flexor pollicis brevis was the most active muscle during grasping a nail. However, it was not activated much when a glass of water was held. It may suggest that the more the thumb is abducted as happens in holding the glass, the less the flexor brevis contributes to a firm

grip. The flexor pollicis brevis, which provides firmness of grip when the abduction is small, is replaced by that of the opponens pollicis when a large amount of abduction is needed. The activity of the opponens coupled with that of the abductor will contribute to a firm grip when there is no flexor activity.

Deficiencies occurred in the intrinsic muscles can severely affect the hand function in prehension. Kozin et al. (1999) simulated low median and/or low ulnar nerve lesions and found: (a) average decrease in grip strength 38% after ulnar nerve block and 32% after median nerve block; (b) the total grip loss 49% as compared with the normal strength; (c) significant decrease in the force production of the long, ring, and small fingers but not the index finger; (d) significant decrease in key pinch force, up to 77% after ulnar block and 60% after median block with a further decrease after combined block to 85%.

Extrinsic muscles pass through the wrist and hence take part not only in finger function but also in wrist motion and stability, which are important elements in prehension. During extension of the wrist the extensor carpi radialis brevis is more active than the carpi radialis longus regardless of the movement speed. However, during prehension or fist-making the roles of these two muscles are reversed and the longus serves as a synergist of the extensor carpi radialis brevis. When the wrist is extended the extensors and flexors are reciprocally activated while such extensors as carpi radials, carpi ulnaris, and the extensor digitorum work synchronously.

In the wrist flexion, the carpi radials, ulnaris and digitorum superficialis act as synergists (Backdahl and Carlsoo 1961) [58]. In abduction and adduction, the appropriate flexors and extensors act reciprocally.

Extrinsic muscles and intrinsic muscles usually work together. The long tendons of the fingers provide the gross motion of opening and closing of the fist at all the joints simultaneously and the intrinsic muscles play important roles in movements departing from simple total opening or closing (Chao et al. 1976 [59]; Long et al. 1970; Maier and Hepp-Reymond 1995ab). In power grip the extrinsic muscles provide the major gripping force (Long et al. 1970). The major intrinsic muscles involved in power grip are the interossei; only the fourth lumbricalis is significantly involved (Long et al. 1970).

Still, the precise value of the relative contribution of the intrinsic and extrinsic muscle into the total force production remains mainly unknown. Li et al (2001) suggested a method for the estimation of the contribution of the intrinsic and extrinsic muscles into the force production in finger pressing tasks. The method is based on application of force at different sites along the finger that allows for different involvement of the intrinsic and

extrinsic muscles (Li et al. 2000b [60]; Latash et al. 2002). To examine the effects of the extensor mechanism on the force production of finger flexors in balancing an external load a mathematical model of a finger was constructed. In this model, the intrinsic muscles were lumped into one virtual intrinsic muscle. The model was based on the static equilibrium conditions and accordingly three equations of the moments around the finger joints were formed. For comparison, a model without extensor mechanism was also evaluated (Figure 3.1). The results indicated that the effects of the extensor mechanism on the flexors were relatively small when the force was applied distally to the PIP joint while the effects were significant when the force was applied proximally to the PIP joint. When the force was applied at the distal phalanx, the flexor digitorum profundus (FDP) and flexor digitorum superficialis (FDS) accounted for over 80% of the flexing force. When the force was applied at the DIP joint, the FDS accounted for more than 70% of the flexing force. The intrinsic muscle accounted for more than 70% of the flexing force when the force was applied at the PIP joint.

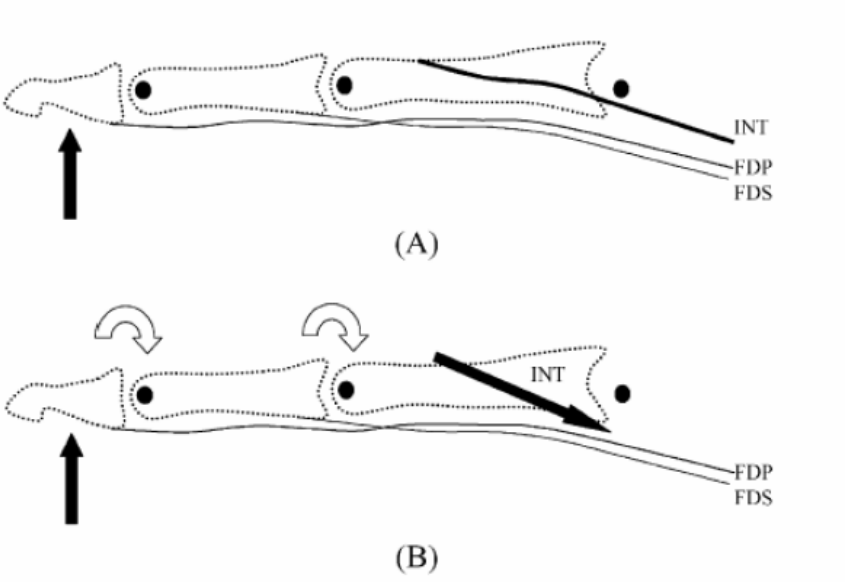

Figure 3.1. (A): Finger model with extensor mechanism. (B): Finger model without extensor mechanism (From Li et al. 2001).

Because all the finger flexors and extensors are multi-joint muscles they generate the moments of force at all the joints that they cross. It can be proved mathematically that a set of joint moments of a kinematic chain (finger) uniquely defines the endpoint force; therefore, it can be said that each finger muscle exerts a finger tip force in a certain

direction (for a detailed explanation see Zatsiorsky 2002, p. 153). If the endpoint force is exerted in other directions, this can only be achieved by combining forces of several muscles. When modulating fingertip force magnitude across the voluntary range, the number of contributing muscles and the relative activity among them is not changed (Valero-Cuevas 2000) [61]. So far, the 'directions of the muscle forces', i.e. the directions of the endpoint force resulting from individual muscle-tendon forces, are reported for only the thumb (Pearlman et al. 2004) [62]. The thumb-tip force vectors do not scale, however, linearly with tendon tensions; the thumb may act as a "floating digit" affected by load-dependent trapezium motion.

3.1.4. Role of tactile sensing

Receptors that convert mechanical stimuli into the neural signals reside in skin, muscles and joints. There are around 17,000 cutaneous mechanoreceptors innervating the glabrous skin of one hand (Vallbo and Johansson 1984) [63]. These cutaneous mechanoreceptors transfer signals to myelinated afferent fibers with fast conduction velocities of 35-80 m/s (Johansson and Vallbo 1983) [64]. When objects are grasped, skin receptors provide information on skin stretch, contact with objects, mechanical deformations and interactions with the object in a hand-centered coordinate system. In addition to mechanoreceptors in the skin and subcutaneous tissues, joint, muscle and tendon receptors provide proprioceptive information during contact and manipulation.

Proprioceptors provide information about the relative position of body segments with respect to one another and about the position of the body in space, including mechanical displacements of muscles and joints.

The hand becomes less sensitive to small forces and vibrations as more force is applied (Howe and Cutkosky 1989) [65]. In psychophysics, two concepts, absolute threshold and differential threshold are widely used. The absolute threshold equals the smallest stimulus level necessary to produce a sensation. The differential, or difference, threshold equals the amount of change in a stimulus required to produce a just noticeable difference in the sensation. Dependence of the difference threshold on the intensity level of a stimulus is known as Weber's law. The scaling factor between the change of stimulus intensity that can be just discriminated and the starting intensity of the stimulus is called Weber's fraction. The Weber's fraction provides an index of sensory discrimination, differential sensitivity. When the hand is lightly loaded the skin is

disassociated somehow from the more rigid bone and muscles of the inner structure of the hand. Small forces or motions can cause substantial motion of the skin, in which many sensors are located, resulting in good tactile sensitivity. As the contact force increases, however, pressure beneath the skin increases and the skin and hand structure become coupled. The fingertip tissue becomes stiffer and task forces produce smaller skin motion and hence the tactile sensitivity decreases.

The human fingertip tissue can be modeled as non-linear viscoelastic material. It has been demonstrated that a non-linear viscoelastic model comprised of an instantaneous stiffness function and viscous relaxations function was capable of predicting fingertip tissue force response under loadings (Jindrich et al. 2003) [66]. A similar non-linear viscoelastic model worked well for the tangential displacement of the finger pad (Pataky 2004) [67].

The placement of finger contacts is also important for the tactile sensitivity. The mechanoreceptors responsible for our most acute tactile sensitivity are concentrated at the fingertips; hence sensitivity will improve if these areas are in contact with the object. Hence, fingertip (precision) grasps provide a better sensitivity than the power (enveloping) grasps.

Extensive studies have been done to better understand the mechanisms and role of tactile sensing during grasping tasks (Jenmalm et al. 2000 [68]; Johansson 2002 [69]). There are four distinct mechanoreceptors in the human skin: Merkel receptors, Meissner corpuscles, Pacinian corpuscles, and Ruffini corpuscles. Johnson (2001) [70] showed that each of the four mechanoreceptive afferent systems innervating the hand serves a distinctly different perceptual function, and that tactile perception can be understood as the sum of these functions. The Merkel cells provide a high-quality neural image of the spatial structure of objects and surfaces that is important to the form and texture perception. The Meissner corpuscles provide signals of a transient skin motion which is critical for grip control and information about the motion of objects contacting the skin. The Pacinian corpuscles provide a neural image of vibrations transmitted to the hand from objects grasped in the hand. The Ruffini corpuscles provide a neural image of skin stretch over the whole hand. Based on tactile sensing, people adjust grip force to load force according to the friction condition at the digit-object interface (Johansson and Westling 1984 [71]; Cole and Johansson 1993 [72]; Forssberg et al. 1995 [73]). This adaptive adjustment is essential for preventing slipping of the object. The effect of surface friction could be dissociated from the effect of either surface texture or coating;

the friction appears to be a more important factor in determining the grip force than surface texture (Cadoret and Smith 1996) [74].

With advanced instruments developed in recent years, more research has focused on the correlation between tactile input and brain function. Magnetic resonance imaging (MRI) of the lateral cerebellar output nucleus (dentate) of humans during passive and active sensory tasks revealed that finger movements that were not associated with tactile sensory discrimination produced no dentate activation. By using functional MRL Stoeckel et al. (2004) [75] found that during tactile object discrimination the anterior portion of the superior parietal cortex was specifically activated by movement evoked kinaesthetic signals while similar area in the contralateral hemisphere was related to the storing of tactile information for subsequent object discrimination.

Prehensions performed by patients with different neuropathies were examined in some studies. Children with cerebral palsy were able to modify their grip force according to friction between the fingertips and the object and could use tactile information for anticipatory control of the force-scaling of the precision grip, but they seemed to need predictable conditions and successive lifts to build up memory representation of an object's friction (Gordon and Duff 1999) [76]. When patients with Huntington's disease lift an object of unpredictable weight they show slowed lift timing and increased variation with lightweight objects. It was concluded that these patients have a reduced ability to process tactile information (Schwarz et al. 2001) [77]. Similarly, Nowak and Hermsdorfer (2003) [78] investigated whether or not cooling of the grasping digits affects scaling of the grip force to the loads when subjects performed continuous vertical arm movements with a grasped object. As the result of cooling, the subjects exerted significantly higher grip force; this indicated that reduced sensory feedback from the grasping fingers impair the economic scaling of grip force level. Similar facts have been observed with digital anesthesia. Hence it seems that cutaneous afferents are required for setting and maintaining the background level of the grip force (Augurelle et al. 2003) [79].

3.1.5. Forces in prehension

When people hold a vertically oriented object statically with a prismatic grasp, they exert a grasp force (*normal force*) and a load force (*tangential force*). The grasp force is larger than or equal to the minimal force necessary to prevent slip; the difference between the actual grasp force and the minimal one was called *safety margin* (Johansson and Westling 1984), $SM = F_n - F_{n\text{-}Slip}$ and $F_{n\text{-}Slip} = F_t/\mu$, where superscript n represent grasp force (normal force), t stands for load force (tangential force), μ is the coefficient of friction. In some studies, *SM* was represented as a percentage of the above difference with respect to the actual grasp force (Burstedt el al. 1999) [80]; in this case $SM = [(F_n - F_{n\text{-}Slip})/ F_n] \times 100\%$. To secure a stable grasp in static's the following conditions should be satisfied:

(1) the object must be in equilibrium (no net forces and torques);

(2) the direction of the applied forces must be within the cone of friction; and

(3) it should be possible to increase the magnitude of the grasping force to prevent any displacement due to an arbitrary applied force.

The hand is a redundant system in terms of both kinematics and kinetics, hence there are many possible solutions which can be used by the CNNS to grasp and manipulate an object. For instance, to secure a stable grasp, there are infinite ways to distribute the digits forces in order to achieve the task goal. Many studies have examined the distribution of grasp forces among the fingers (Kinoshita *et al*. 1995 [81]; Li *et al*. 1998b; Zatsiorsky 2002ab) during prehension. Three phenomena have been observed during precision gripping as well as in pressing tasks:

(1) *force sharing* – the total fingers force is shared among the fingers in a certain manner (Kinoshita *et al*. 1995, Li *et al*. 1998ab);

(2) *force deficit* – the force produced by a given finger in a multi-finger maximal voluntary contraction (MVC) task is smaller than the maximal force generated by this finger in a single-finger task (Li *et al*. 1998ab, 2001b); and

(3) *enslaving* – the fingers that are not required to produce any force by instruction are involuntarily activated (Latash *et al*. 1998; Li *et al*. 1998ab; Zatsiorsky *et al*. 1998, 2000).

Enslaving effects can be attributed to the three sources/mechanisms:

- peripheral connections, both tendinous (Leijnse 1997) [82] and intermuscular myofascial (Huijing 1999ab) [83]

- multi-digit motor units in the extrinsic muscles (Kilbreath and Gandevia 1994) [84], and
- central neural connections. Control of movements of individual fingers is distributed widely in the M1 hand area (Schieber and Poliakov 1998) [85].

Although the hand is mechanically redundant and the potential solutions are seemingly innumerous, the number of practical solutions is limited by a variety of constraints. The constraints may be grouped into

1. physical constraints, such as object properties, mechanical constraints;
2. neuro-physiological constraints, such as anatomy and physiology of the hand, and
3. high level constraints, such as task requirement, motivation etc.

The laws of physics impose limitations on the forces of prehension. For example, holding a vertically oriented object in the air at rest requires that the normal force of the thumb and the total force of the opposing fingers be equal in magnitude and opposite. To prevent the rotation of an object during grasping, the individual fingers should produce forces such that the total moment of force balances the total torque applied on the object. Hence, force sharing patterns in gripping tasks are partially determined by mechanical constraints. In particular, force sharing patterns among fingers during prehension are strongly dependent upon the thumb location (Li *et al*., 1998b) and handle shape (Cochran and Riley 1986) [86]. It was also demonstrated that subjects adjust fingertip forces at each contact to the local friction (Burstedt et al. 1999).

The anatomy and physiology of the hand create structural limitations on force and control of prehension. One example is the well-documented phenomenon, enslaving. The grip force, as well as individual finger forces, also depends on the wrist angle (Li 2002). Lamoreaux and Hoffer (1995) [87] reported dramatic drop of total grip force with the wrist in maximal ulnar and maximal radial deviation as compared with the neutral anatomic position. Li (2002) explored the individual finger forces during voluntarily movement at the wrist joint. The maximum finger forces were produced at 20 degrees of wrist extension and 5 degrees of ulnar deviation with the force-sharing percentages 32.2%, 32.67% 23.5% and 11.7% for the index, middle, ring and little finger, respectively. With the wrist deviated further away from this position, the forces produced by individual fingers decreased but not in a proportional manner. Napier (1993) showed that the wrist in 30-40 degrees of extension is in the optimal position for gripping. In full flexion of the wrist the hand can exert only 25 percent of its force in full extension.

At the highest level, the constraints can be informational, motivational, social, etc. For example, the subject may be instructed to hold the handle with minimum effort. Since subjects have individual differences, they will interpret the instruction differently and, as a result, different patterns of digit forces, e.g. different force magnitudes and force sharing will be recorded.

3.1.6. Motor Redundancy in Prehension

It was already mentioned in the preceding section that the grasping hand is a mechanically redundant system: while a grasped rigid object has only six degrees of freedom (DoF) the grasping digits produce 30 force/moment components (5 digits × 6 force & moment components per digit). Hence the dimensionality of a transformation matrix that relates the individual finger forces and moments with the resultant forces and moments acting on the object is 6×30 and the matrix is not a full rank. It has been mentioned in the literature, that the grasping hand is a convenient object for studying motor redundancy in human motion because all the digit forces can be measured (Li et al. 1998b). This section deals with the approaches used for studying motor redundancy in prehension. I start, however, with a brief discussion of the motor redundancy problem in general.

3.1.6.1 Motor Redundancy in Human Movement

The problem of controlling the redundant DoFs was first addressed by N. Bernstein (1967) and is known as the Bernstein problem. Bernstein (1967) noted that the moving body possessed many independent DoFs in the potentially controllable number of joints, muscles and neurons. The computational load of controlling so many degrees of freedom is enormous. How, then, Bernstein asked can these degrees of freedom 'be regulated in the course of activity by a minimally intelligent executive intervening minimally?'. Bernstein's solution was that movements are organized into functional groupings or synergies, flexibly adapted by people to meet specific tasks. According to Latash et al. (2004), synergy can be viewed as a neural organization of elements that stabilize important performance variables. Synergy has two major characteristics:

1. Elements typically share a common input or neural drive that leads to stable relationships among them over time;

2. Elements show error compensation.

Synergies in human movement may be revealed in three contexts:

1. Coordinated movements,
2. Neural circuits and
3. Muscle activation patterns.

For example, postural reactions involve the coordinated production of forces and movements by all segments of the body for the maintenance of balance and equilibrium. These coordinated movements may be referred to as synergies. At the neural level, there are a number of identified neural circuits that could principally bring about coordinated activation or inactivation of motoneurons, e.g.

1. reciprocal inhibition,
2. recurrent inhibition connecting different motoneuron pools,
3. interneurons projecting to motoneurons of different muscles (Latash 1998).

Muscle synergy may be defined simply as a group of muscles acting together. However— since the spatial and temporal patterns of muscle activation are highly variable—the applicability of the term 'synergy' for describing muscle activation patterns was questioned by some authors (Macpherson 1991) [89].

In the study of motor redundancy, several research approaches became popular.

Among them are (a) optimization and (b) methods used to explore the movement variability.

Usually, different people solve same motor tasks in a similar way. For instance, we all walk more or less similarly. An idea of the optimization approach is that when selecting a coordination pattern the central controllers of different people use the same strategy: they minimize a certain 'cost function', e.g. they select the movement pattern that corresponds to minimal energy expenditure. In spite of popularity of optimization methods in the literature, the methods have evident delimitations, e.g. different cost functions may yield similar solutions, very often the validity of the optimization approach cannot be verified (for instance the predicted individual muscle forces cannot be directly measured), etc. A very important delimitation of the method is that it provides a unique solution while real movements are variable: if the same movement is performed several times it is never reproduced identically. The movement realizations are similar on a rough-grain scale and they are different on a fine-grain scale.

During the last years, movement variability attracted great interest. In addition to the documenting movement variability in different situations a question about the role and

mechanisms of the variability has been addressed. According to the uncontrolled manifold (UCM) hypothesis, which is suggested by Scholz and Schoner (1999) and further explored by Latash et al. (2002), the controller acts in the space of elemental variables and selects in that space a subspace (a manifold, UCM) corresponding to a stable value of an important performance variable. In addition, the controller organizes covariation of elemental variables to limit their variability in directions orthogonal to the UCM while allowing relatively more variability within the UCM. The UCM theory provides a quantitative measure for a synergy by comparing the amounts of the total variance per DoF within the UCM and orthogonal to the UCM. If the former is larger than the later, it reveals a synergy. Another point of view is advanced by Todorov and Jordon (2002) [91]. They propose an alternative theory based on stochastic optimal feedback control. They showed that the optimal strategy in the face of uncertainty is to allow variability in redundant (task-irrelevant) dimensions.

Based on this framework, task-constrained variability, goal-directed corrections, motor synergies, controlled parameters, simplifying rules and discrete coordination modes might emerge naturally.

All the above ideas (synergies, optimization, the UCM approach, etc.) were used to study prehension.

3.1.6.2 Prehension Synergies

When performing similar tasks people use similar force production patterns (Santello and Soechting 2000). A central goal of the prehension research is to discover these rules. A more immediate goal is to find and describe the reproducible patterns of coordination.

The ensuing review addresses the following topics: (a) the concept of prehension synergy, (b) hierarchical control of prehension, (c) principle of superposition.

Prehension synergy was defined as the conjoint change of digits forces (Zatsiorsky and Latash 2004). Prehension synergies are manifested in different ways. They can be revealed by (a) adjustments to changes in task parameters (Zatisorsky et al. 2003), (b) compensation for self-induced and/or externally-imposed perturbations (Johansson et al. 1992abc; Flanagan and Tresilian 1994; Johansson and Cole 1994), and (c) error compensation revealed in a negative covariation among elemental variables recorded in different trials (Shim et al. 2003) or in a single trial of long duration (Santello and Soechting 2000).

With the variation of task parameters, the forces at the virtual finger level show qualitatively different patterns from the finger forces at the individual finger level (Santello and Soechting 1997; Baud-Bovy and Soechting 2001, 2002; Zatsiorsky and Latash 2004). Based on these observations a theory was proposed that prehension synergies are organized in a hierarchical fashion and include at least two levels of control. At the higher lever, the forces exerted by the thumb and VF are defined. At the lower level, the forces exerted by the individual fingers are determined (Zatsiorsky and Latash 2004).

One of the control mechanisms that can simplify the control of prehension is the principle of superposition. The principle has been recently suggested in robotics (Arimoto et. al. 2001). According to this principle, some skilled actions can be decomposed into several elemental actions that can be controlled independently by separate controllers. In particular, it has been shown that a dexterous grasp and manipulation of an object by two soft-tip robot fingers can be realized by a linear superposition of two commands, one command for the stable grasping and the second one for regulating the orientation of the object. Such a decoupled control decreases the computation time. By studying repetitions of a standard task, it was demonstrated that the principle of superposition can be applied to human prehension: the digit forces and moments fall in one of two subsets (Shim et. al. 2003; Zatsiorsky et. al. 2004). The variables belonging to the same subset highly correlate with each other while there is no correlation between the variables from different subsets. In the first subset, the normal forces of the thumb and VF are grouped; these forces prevent the object from slipping out the hand. In the second subset, the tangential forces of the thumb and VF, the moments produced by the tangential and normal forces and the moment arm of the VF normal force are grouped; these variables maintain the orientation of the handle constant. In another experiment (Zatsiorsky et. al. 2004) in which the resisted load and torque are varied systematically, it was found that the control of load and control of torque are independent and control commands can be simply added together. These findings lend support to the validity of the principle of superposition in human grasping.

Prehension synergies are revealed not only in static but also in dynamic tasks, specifically when a subject is instructed to perform point to point/cyclic arm movement. When a subject moves a hand-held object up or down, an inertial force acts in the vertical direction in addition to the gravity force. The load force (L, tangential force) equals $L=W+ma$, where W is the weight, m is mass of the object and a is its acceleration. When

the load force increases, the grip force increases accordingly (Johansson and Westling 1984) to prevent slip.

The relation between normal and tangential digit forces during lifting an object, a grasping synergy (Zatsiorsky and Latash 2004), has been extensively examined. It was demonstrated that this relation develops at an early age (Forssberg et al. 1991; Blank et al. 2001). The grip force is modulated by the weight of the object (Johansson and Westling 1984; Winstein et. al. 1991), abrupt load perturbations (Eliasson et al. 1995, Serrien et. al. 1999ab), friction conditions (Cole and Johansson 1993; Burstedt et. al. 1999), tangential torques (Kinoshita etl. al. 1997), gravity changes during parabolic flights (McIntyre et. al. 1998 [94]; Hermsdorfer et. al. 1999a; Augurelle et. al. 2003), and inertial forces that act during shaking and point to point arm movements (Flanagan and Wing 1993, 1995) as well as during locomotion (Gysin et al.2003).

The coupling between normal and tangential forces is very robust. In similar load conditions, the grip forces are larger in senior adults (Vandervoort et. al. 1986; Kinoshita and Francis 1996; Cole and Rotella 2002) and patients with neurological disorders (Gordon and Duff 1999; Babin-Ratté et al. 1999; Hermsdörfer et. al. 1999b; Serrien and Wiesendanger 1999; Fellows et al. 2001). During similar manipulations, local skin anesthesia and digit cooling make the coordination of the load and grip force less precise but does not change the general pattern of coordination (Nowak et. al. 2001; Monzee et. al. 2003; Nowak and Hermsdörfer 2003). Based on these observations it has been concluded that the grip force-load force coupling is mainly controlled by a feed-forward mechanism: A central controller regulates the grip force according to the expected load force (Johansson and Westling 1984; Flanagan and Wing 1995) while feedback mechanism triggered by cutaneous sensation acts if an assessment of an expected load force happens to be erroneous.

3.2. Mechanics of grasp

In this section, mechanics of grasp will be examined and reviewed. Four related topics—contact models, grasp map, internal force and grasp stability—will be described.

3.2.1. Contact models

Contact is defined as a collection of adjacent points where two bodies touch each other (Mason and Salisbury 1985) [96]. A contact between a finger and an object can be described as a mapping between forces and moments exerted by the finger at the area of contact and the resultant wrenches at some reference point on the object (A wrench is a generalized force, a 6×1 vector that consists of three linear components and three angular components).

TABLE 3.2. CONTACT TYPE AND CORRESPONDING DOFS

Contact type	Remaining DoFs
No contact	6
Frictionless point	5
Frictionless line	4
Point with friction	3
Frictionless plane	3
Soft finger	2
Line with friction	1
Plane with friction	0

Based on the screw theory Mason and Salisbury (1985) proposed a system to categorize contact models. In this system, six classes of contacts (excluding the no contact case) were introduced (Table 3.2). The classification is based on three types of contact: point contact, line contact, and plane contact. Adding or eliminating friction will give six combinations of contact. For each contact model, the imposed constraints are described in terms of the DoFs as well as in terms of screw systems of associated

motions and forces. This formulation is neat and simplifies the calculation. However, it is not accurate under certain circumstances. For example, this classification does not take into account surface deformation under load, which could affect the strength and stability of grasp.

The discussion below is limited to the three types of contact that are relevant to the present research, point contacts with and without friction and the soft finger contact. Point contact models are widely applied in robotics.

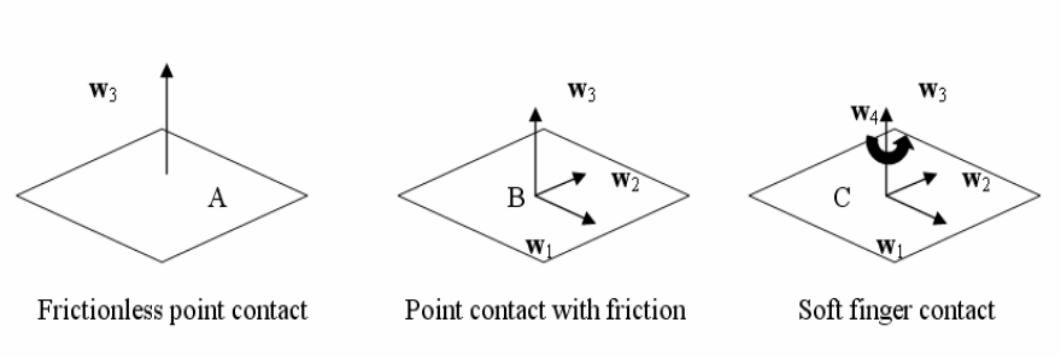

Figure 3.2. (A) Frictionless point contact; such a contact can resist force only in normal direction. (B) Point contact with friction; it can resist forces along three axes. C) Soft finger contact can resist forces along three axes and a moment of force about an axis normal to the contact surface (torsional moment). ***w*** *represent wrench basis:* ***w1*** *, [1 0 0 0 0 0]T is in a positive x direction,* ***w2*** *, [0 1 0 0 0 0]T , is in a positive y direction,* ***w3*** *, [0 0 1 0 0 0]T is in a positive z direction.*

3.2.1.1. A frictionless point contact:

When there is no friction between the fingertip and the object, forces can only be applied in the direction normal to the surface of the object. The applied wrench F_{c_i} is:

$$F_{c_i} = \begin{bmatrix} 0 \\ 0 \\ 1 \\ 0 \\ 0 \\ 0 \end{bmatrix} f_{c_i} \quad f_{c_i} \geq 0, \qquad (0.1)$$

where $f_{c_i} \in ¡$ is the magnitude of the force applied by the finger in the normal direction, the column vector represents a wrench basis w3 in the normal direction (Figure 3.2A).

The requirement that f_{c_i} is positive indicates that at this type of contact a force along w3 can only push on an object but cannot pull it.

3.2.1.2. A point contact with friction model

In practical situations, we can experience contact without friction quite rare (an in exact example can be a contact with a wet soap). A simple widely used model of friction is called *Coulomb friction model*. The Coulomb friction model is an empirical model which dictates that the tangential force is proportional to the normal force and the coefficient is a function of the materials of contact. The range of the magnitude of tangential force is determined by:

$$\left|f^t\right| \leq \mu f^n \qquad (0.2)$$

where $\mu > 0$ is the static coefficient of friction, f^t represents tangential force and f^n represents normal force. In three dimensions, the above relation can be represented geometrically as *friction cone* (Figure 3.3). To maintain a stable contact, the contact forces must lie in the friction cone (*FC*).

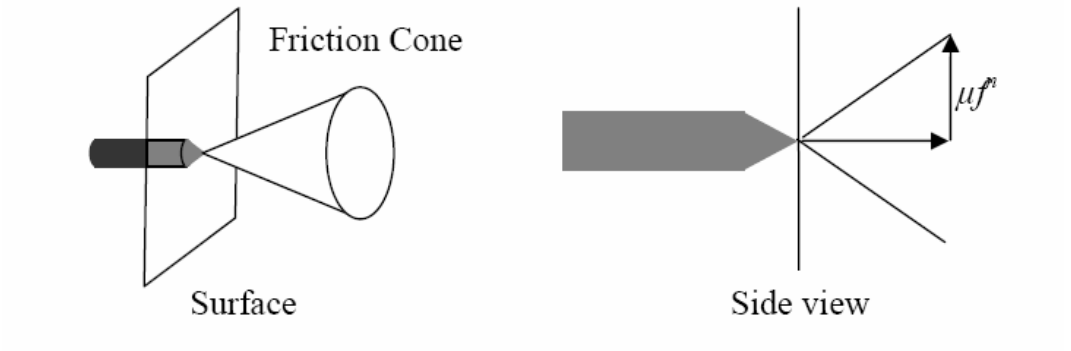

Figure 3.3. Geometric representation of the Coulomb friction model.

In the point-contact-with-friction model, existence of friction between the fingertip and the object is assumed. In such a case, forces can be exerted in any direction within the friction cone (Figure 3.2.B).

$$F_{c_i} = \begin{bmatrix} 1 & 0 & 0 \\ 0 & 1 & 0 \\ 0 & 0 & 1 \\ 0 & 0 & 0 \\ 0 & 0 & 0 \\ 0 & 0 & 0 \end{bmatrix} f_{c_i} \quad f_{c_i} \in \mathrm{FC}_{c_i}, \qquad (0.3)$$

$\mathrm{FC}_{c_i} = \left\{ f \in \mathbb{R}^4 \mid \sqrt{f_1^2 + f_2^2} \le \mu f_3, f_3 \ge 0, |f_4| \le \gamma f_3 \right\}$, and f_{c_i} is a (3×1) vector.

3.2.1.3. Soft contact

In addition to the classification of contacts described in the preceding paragraphs, Cutkosky (1985) proposed a different set of contact models in which the fingertip geometry and deformation were also taken into account. Finger pad can deform under loading; therefore the fingertip compliance is considered in the model in addition to the finger joint compliance. For a small contact area, the fingertip becomes more compliant with respect to rotations and can approximate point contact model well. For a larger contact area, the resistance to rotation (torsion) increases, the translational compliance is larger and the contact can approach a planar contact with friction. Under contact with object the human fingertips exhibit rolling and deformation so in a realistic model the fingers are assumed to be soft and curved. A model of a *soft-finger contact* (Figure 2C) can be written as:

$$F_{c_i} = \begin{bmatrix} 1 & 0 & 0 & 0 \\ 0 & 1 & 0 & 0 \\ 0 & 0 & 1 & 0 \\ 0 & 0 & 0 & 0 \\ 0 & 0 & 0 & 0 \\ 0 & 0 & 0 & 1 \end{bmatrix} f_{c_i} \qquad f_{c_i} \in \mathrm{FC}_{c_i} \qquad (0.4)$$

$\mathrm{FC}_{c_i} = \left\{ f \in \mathbb{R}^4 \mid \sqrt{f_1^2 + f_2^2} \le \mu f_3, f_3 \ge 0, |f_4| \le \gamma f_3 \right\}$, where the γ is the coefficient of torsional friction and f_{c_i} is a (4×1) vector.

In general, a set of contact forces applied by a given contact is:

$$F_{c_i} = W_{c_i} f_{c_i}$$

where W_{c_i} represents a ($6\times m$) wrench basis for the i^{th} contact (*ci* represents ith contact) and f_{c_i} is a $m\times 1$ vector.

3.2.2. Grasp map

To determine the effect of the contact forces on the object, the forces and moments should be transformed to the object coordinate frame. The basic theory that is briefly described below is mainly due to screw theory and is presented in the monograph by Murray et al. (1994) [97].

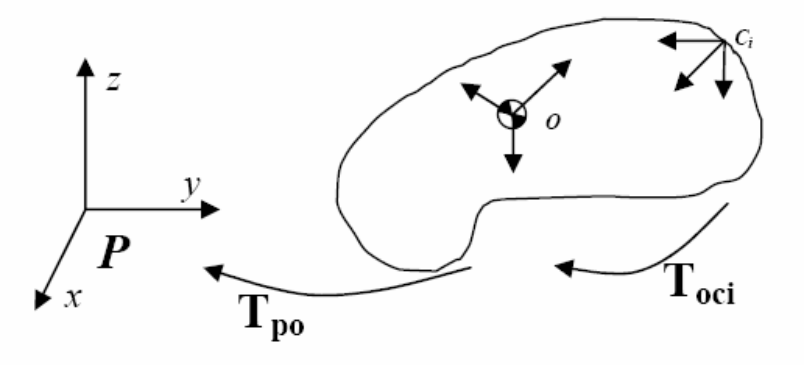

Figure 3.4. Coordinate frames for contact and object forces.

Let (p_{oc_i}, R_{oc_i}) be the configuration of the i^{th} contact frame relative to the object frame, where p_{oc_i} is the displacement vector between the origins of the two frames and R_{oc_i} is the rotation matrix which transform the local frame of contact to object frame (Figure 5). The generalized force exerted by a single contact can be written in object coordinates as

$$F_o = W_{oc_i} F_{ci} = \begin{bmatrix} R_{oc_i} & 0 \\ \hat{p}_{oc_i} R_{oc_i} & R_{oc_i} \end{bmatrix} W_{ci} f_{ci}, \qquad f_{ci} \in FC_{ci} \qquad (0.5)$$

where the matrix W_{oc_i} is the wrench transformation matrix (6×m) which maps contact wrenches to object wrenches; $\hat{p}_{oc_i}$ (3×3) is the screw symmetric matrix of vector p_{oc_i} (*ci* represents i^{th} contact); f_{ci} is the generalized force vector and F_{ci} is the applied wrench. The screw symmetric matrix signifies a cross-product operator, $\mathbf{a} \times \mathbf{b} = \hat{\mathbf{a}}\mathbf{b}$ where **a** and **b** are vectors. The transformation described by equation (5) rotates the force and moment vectors from the contact frames to the object frame and adds a moment of the

contact force about the origin of the object frame. If we have *n* fingers contacting an object, the total wrench on the object is the sum of the object wrenches due to each finger.

The map between the contact forces and the total object force is called the *grasp map*, $G : ¡^{m} \to ¡^{6}$, where *m* is the dimension of column space of wrench basis. Since each contact map is linear and wrenches can be superposed (as long as they are all written in the same coordinate frame), the net object wrench is

$$F_0 = G_1 f_{c1} + \ldots + G_n f_{cn} = \begin{bmatrix} G_1 & \text{L} & G_n \end{bmatrix} \begin{bmatrix} f_{c1} \\ \text{M} \\ f_{cn} \end{bmatrix} \qquad (0.6)$$

where *n* represent the n^{th} contact and the grasp map is

$$G = \begin{bmatrix} W_{oc_1} & W_{c1} & \text{L} & W_{oc_n} & W_{cn} \end{bmatrix}$$

With this definition, the object wrench can be written as

$$F_0 = G f_c \qquad f_c \in FC, \qquad (0.7)$$

where **G** is a 6×*mn* matrix (*n* equals the total number of contacts).

3.2.3. Internal force

To balance external object wrenches appropriate finger wrenches should be applied at the contacts. If a grasp can resist any applied wrench, such a grasp is called the *force-closure* grasp and can be written as: $\mathbf{G}\mathbf{f}_c = -\mathbf{F}_e$ where $-\mathbf{F}_e = \mathbf{F}_o$ (Murry et. al. 1994). A major feature of a force-closure grasp is the existence of internal forces. An internal force is a set of contact forces which result in no net force on the object (Mason and Salisbury 1985; Murry et. al. 1994). In the above equation, **G** is a 6×*mn* matrix, where *mn*>6. Because **G** has more columns than rows it defines an under-determined set of equations and for a given value of $\mathbf{F}_e$, a unique solution for $\mathbf{f}_c$ does not exist. In other words, a set of resultant forces and moments acting on a hand-held object does not prescribe in a unique way the finger forces acting on it.

Any solution for $\mathbf{f}_c$ consists of two vectors $\mathbf{f}_m$ and $\mathbf{f}_i$ such that $\mathbf{f}_c = \mathbf{f}_m + \mathbf{f}_i$ (Kerr and Roth 1986), where $\mathbf{f}_m$ is orthogonal to $\mathbf{f}_i$ and where $\mathbf{f}_i$ lies in the null space of $\mathbf{G}$. If a set of orthonormal basis vectors which span the null space of $\mathbf{G}$ are assembled into the columns of matrix $\mathbf{N}$, then $\mathbf{f}_i$ can be written in terms of the $m \times 1$ vector $\boldsymbol{\lambda}$ (m is the dimension of null space) as $\mathbf{f}_i = \mathbf{N}\boldsymbol{\lambda}$.

The mathematical independence of the internal and manipulation forces allows for their independent (decoupled) control and such a decoupled control is realized in some robotic manipulators (e.g., Zuo and Qian 2000). People, however, most probably do not use this option: It has been shown that when people move a vertically oriented object in the vertical direction the grip force F_G increases in parallel with the load force F_L ($F_L = W + ma$ where W is the object's weight, m is its mass and a is acceleration) to prevent slip (Johansson and Westling 1984; Flanagan and Wing 1993, 1995; Flanagan et al. 1993; Flanagan and Tresilian 1994; Nakazawa et al. 1996, 1999; Kinoshita et al. 1996, Gordon et al. 1999; Gysin et al. 2003; see also Flanagan and Johansson 2002 for a recent review).

The F_G - F_L coupling is so robust that people increase F_G in parallel with F_L even when F_G is already much above the slipping threshold, e.g. when a performer purposefully grasps the object with a very high force before lifting the object (Flanagan and Wing 1995a).

3.2.4. Grasp stability

A grasp is called stable if the grasped object after being subject to small disturbances returns to equilibrium. A grasp should be stable both when it is stationary and during manipulation. Usually, in stationary conditions, grasp stiffness is sufficient for the grasp stability. However, when manipulating at a higher speed the damping and inertia effects might not be negligible; therefore grasp impedance —which is understood here as a complex mechanical resistance depending on the displacement magnitude, its speed and acceleration— should be considered.

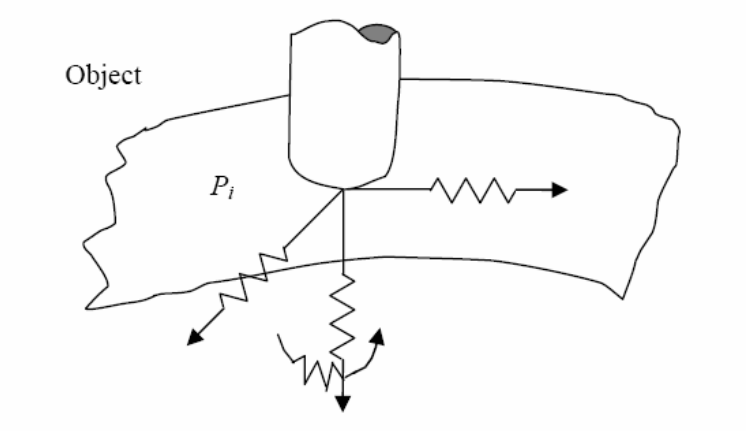

Figure 3.5. Soft finger contact model with stiffness components. Four springs shown in the figure represent elastic resistance of the finger tip to the linear deformation in three orthogonal directions and the resistance with respect to fingertip torsion about an axis normal to the contact surface.

In grasping and manipulation we can think of the stiffness matrix as a measure of interaction between fingers and the object surface when external forces and moments are applied to the system. Intuitively, we can think of the fingertip as having been replaced by a set of "virtual springs" (see Figure 3.5). Grasp stiffness characteristics can be obtained empirically by applying a set of forces to the fingertips and measuring their deflections. It has been shown that at relatively low speeds it is possible to characterize the behavior of a grasp with stiffness matrices (Kao et al. 1997) [98]. The stiffness matrix at the finger/object contacts is an instantaneous static relation between contact forces and compliant deflections as follows:

$$K_i = -\frac{\partial f_i}{\partial x_i} \qquad \text{or} \qquad \delta f = -K_i \delta x_i \qquad (0.8)$$

where $\partial \mathbf{f}_i$ includes the linear force and moment with respect to the local coordinates and $\partial \mathbf{x}_i$ is a small change in the position and orientation of the contact. Notice that for finite rotations or large deflection, the linearized approximation of $\mathbf{K}_i$ becomes inaccurate. The stiffness $\mathbf{K}_i$ associated with individual i^{th} finger/object contact can be computed as a function of the finger joint stiffness, the structural compliance of the finger, and the contact types (Cutkosky and Kao 1989) [99].

For further analysis of stiffness, a stiffness matrix **K**, can be resolved into two components, a symmetric, **K***s* and an anti-symmetric, **K***a*, (Chen and Kao 2000) where

$$K_s = \frac{(K + K^T)}{2} \quad \text{and} \quad K_a = \frac{(K - K^T)}{2} \qquad (0.9)$$

The symmetric component can be derived from a conservative quadratic potential function; whereas, the non-symmetric components is related to the work done by the grasping force moving along a closed path during manipulation.

Grasp stiffness plays an important role in grasp stability and it has been extensively examined in robotics. Hanafusa and Asada (1977) [100] were the first to study the stability of an articulated grasp. They consider the grasp as an elastic system with each finger having a controlled stiffness. Based on minimizing the total elastic energy of the grasp they quantified quasi-static stability. Nguyen (1989) [101] proposed a systematic stability analysis and a method of constructing stable planar and spatial grasp of *n* elastic fingers. The stiffness matrix of each finger was formed, and it was 3 by 3 in plane and 6 by 6 in space. The grasp stiffness matrix **K** in the object frame can be obtained by applying a congruent transformation to the stiffness matrices at the contact frames. (A transformation is called congruent if $\mathbf{U} = \mathbf{D}^T\boldsymbol{\eta}\mathbf{D}$, where $\det(\mathbf{D}) \neq 0$. In this expression, **U** and $\boldsymbol{\eta}$ are matrices and det is a determinant.) The grasp stiffness matrix must be positive definite in order for the grasp to be quasi-statically stable.

Recently, analyses of stiffness developed in robotics were also applied to human studies. Milner and Franklin (1998) [102] measured the two-dimensional static stiffness of the index finger at different finger postures and target force directions. It was demonstrated that the finger stiffness was anisotropoic, with the direction of greatest stiffness being approximately parallel to the proximal phalanges of the finger. Kao et al. (1997) applied the methods of robotic stiffness control and calibration to human grasping tasks (pinch grip). They showed that linear relation between force and displacement is capable of capturing the characteristics of the experimental data of human grasps when displacements are relatively small. By studying the effect of grasp force and finger span on the grasp stiffness, Van Doren (1998) [103] found that stiffness increased significantly in proportion to initial force but was changed only slightly by initial span.

To study dynamic perturbations, i.e. the perturbations occurring at large velocity and acceleration, a concept of grasp stiffness can be generalized to the concept of grasp impedance.

When a finger is in contact with an object the finger has an ability to exhibit itself as a six-dimensional spring-mass-damper system to the object. However, the grasped object can experience only a subset of these dynamic properties at each contact location. For a soft finger contact, only four of the six components are experienced by the object (Figure 5). The linear impedances (spring, mass, dampers) related to *x*, *y* and *z* directions and the angular impedances about the *z*-directions of the contact frame are the only ones seen by the object. With an assumption that the fingertip frame and the contact frame are coincident, only such components are considered to exist at the contact point on the object. Thus, the impedance matrices of the finger at the contact point are:

$$\begin{aligned} K_{fi} &= \mathrm{Diag}\begin{bmatrix} K_{fix} & K_{fiy} & K_{fiz} & K_{fi\theta z} \end{bmatrix} \\ B_{fi} &= \mathrm{Diag}\begin{bmatrix} b_{fix} & b_{fiy} & b_{fiz} & b_{fi\theta z} \end{bmatrix} \\ M_{fi} &= \mathrm{Diag}\begin{bmatrix} m_{fix} & m_{fiy} & m_{fiz} & m_{fi\theta z} \end{bmatrix} \end{aligned} \qquad (0.10)$$

for $i=1\ldots n$, where n is the number of fingers in the grasp, **K**, **B**, **M** represents stiffness, damping and mass, respectively. By combining the stiffness, damping coefficients, and the masses of all fingers the three diagonal matrices in contact space can be formed as

$$\begin{aligned} K_f &= \mathrm{Diag}\begin{bmatrix} K_{f1} & K_{f2} & \mathrm{L} & K_{fn} \end{bmatrix} \\ B_f &= \mathrm{Diag}\begin{bmatrix} B_{f1} & B_{f2} & \mathrm{L} & B_{fn} \end{bmatrix} \\ M_f &= \mathrm{Diag}\begin{bmatrix} M_{f1} & M_{f2} & \mathrm{L} & M_{fn} \end{bmatrix} \end{aligned} \qquad (0.11)$$

The next step is to find the grasp impedance matrices **K**, **B**, and **M** in the object frame resulting from the impedance matrices at the contact frames given by (11). The relation between the stiffness matrices in these two frames is given by a congruent transformation, $K_f = J_g^T K J_g$, where J_g is the grip Jacobian and **K** is obtained as $K = \begin{bmatrix} J_g K_f^{-1} J_g^T \end{bmatrix}^{-1}$ (Shimoga 1996) [104].

4. The State of the Art of the Tactile Sensors

4.1. Introduction

Equation Chapter 2 Section 14

This subchapter reviews the current state of the art and outlook in robotic tactile sensing for real-time control of dexterous manipulation. Tactile sensor devices are described, including tactile array sensors, force-torque sensors, and dynamic tactile sensors. The information provided by these devices can be used in manipulation in many ways, such as finding contact locations and object shape, measuring contact forces, and determining contact conditions.

Although touch sensing is the basis of dexterous manipulation, early work in tactile sensing research focused on the creation of sensor devices and object recognition algorithms. Particular attention was devoted to skin-like array sensors. The creation of multi-fingered robot hands increased interest in tactile sensing for manipulation, beginning with preliminary work on incorporating tactile information in manipulation. In the last few years studies on the use of tactile sensing in real-time control of manipulation have appeared. In these studies, tactile sensors have provided information that has guided the execution of the tasks including automatic grasping, edge tracking, and rolling manipulation.

Robotic sensing can be classified as either of the non-contact or contact type [105]. Non-contact sensing involves interaction between the robot and its environment by some physical phenomena, such as acoustic or electromagnetic waves. The most important types of robotic sensors of the non-contact type are vision and proximity sensors.

Contact sensing, on the other hand, implies measurement of the general interaction that takes place when the robot's end-effector is brought into contact with an object. Contact sensing is further classified into force and tactile sensing.

Force sensing is defined as the measurement of the global mechanical effects of contact, while tactile sensing implies the detection of a wide range of local parameters affected by contact. Among those contact-based effects the most significant ones are contact stresses, slippage, heat transfer, and hardness. The properties of a grasped object that can be derived from tactile sensing can be classified into geometric and dynamometric types

[106]. Among the geometric properties there are presence, location in relation to the end-effector, shape and dimensions, and surface conditions [107–111]. Among the dynamometric parameters associated with grasping there are: force distribution, slippage, elasticity and hardness, and friction [112–116].

Tactile sensing requires sophisticated transducers; yet the availability of these transducers alone is not a sufficient condition for successful tactile sensing. It is also necessary to accurately control the modalities through which the tactile sensor interacts with the explored objects (including contact forces, as well as end-effector position and orientation) [117–119]. This leads to active tactile sensing, which requires a high degree of complexity in the acquisition and processing of the tactile data [120].

Tactile sensing normally involves a rigid object indenting the compliant cover layer of a tactile sensor array [121]. The indentation of a compliant layer due to contact can be analyzed from two conceptually different points of view [105]. The first one is the measurement of the actual contact stresses (force distribution) in the layer, which is usually relevant to controlling manipulation tasks. The second one is the deflection profile of the layer, which is usually important to recognize geometrical object features. Depending on the approach adopted, different processing and control algorithms must be utilized.

In general, the study of tactile sensors comprises two steps:

(1) the forward analysis, related to the acquisition of data from the sensor (changes on the stress or strains, induced by the indentation of an object on the compliant surface of the transducer);
(2) the inverse problem, normally related to the recovery of force distribution or, in some cases, the recovery of the indentor's shape.

4.2. Requirements for Tactile Sensors

In 1980, Harmon conducted a survey to determine general specifications for tactile sensors [122]. Those specifications have been used subsequently as guidelines by many tactile sensor designers:

1. Spatial resolution of 1 to 2 mm
2. Array sizes of 5*10 to 10*20 points

3. Sensitivity of $0.5*10^{-2}$ to $1*10^{-2}$ N for each force-sensing element (taxel)
4. Dynamic range of 1000:1
5. Stable behavior and with no hysteresis
6. Sampling rate of 100 Hz to 1 kHz
7. Monotonic response, though not necessarily linear
8. Compliant interface, rugged and inexpensive

While properties (109), (111), and (112) above should apply to any practical sensor, the others are merely suggestions, particularly with respect to the number of array elements and spatial resolution. Developments on tactile sensing following [122] have identified additional desirable qualities; namely, reliability, modularity, speed, and the availability of multisensor support [120].

4.3. Technologies for Tactile Sensing

The technologies associated with tactile sensing are quite diverse: extensive surveys of the state-of-the art of robotic-tactile-transduction technologies have been presented in [106, 107, 120, 121]. Some of these technologies will be discussed briefly.

4.3.1. Resistive

The transduction method that has received the most attention in tactile sensor design is concerned with the change in resistance of a conductive material under applied pressure. A basic configuration of a resistive transducer is shown in Figure 4.1. Each resistor, of which value changes with the magnitude of the force, represents a resistive cell of the transducer. Different materials have been utilized to manufacture the basic cell.

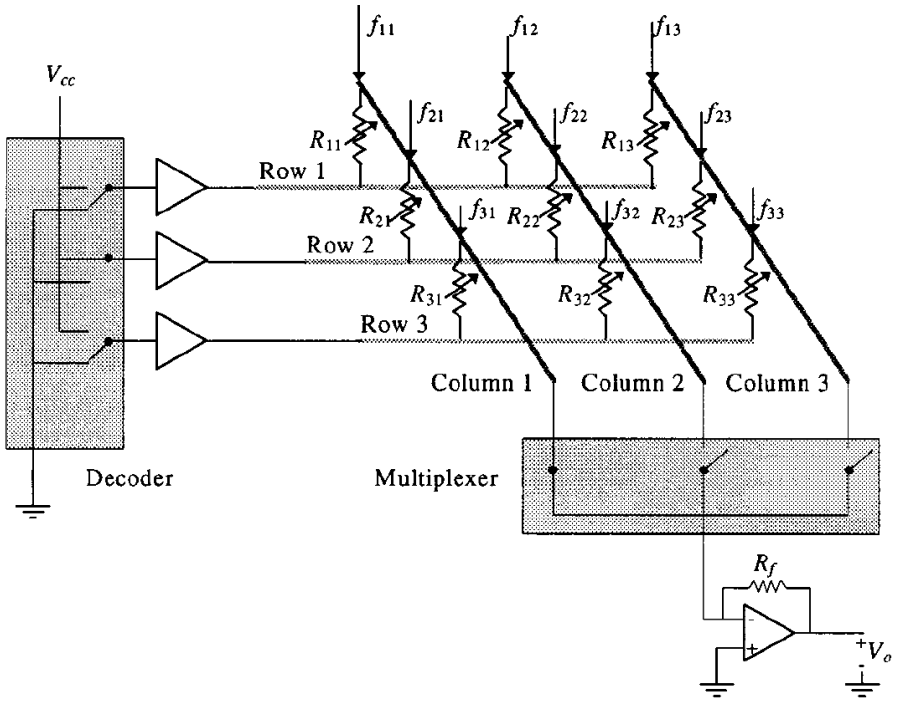

Figure 4.1. General configuration of a resistive transducer.

Conductive elastomers were among the first resistive materials used for the development of tactile sensors. They are insulating, natural or silicone-based rubbers made conductive by adding particles of conductive or semiconductive materials (e.g., silver or carbon). The changes in resistivity of the elastomers under pressure are produced basically by two different physical mechanisms. In the first approach, the change in resistivity of the elastomer under pressure is associated with deformation that alters the particle density within it. In the second approach, while the bulk resistance of the elastomer changes slightly when it is compressed, the design allows the increase of the area of contact between the elastomer and an electrode, and correspondingly a change in the contact resistance. A typical design of this kind is given in [123]. In [124], a newer tactile sensor is reported with both three-axis force sensing and slippage sensing functions. In the former case, the pressure sensing function is achieved by utilizing arrays of pressure transducers that measure a change in contact resistance between a specially treated polyimide film and a resistive substrate.

Piezoresistive elements have also been used in several tactile sensors. This technology is specifically attractive at present because, with micromachining, the piezoresistive elements can be integrated together with the signal-processing circuits in a single chip. A

64*64 - element silicon pressure sensor array incorporating CMOS processing circuits for the detection of a high-resolution pressure distribution was reported in [125].

The array, composed of 4096 (64*64) individual stress sensing elements, was constructed with a fully CMOS-compatible fabrication process, allowing integration of the sensing structures with digital control circuitry. The individual array elements have linear responses to both applied normal stress (1.59 mV/kPa, 0–35 kPa) and applied shear stress (0.32 mV/kPa, 0–60 kPa). A spatial resolution comparable to the spacing of the papillary ridges of the human dermis (300 μm) has been achieved within the 1.92*1.92 cm active sensing area of the array

When piezoresistors and circuits are fabricated on the same silicon substrate, the sensor array can be equipped with a complex switching circuit, next to the sensing elements, which allows a better resolution in the measurements [113].

4.3.2. Capacitive

Tactile sensors within this category are concerned with measuring capacitance, which varies under applied load. The capacitance of a parallel-plate capacitor depends on the separation of the plates and their areas.

A sensor using an elastomeric separator between the plates provides such compliance that the capacitance will vary according to the applied normal load. The intersections of rows and columns of conductor strips form capacitors. Each individual capacitance can be determined by measuring the corresponding output voltage at the selected row and column. To reduce cross-talk and electromagnetic interference, the rows and columns that are not connected are grounded.

When a load is applied to the transducer, the capacitor is deformed as shown in Figure 4.2. For modeling purposes, we assume that the plate capacitor is only under compression. When no load is applied, the capacitance due to the element in the i-th row and the j-th column, C0 ij, is given by:

$$C_{ij}^{0} = \varepsilon \frac{wl}{h_0} \tag{2.1}$$

where e is the permittivity of the dielectric, w and l are the width and the length of the plate capacitor, respectively, and h0 is the distance between plates when no load is applied.

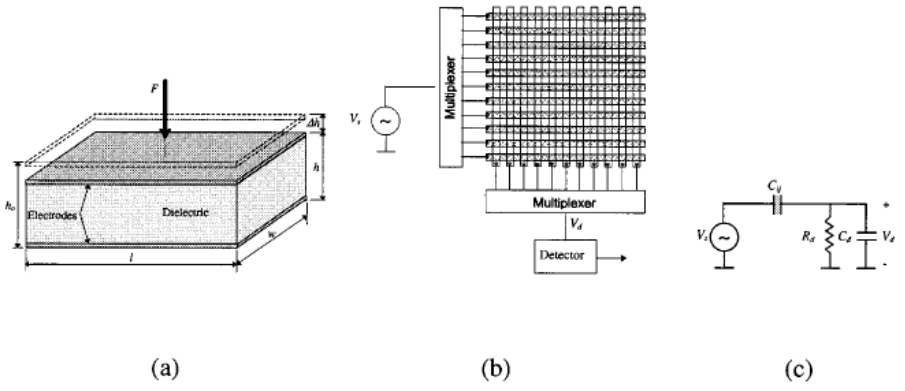

Figure 4.2. (a) Basic cell of a capacitor tactile sensor. (b) Typical configuration of a capacitive tactile sensor. (c) Equivalent circuit for the measurement of the capacitance C_{ij}.

When a load is applied, the capacitor is under compression and the capacitance is given by:

$$C_{ij} = \varepsilon \frac{wl}{h_0 - \Delta h} \tag{2.2}$$

where Δh is the displacement of the top metal plate and $\Delta h \ll h_0$. The strain can be measured by:

$$\frac{C_{ij} - C_{ij}^0}{C_{ij}} = 1 - \frac{h_0 - \Delta h}{h_0} = \frac{\Delta h}{h_0} \cong \zeta_Z \tag{2.3}$$

Consequently, the strain at each taxel can be determined by measuring the magnitudes of C_{ij} and C_{ij}^0 for each element.

Note that the presence of a tangential force would offset the plates tangentially and change the effective area of the capacitor plates. An ideal capacitive pressure sensor can quantify basic aspects of touch by sensing normal forces, and can detect slippage by measuring tangential forces. However, distinguishing between the two forces at the output of a single sensing element is a difficult task and requires a more complex transducer than the one presented in Figure 4.2 [126].

Micromachined silicon-based capacitive devices are especially attractive due to their potential for high accuracy and low drift. A sensor with 1024 elements and a spatial resolution of 0.5 mm was reported in [127]. Several possible structures for implementing capacitive high-density tactile transducers in silicon were reported in [128]. A cylindrical finger-shaped transducer was reported in [129].

The advantages of capacitive transducers include wide dynamic range, linear response, and robustness.

Their major disadvantages are susceptibility to noise, sensitivity to temperature, and the fact that capacitance decreases with physical size, ultimately limiting the spatial resolution. Research is progressing toward the development of electronic processing circuits for the measurement of small capacitances using charge amplifiers, and the development of new capacitive structures.

4.3.3. Piezoelectric

A material is called piezoelectric, if subjected to a stress or deformation, it produces electricity. Longitudinal piezoelectric effect occurs when the electricity is produced in the same direction of the stress, Figure 4.3. In this figure, a normal stress s (= F/A) is applied along the Direction 3 and the charges are generated on the surfaces perpendicular to Direction 3. A transversal piezoelectric effect occurs when the electricity is produced in the direction perpendicular to the stress.

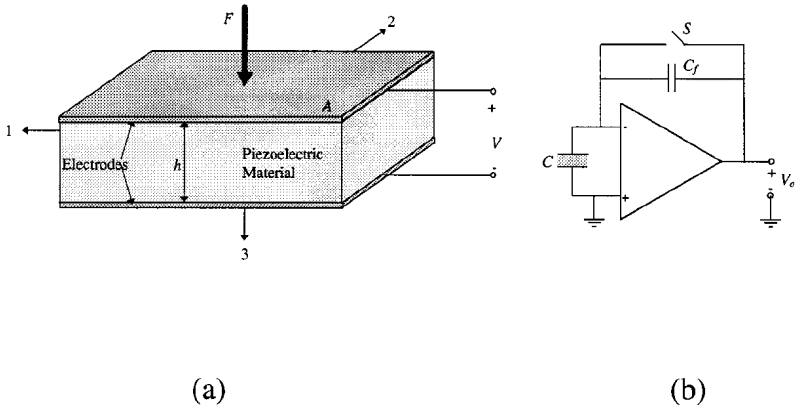

Figure 4.3. (a) Basic cell of a pizoelectric transducer. (b) Charge amplifier utilized for the measurement of the applied force.

The voltage V generated across the electrodes by the stress s is given by:

$$V = d_{33}\frac{h}{\varepsilon}\sigma \qquad (2.4)$$

where d33 = Piezoelectric constant associated with the longitudinal piezoelectric effect

e = Permittivity

h = Thickness of the piezoelectric material

The piezoelectric material most widely used in the implementation of tactile transducers is PVF2. It shows the largest piezoelectric effect of any known material. Its flexibility, small size, sensitivity, and large electrical output offer many advantages for sensor applications in general, and tactile sensors in particular. Examples of tactile sensors implemented with this technology can be found in [105].

The major advantages of the piezoelectric technology are its wide dynamic range and durability. Unfortunately, the response of available materials does not extend down to dc and therefore steady loads cannot be measured directly. Also, the PVF2 material produces a charge output that is prone to electrical interference and is temperature dependent.

The possibility of measuring transient phenomenon using piezoelectric material has encouraged some researchers recently to use the piezoelectric effect for detecting vibrations that indicate incipient slip, occurrence of contact, local change in skin curvature, and estimating friction and hardness of the object [111, 114, 115].

4.3.4. Optical

Recent developments in fiber optic technology and solid-state cameras have led to numerous novel tactile sensor designs. Some of these designs employ flexible membranes incorporating a reflecting surface, Figure 4.4.

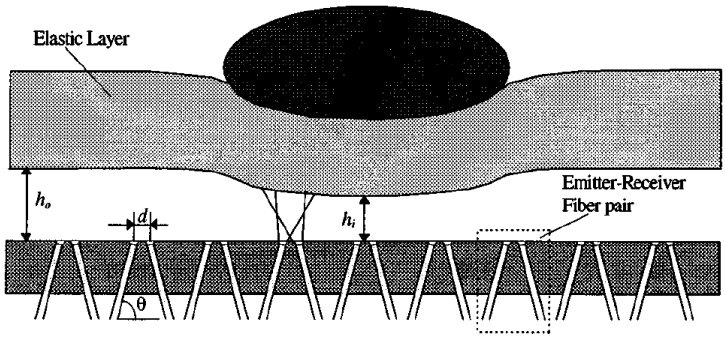

Figure 4.4. Reflective transducer

Light is introduced into the sensor via a fiber optic cable. A wide cone of light propagates out of the fiber, is reflected back from the membrane, and is collected by a second fiber. When an external force is applied onto the elastomer it shortens the distance between the reflective side of the membrane and the fibers, h. Consequently, the light gathered by the receiving fiber changes as a function of h.

Another optical effect that can be used is that of frustrated total internal reflection [109]. With this technique, an elastic rubber membrane covers, without touching, a glass plate (waveguide); light entering the side edge of the glass is totally reflected by the top and bottom surfaces and propagates along it, Figure 4.5.

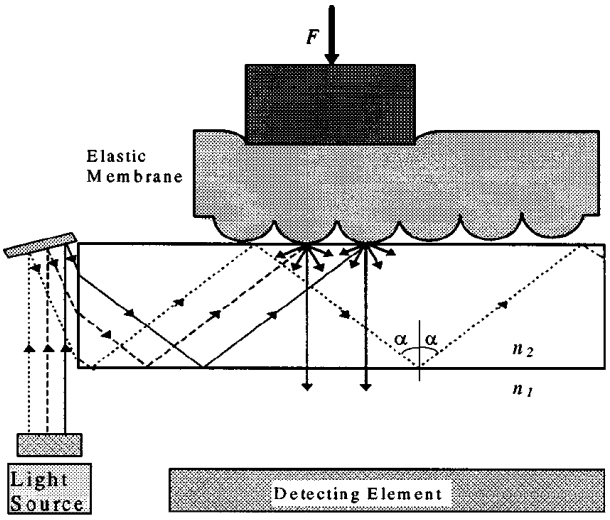

Figure 4.5 Tactile transducer based on the principle of internal reflection.

Objects in contact with the elastic membrane deform it and induce contact between the bottom part of the membrane and the top surface of the waveguide, disrupting the total internal reflection. Consequently, the light in the waveguide is scattered at the contact location. Light that escapes through the bottom surface of the waveguide can be detected by an array of photodiodes, a solid-state sensor, or, alternatively, transported away from the transducer by fibers [107]. The detected image is stored in a computer for further analysis. A rubber membrane with a flat surface yields a high-resolution binary (contact or non-contact) image [109]. If the rubber sheet is molded with a textured surface (Figure 4.5), an output proportional to the area of contact is obtained and, consequently, the applied forces can be detected [107]. Shear forces can also be detected using special designs. Sensors based on frustrated internal reflection can be molded into a finger shape [109] and are capable of forming very high-resolution tactile images. Such sensors are commercially available.

Other types of optical transducers use “occluder” devices. One of the few commercially available tactile sensors uses this kind of transducer [130]. In one of the two available designs, the transducer’s surface is made of a compliant material, which has a grid of elongated pins on its underside.

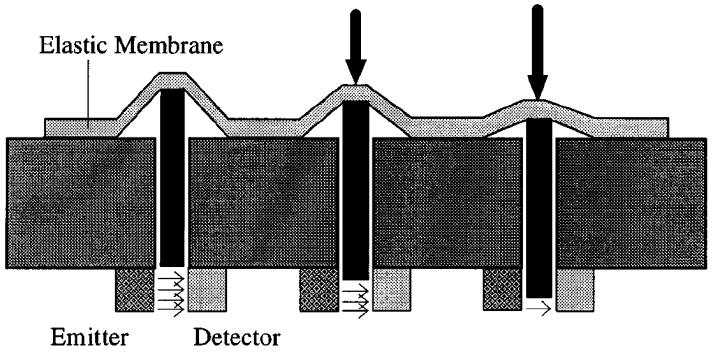

Figure 4.6. Principle of operation of an occluder transducer.

When force is applied to the compliant surface, the pins on the underside undergo a mechanical motion normal to the surface, blocking the light path of a photoemitter–detector pair. The amount of movement determines the amount of light reaching the photoreceiver. Correspondingly, the more force is applied, the less amount of light is collected by the photoreceiver, Figure 4.6. The major problems with this specific device are associated with creep, hysteresis, and temperature variation. This scheme also requires individual calibration of each photoemitter–photodetector pair.

Fibers have also been used directly as transducers in the design of tactile sensors. Their use is based on two properties of fiber optic cables: (1) if a fiber is subjected to a significant amount of bending, the angle of incidence at the fiber wall can be reduced sufficiently for light to leave the core; and (2) if two fibers pass close to one another and both have roughened surfaces, light can pass between the fibers. Light coupling between adjacent fibers is a function of their separation [107].

When an object is forced into contact with the transducer a light distribution is detected at each detector. This light distribution is related to the applied force and the shape of the object. Using complex algorithms and active sensing (moving the object in relation to the transducer), the object position, orientation, size, and contour information can be retrieved.

4.3.5. Photoelastic

An emerging technology in optical tactile sensing is the development of photoelastic transducers. When a light ray propagates into an optically anisotropic medium, it splits into two rays that are linearly polarized at right angles to each other and propagate at different velocities. This splitting of a ray into two rays that have mutually perpendicular

polarizations results from a physical property of crystalline material that is called optical birefringence or simply birefringence. The direction in which light propagates with the higher velocity is called the fast axis; and the one in which it propagates more slowly is called the slow axis. Some optically isotropic materials — such as glass, celluloid, bakelite, and transparent plastics in general — become birefringent when they are subjected to a stress field. The birefringent effect lasts only during the application of loads. Thus, this phenomenon is called temporary or artificial birefringence or, more commonly, the photoelastic phenomenon.

If force is applied, stresses are induced in the photoelastic layer, making the material birefringent. This introduces a certain phase difference between the components of the electric field associated with the light-wave propagation. The two directions of polarization are in the plane perpendicular to the direction of propagation. As a consequence of this effect, the output light is elliptically polarized, creating a phase difference distribution, p, between the input light ant the output light. The phase difference distribution carries the information of the force distribution applied to the transducer.

A polariscope is a practical method to observe the spatial variation on light intensity (fringes) due to the effect of induced phase difference distribution. A technique for the recovery of the forces from the polariscope is described in [131].

Photoelasticity offers several attractive properties for the development of tactile sensors: good linearity, compatibility with vision-base sensing technologies, and high spatial resolution associated with the latter, which could lead to the development of high-resolution tactile imagers needed for object recognition and fine manipulation. Also, photoelastic sensors are compatible with fiber optic technology that allows remote location of electronic processing devices and avoidance of interference problems.

Other technologies for tactile sensing include acoustic, magnetic, and microcavity vacuum sensors.

5. The System Description

People can grasp a wide variety of shapes and sizes, perform complex tasks, and switch between grasps in response to changing task requirements. This is due, in part, to the physical structure of our hands (multiple fingers with many degrees of freedom), and in part to our sophisticated control capabilities.

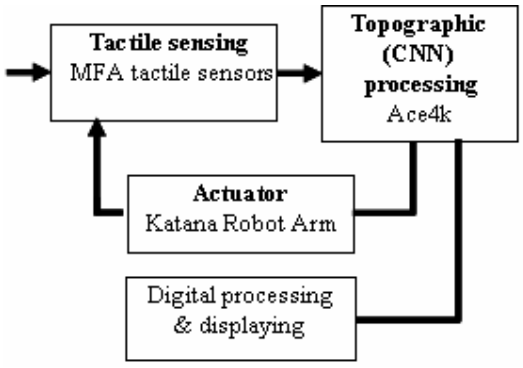

Figure 5.1: The block-diagram of the experimental system

In living structures the sensing and "processing" parts are closely coupled providing "intelligent sensing".

The functions of an intelligent sensor system may be described in terms of compensation, information processing, communications and integration. The combination of these respective elements allows the development of intelligent sensors that can operate in a multi-modal fashion.

We built a prototype system (Figure 5.1.) where the sensory array output is processed by a CNN-UM (Cellular Neural/Nonlinear Network – Universal Machine) processor.
The sensing elements are Si based tactile sensors (MEMS) [149], they are mounted on a two-fingered robot hand [150]. The actuator is controlled in closed loop.

5.1. The Sensors

Humans guide dexterous manipulation tasks largely through tactile perception of objects. When a fingertip comes into contact with an object, a contact stress profile is induced at the interface. The resulting stress profile has three components: one normal to the surface (normal stress), and two oriented tangentially to the surface (shear stress). Sensing and processing these tri-axial stress profiles provide humans with a rich source of information

about their physical environment. Measuring and processing contact stress information are of great importance in robotic dexterous manipulation.

At the beginning of the experiments we tried a few commercially available tactile sensors. One of them is TactArray made by The Pressure Profile System (PPS) [151]. The sensing mechanism is a capacitive one, namely there is an air gap between the electrodes and this can be changed by the pressure. Only the normal stress can be measured with this method. The tactile-array may have 16*16 or 32*32 taxels with 5 kHz scan rate. The tactile array can be connected by USB port to a PC. The interface software supports acquisition and visualization of the sensed data. The resolution of data is 12 bit.

5.2. Piezorezistiv sensors

Our group developed a monocrystalline silicon tactile sensor (MEMS) [152]. The signal conversion (from mechanical to electrical) is based on the piezorezistive effect. A single crystalline silicon as a structural material provides excellent and controllable mechanical proprieties in all directions; moreover, the manufacturing process can be integrated into the microcircuit technology. The main advantage of the method used in the fabrication of the sensor lies in the freedom provided by the use of the single-side porous silicon micromachining for the formation of the suspended n-type single crystal membrane. In this way there is no orientation restriction in the membrane design whatsoever. Moreover, it also facilitates the formation of the optimum p^+ piezoresistors.

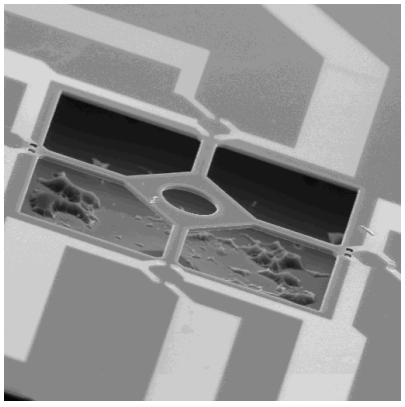

Figure 5.2: One Taxel (Touching element)

Taxel size is 500x500µm2 with wiring. The hole in the middle serves for bumper formation. Each individual sensor is composed of a central shuttle plate suspended by

four bridges over an etched pit. Embedded in each of the four bridges a piezoresistor is placed. The suspension of the structure over the substrate may result in deformation occuring in the bridges, as normal and shear loads are applied to the central plate through an overlying protective elastomer layer. Each of the piezoresistors acts as the variable leg of a resistive half-bridge circuit. By monitoring the intermediate node voltage of the half-bridge, a direct measure of the state of strain in each of the four bridges is obtained.

A method has been published regarding the reconstruction of the stress tensor elements from the four measured voltages of a bare four-bridge sensor [125]. The equations describing the connection between the measured voltages and the strain are presented in Equation 4.1:

$$T_x = \frac{1}{\alpha_s}(V_{Left} - V_{Right})$$

$$T_y = \frac{1}{\alpha_s}(V_{Down} - V_{Up}) \qquad (4.1)$$

$$S_n = \frac{1}{2\alpha_s}(V_{Down} + V_{Up} + V_{Left} + V_{Right})$$

where T_x, T_y, S_n are the two shear and one normal strain components, respectively, V_i are the four measured voltages, the α_s constants contain the piezoresistive coefficients and all the information about the geometry of the sensor and the amplification.

5.3. The Sensory Array

In this setup we use a pair (one for each finger) of 2*2 array of tactile sensors, capable of measuring full triaxial stress profiles with high stress measurement resolution and a spatial resolution comparable to the spacing of the papillary ridges of the human dermis (0.8-1 mm) [10]. The sensory array is mounted on the fingertips of the Katana Arm®.

The symmetrical placement of the sensors and the sensor arrays increases the flexibility and robustness of this prototype system. This configuration allows the robot to perform tasks which demand the distribution of the sensors that is similar to the placement of human beings' thumb and other fingers, i.e. opposite.

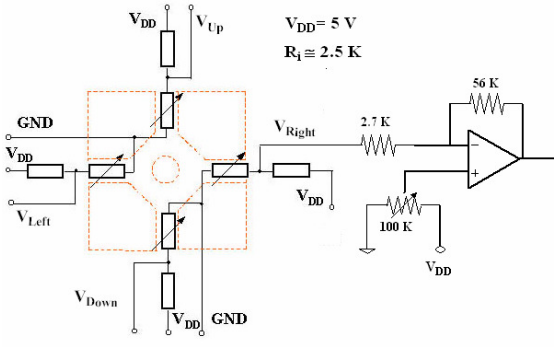

Figure 5.3: Circuit diagram and the signal conditioning unit

The complete system consists of 32 signal channels, two fingers, each of them with a 2*2 array where each taxel is composed of four piezorezistive sensors (2*2*2*4).

Each piezorezistive sensor has a pair resistor on the chip (Figure 5.3.), but this resistor's value doesn't change. These pairs of resistors are connected in series, and constant 5 Volts are applied to them. In normal unloaded state the resistors' value (both piezorezistive and normal) is around 2.5 KOhm, in this case the output of the voltage divider is 2.5V. After applying a force to the piezoresistive sensor the value of the resistor will change and the output of the voltage divider will change positively or negatively, depending on the force direction, whether the sensor is pressed or pulled. The maximum change in the piezorezistors' value is around 2%. This means that the measured 2.5V output has a ±50mV shift. Since usually the AD converters work on 8-12 bits, their resolution is not enough to detect the min. 2mV change on the 2.5V. To overcome this, a signal conditioning unit is placed between the sensor output and AD converter. This unit is a differential amplification unit; the reference voltage is on the positive input, which is equal to the unloaded voltage divider output. This reference voltage is variable, because the sensors and the reference resistor pairs are not identical, so the signal conditioning unit must be calibrated for the given sensor array. The sensor's half-bridge output is connected on the negative input. This circuit amplifies the difference between the reference voltage and the sensor output, the amplification factor is 20. The output of the signal conditioning unit is not the absolute voltages on the bridges, but its relative changes to the normal, unload state.

The analog signals are converted into digital signals with an Advantech PCI 1713 A/D converter, after amplification and calibration.

5.4. Katana Arm®

Contrary to vision (usually a CCD camera), the tactile sensors need to make a contact with the surface of the object. In this experiment we use the Katana Arm® as the actuator for the sensors.

Katana Arm® is a high-quality programmable robot arm with fully integrated electronics, controlled via a serial interface by a PC. It is of four degrees of freedom. The end effector is a two-fingered gripper, which is able to grasp both smaller and larger objects. Most parameters are accessible and changeable online, a feature which enables controller optimization during work.

Controlling Unit

The main processing and controlling tasks are accomplished on the PC. The Graphical User Interface is written in C++. The main tasks of this application are:

- to read the data from the sensor
- to process the data
- to extract, detect and classify the significant events
- to display the forces acting on the surface of the sensor array
- to give the proper feedback to the Robotic Arm and Grasper (control)

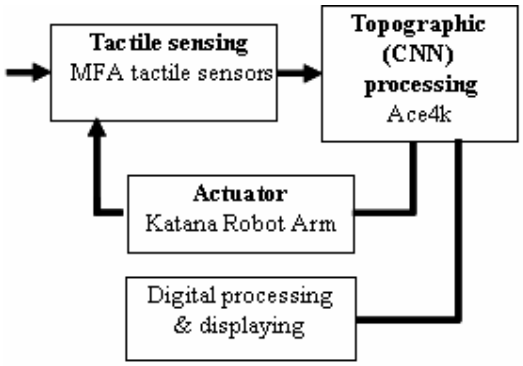

Figure 5.4: System diagram

The experimental system presented in Figure 5.4 is a closed loop system. The sensing, processing and actuating parts are linked, and they realize a real-time exploration system, gathering information about the grasped objects in a proactive-adaptive way.

6. Gentle Grasping

When the task is to grasp a fragile object such as a glass or an egg, it is sufficient to have information about the exact moment when the contact is made, and an adequate bandwidth in the control loop in order to stop the grasper. In the case of a complex grasping task there is a need for special sensors and algorithms. We consider it a simple case when the robot has to hold a glass, which is filled with water, so the weight of the glass is changing. In this case the grasping force has to change adaptively, proportionately with the weight of the object. If the force is too small, the object starts to slip out of the fingers and this must be detected by the system, in order to be able to give an adequate response. Tactile sensors can provide better sensory information for this task than can be obtained by vision or torque sensors placed in the DC-motors of the arm.

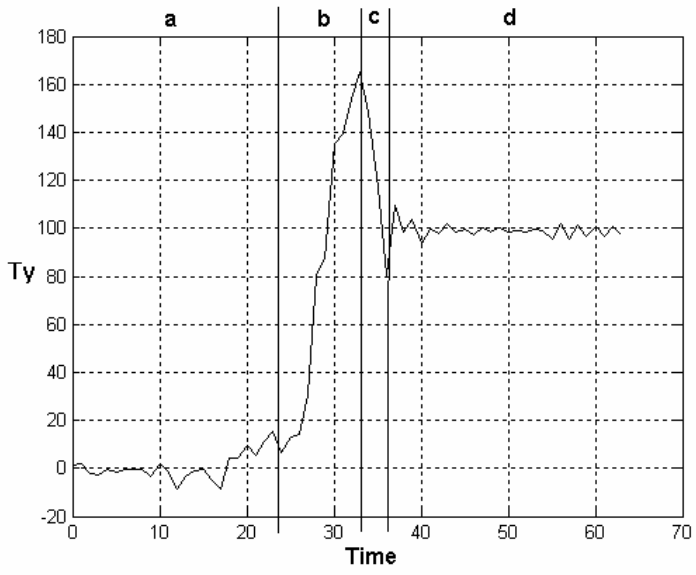

Figure 6.1: a) nothing is grasped, b) Ty growing proportionally with the weight; c) object starts to slip out, d) static Ty, equal with kinetic friction force

As a solution to this problem, we considered the tri-axial tactile sensor where the tactile sensor can sense not only the normal component of the grasping force, but the shear stress, too. If the robot grasps with a constant force, when the glass is filled up, the normal component (Sn) will remain constant, but the vertical component (Ty) of the grasping force will grow proportionately with the weight of the grasped object (Figure 67.1.b), because the vertical component is directly proportional with the weight of the glass. Actually, after a calibration the Ty component could work as a balance. The condition of not slipping is that the sensed Ty force must always be smaller than the

sticking friction force between the glass and gripper, as described in Equation (5.1). The sticking friction force holds the weight of the glass, and it is proportional with the normal component (Sn) of the applied force.

$$|Ty| \leq \mu s * Sn \quad (5.1)$$

where μ_s - static friction coefficient, Sn – normal component, Ty – vertical shear stress

The glass starts to slip out of the fingers if Equation 5.1 is not satisfied. In that moment Ty will suddenly decrease (Figure 6.1.c) and will be seated on a constant level (Figure 6.1.d), given by (5.2).

$$|Ty| = \mu k * Sn \quad (5.2)$$

where: μ_k - kinetic friction coefficient, Sn – normal component, Ty – vertical shear stress

A possible application of this system is, after a calibration, to determine both the static and kinetic friction coefficients between the grasper and the object grasped.

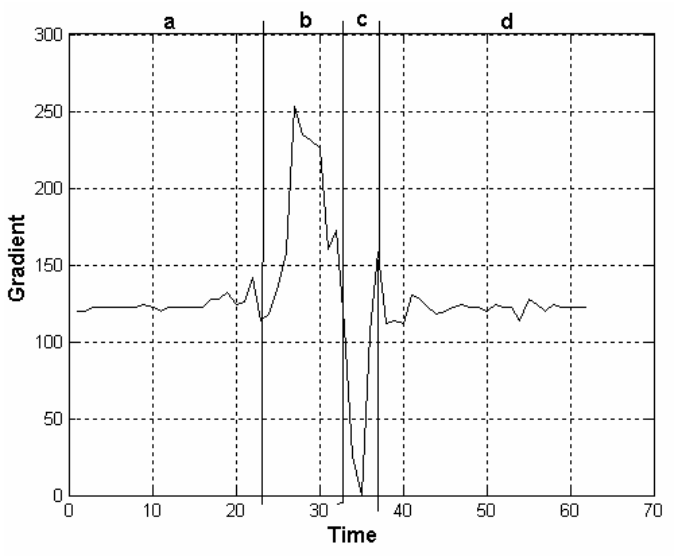

Figure 6.2: The gradient of the Ty (Sobel.tem)

6.1. The Analogic Algorithm

Aladdin Pro System [154] provides a common framework for developing analogic CNN algorithms. The algorithms can be run on software simulators or a 64*64 CNN-UM analog VLSI chip [155]. ACE4k is a platform that contains a CNN-UM chip built in a board type PC104. The platform is connected to the host PC by a PCI bus interface, and provides a fast capability for loading data up-and-down to the 64*64 CNN-UM.

The algorithm follows the evolution of Ty, calculates the first derivative giving the direction and the speed of Ty's change. As a first step, we have to transform the signals coming from the sensors into images. In the present configuration the sensory array is

only 2*2 consequently there are only four Ty signals on each finger. These signals are multiplied in order to obtain the same number of columns as rows (64 in the case of 64*64 CNN-UM). Since in this moment our tactile sensor array has only 2*2 elements, the need for this algorithm, i.e. parallel processing, is not so obvious. The efficiency of this method comes out in the case of a larger array size, at least 8*8. The 8*8 touching sensor array is already in testing phase, but it is not yet integrated in the system. In this contribution the main principle of gentle grasping is described, and this can be applied to arrays larger than 2*2.

Vertical “axe” represents a Ty signal, the horizontal “axe” the time. The value of a Ty in a given time is coded on the pixel’s gray-scale level.

The Universal Machines on Flows (UMF) [156] description of the algorithm can be seen in Figure 6.3. As a first step, the algorithm applies a Sobel template (see the corresponding template in Appendix A) to calculate the gradient. The gradient of one Ty is plotted in Figure 6.2. The positive rise (Figure 6.2.b) shows how the weight of the object grows. After this positive deflection, a sudden negative fall occurs (Figure 6.2.c). In this period the value of Ty changes from static friction force (μs*Sn) to kinetic friction force (μk*Sn). The algorithm is of two branches: one for detecting the positive rise and the other is to detect the fall.

On the first branch the algorithm extracts the white strip. As a first step, it globally adds one to the image in order to cut any inverse bulge. This takes place because the representation of a gray-scale image is in the range of [-1, 1]. In order to be able to apply a threshold template, we must invert the image. After these steps, only a black strip remains on the image, corresponding to the positive rise. For us the width of this strip is of a major importance. Applying a Horizontal_CCD template and then counting the black pixels we can get the exact width of the line. In our case the positive line width is represented by 9 pixels (Figure 6.1.b).

The second branch is to detect the negative fall of the derivative. In order to cut the positive part, we add globally -1 to the image by the algorithm. Applying the threshold and Vertical_CCD template, we can get the width of the negative strip. In the presented case the width is 2 pixels (Figure 6.1.c). These fast changes in the negative direction in the evolution of Ty occures because the object started to slip out of the fingers.

The 9-pixel width of the positive evolution shows that this is a change slower than that of the negative fall, which is only 2-pixel wide.

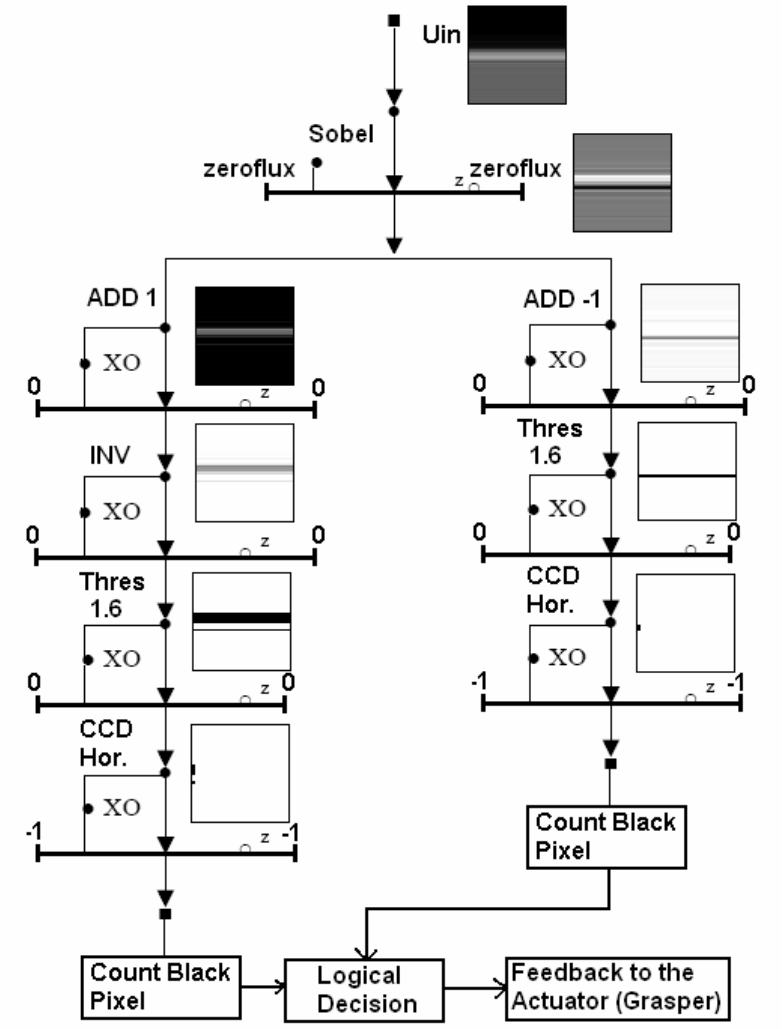

Figure 6.3: UMF Diagram of the algorithm

7. Sensing, Detecting And Analyzing Active Forces Between Contacting Surfaces

Position control strategies are adequate for tasks such as materials transfer and spot welding where the manipulator is not interacting significantly with objects in the workspace. However, tasks such as assembly, grinding, and deburring, which involve extensive contact with the environment, are better handled by controlling the forces (force and/or torque) of interaction between the manipulator and the environment directly. For example, consider an application where the manipulator is required to wash a window, or to write with a felt tip marker. In both cases pure position control scheme is unlikely to work. Slight deviations of the end-effector from the planned trajectory will cause the manipulator either to lose contact with the surface or to press too strongly on the surface. For a highly rigid structure such as a robot, a slight position error could lead to extremely large forces of interaction with disastrous consequences (broken window, smashed pen, damaged end-effector, etc.). The above mentioned applications are typical as they involve both force control and trajectory control. In writing application we clearly need to control the forces normal and tangential to the plane of the paper and position in the plane of the paper in order to generate the appropriate text. It is clear that we should modify the position commands based on externally sensed force information. Therefore a force feedback control algorithm should accept force and motion commands, measure 3D forces and positions, and produce motion commands to the manipulator.

Interaction of the manipulator with the environment will produce forces and moments at the end-effector or tool. Let $\mathbf{F} = (F_x, F_y, F_z, n_x, n_y, n_z)^T$ represent the vector of forces and torques at the end-effector, expressed in the tool frame. Thus F_x, F_y, F_z are the components of the force at the end-effector, and n_x, n_y, n_z are the components of the torque at the end-effector.

I propose an efficient and fast method to detect and identify the twisting or pulling motion of the touching objects. The **F** vector of forces and torques cannot be measured with sensors sensing only the normal (perpendicular) component of the forces acting between the surfaces.

The smallest sensing unit (from now on sensory unit), capable of detecting the **F** vector of forces and torques and differentiating the basic events is of two by two sensory elements, so called taxels (touching element). With a special combination of these

sensors and an adequate processing unit this sensing unit is a fully operational, sterling 6 DOF force and torque sensor.

The method presented in this chapter detects the spatio-temporal tactile events, thru processing the pressure fields between the fingertips and the grasped object. The 3D pressure fields are decomposed in three orthogonal pressure maps. These maps are processed separately and the typical features (positive or negative pressure levels) are extracted, detected. The typical spatio-temporal tactile events are classified with a logical combination of these 3D features.

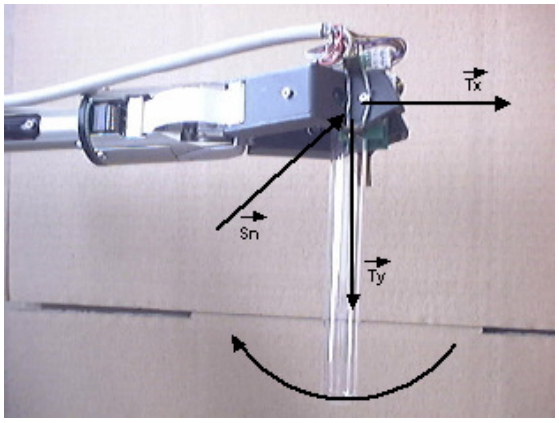

Figure 7.0: grasper with the object

According to the 6DOF, 6 basic events can be described: shift along the one of the OX, OY, OZ directions and rotation around one of the OX, OY, OZ axes.

As a reference coordinate frame let consider the fingers contact point as an origin. The OX direction is the horizontal plane, with the positive direction “out” from the gripper point of view. The OY direction is the vertical plane, positive direction “up”. The OX and OY are the tangential components. The OZ direction (here notated as N) is perpendicular to the finger surface (normal component), the positive direction is “in”, which means “pushing the finger”. The two fingers are mirrored to each other (Figure 7.0).

7.1. Shift along the OX direction

The Tx component will increase in each sensor if the movement is in the positive direction and will decrease if the movement is in the negative direction. All the other components (Ty and Sn) will remain constant.

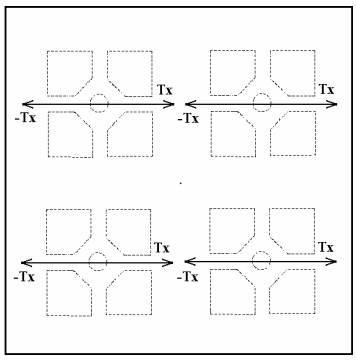

Figure 7.1 Direction of the forces acting during the shift along the OX direction

7.2. Shift along the OY direction

If the direction of the forces is up (positive), all the Ty components will grow. In opposite to that, if the direction of acting forces is down (negative), the Ty components will decrease (the magnitude of the force will grow but the orientation is negative). All the other components (Tx and Sn) will remain constant.

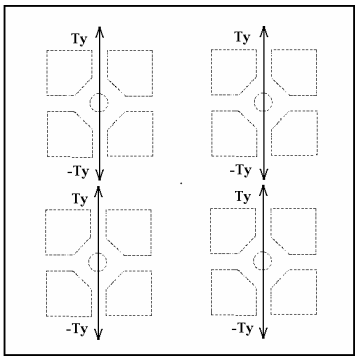

Figure 7.2 Direction of the forces acting during the shift along the OY direction

7.3. Shift along the OZ direction

The *OZ* is the normal direction to the surface of the sensors. Pushing the grasped object toward the left finger the normal pressure on that sensor array will grow (the Sn component), meanwhile the Sn component on the right sensor array will decrease. The Sn component describes (characterizes) the magnitude of the grasp of the robotic hand, and grows proportionally with the grasping force.

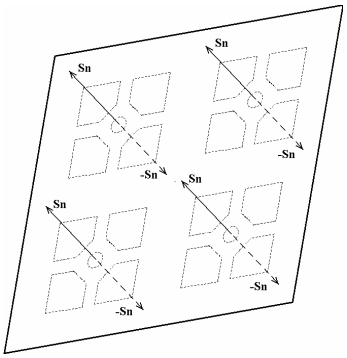

Figure 7.3 Direction of the forces acting during the shift along the OY direction

7.4. Rotation around the OZ axe

The most challenging situation is the grasping of an object with a two fingered robot hand, when the object starts to twist around the direction of the grasping force, i.e. the normal axe to the grasper's surface, see Figure 7.0.

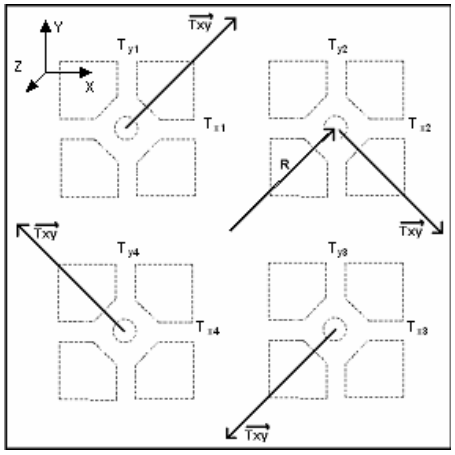

Figure 7.4: Shear forces

During this experiment, a rotating force is applied to the grasped object, in order to raise a torque on the sensor surface. This torque will induce forces proportional to its direction and size in each sensor, see Figure 7.4. These emerged forces have three components, one normal to the surface S_n, and two tangential (T_x and T_y). The normal force is due to the grasping force, and shows how much the probe is pressed by the fingers. The twisting motion is sensed by the tangential components of the original force. Due to the sensors properties both compression and distention are measurable. The measured values of the forces in the *OX* direction (in our case horizontal, outwards from

the fingers) are plotted in Figure 7.4.1. In the case presented the rotation of the grasped test-tube will result in the change of the T_{Xi} components of the forces as follows: T_{X1} and T_{X2} will grow, but T_{X3} and T_{X4} will decrease.

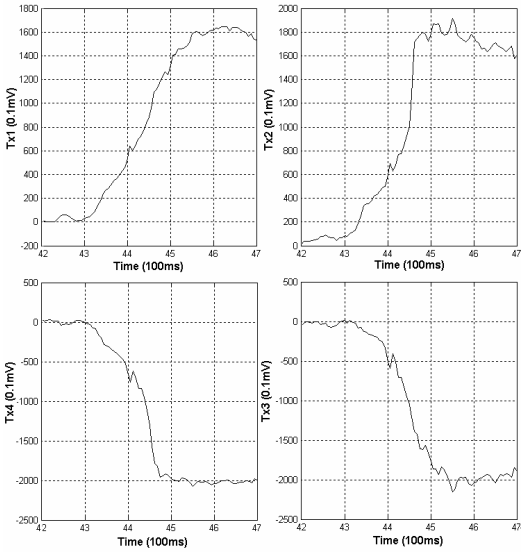

Figure 7.4.1: The evolution of the four T_x components during the twisting force (in time)

In the same time, in the *OY* direction (vertical) the force will evolve in the following way: T_{Y1} and T_{Y4} will grow, but T_{Y2} and T_{Y3} will decrease (Figure 7.4.2).

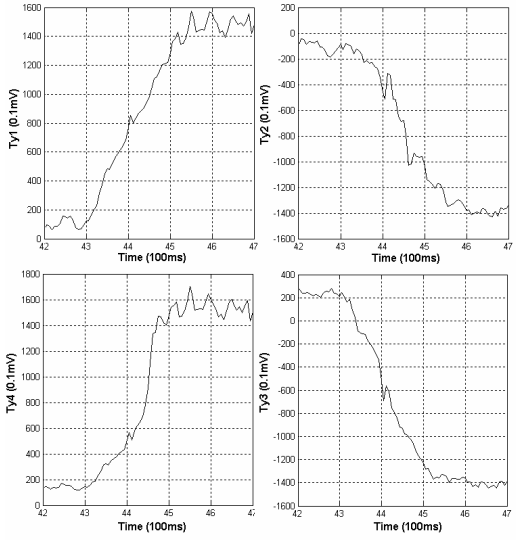

Figure 7.4.2: The evolution of the four T_y components during the twisting force (in time)

In Figure 7.4.1-7.4.2 the relative changes of the force components are plotted against time. When no torque is present T_x and T_y are equal to zero. As the torque grows-changes in a given direction the T_x and T_y components grows up or falls down.

Plotting Tx on the horizontal axe, and Ty on the vertical axe, we can follow the evolution of the forces (the size and direction), see Figure 7.4.3.

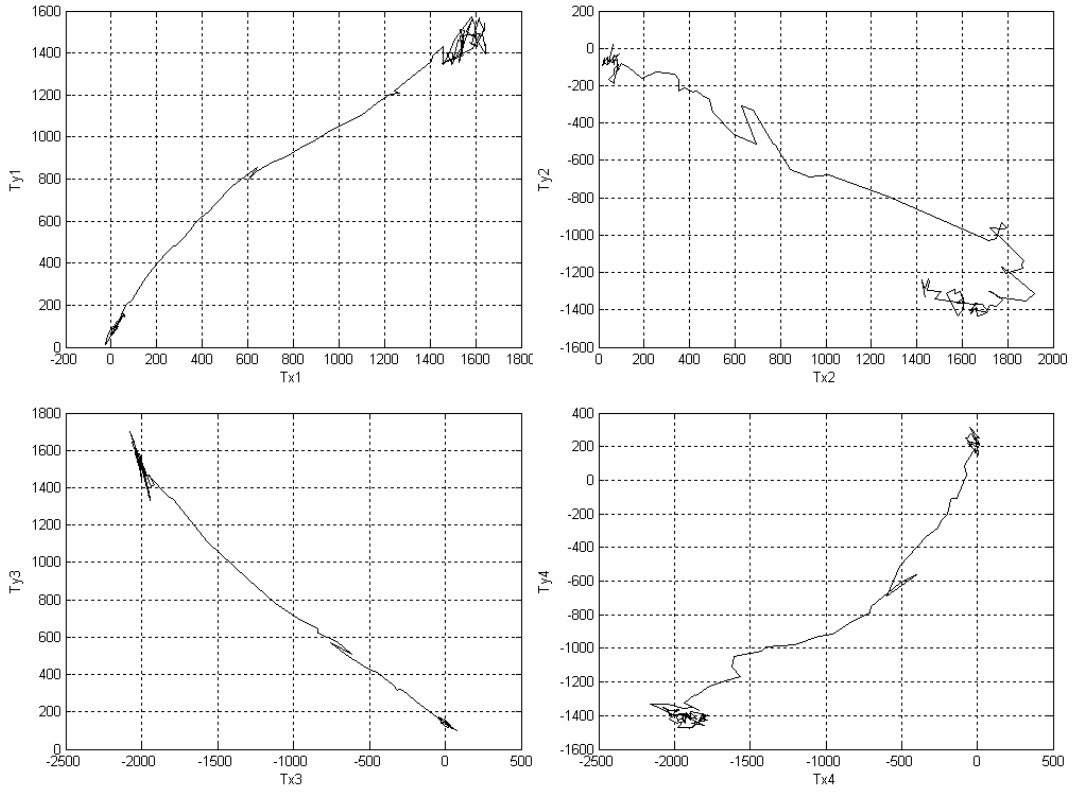

Figure 7.4.3: The evolution of the four Tx and Ty during the twisting force (Tx against Ty)

The torque exerted on the sensor by external forces about the surface normal can be calculated based on the four T_x, T_y pairs of the tactile sensor unit with Equation 6.1.

$$T = R\left(\sqrt{T_{x1}^2 + T_{y1}^2} + \sqrt{T_{x2}^2 + T_{y2}^2} + \sqrt{T_{x3}^2 + T_{y3}^2} + \sqrt{T_{x4}^2 + T_{y4}^2}\right) \quad (6.1)$$

Where T is the torque, R- torque arm, T_{xi} and T_{yi} respective share force components.

7.5. Rotation around the OX axe

In this case the positive direction is the Clockwise from the arm perspective. Both the Ty and Sn components are active during this event, Tx will remain constant. The obvious result of this rotation is that on the right finger's two upper taxel the Sn component will grow and the lower two will decrease. On contrary, the left finger's two lower taxel the Sn component will increase and the upper two will decrease. Due to the fact that the distance between the taxels is much smaller than the thickness of the grasped object (d <<l, Figure 7.5) it is better to analyze the changes of the Ty pressure field.

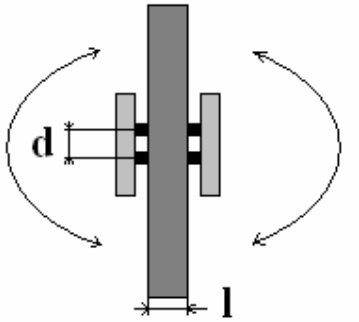

Figure 7.5 Rotation around the OX axe, the distance between the taxels is much smaller than the thickness of the grasped object (d <<l), (front view of the hand)

During the rotation in the positive direction the four Ty on the right side will grow in negative direction, meanwhile on the left side the Ty components will grow in positive direction.

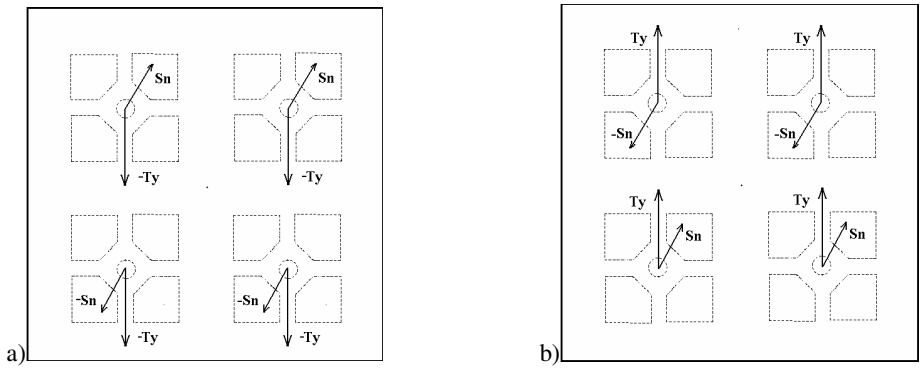

Figure 7.5.1 Direction of the forces acting during the rotation around the OX axe in positive direction: a) Right finger, b) Left finger

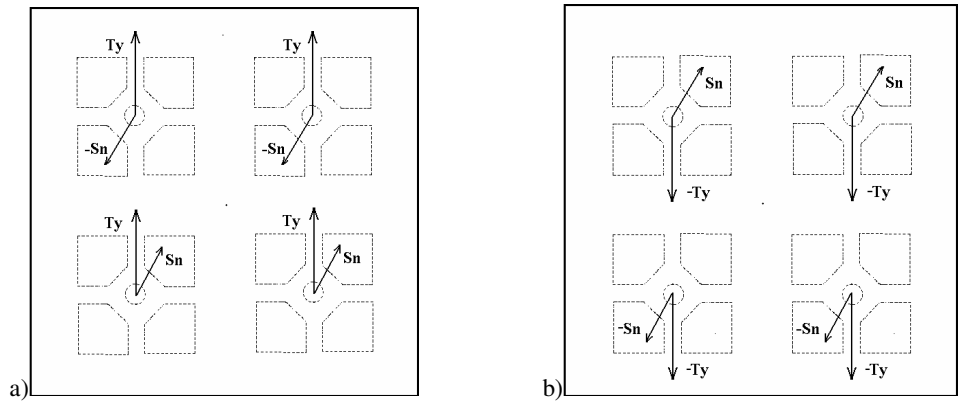

Figure 7.5.2 Direction of the forces acting during the rotation around the OX axe in negative direction a) Right finger, b) Left finger

7.6. Rotation around the OY axe

This case is similar to the precedent. In this case the positive direction is rotating the object to right. Both the Tx and Sn components are active during this event, Ty will remain constant. On the right finger's two outer taxel the Sn component will grow and on the inner two will decrease. On contrary, on the left finger's two inner taxel the Sn component will increase and on the outer two will decrease. The changes in the Ty pressure field will be more pre-eminent in this case as well.

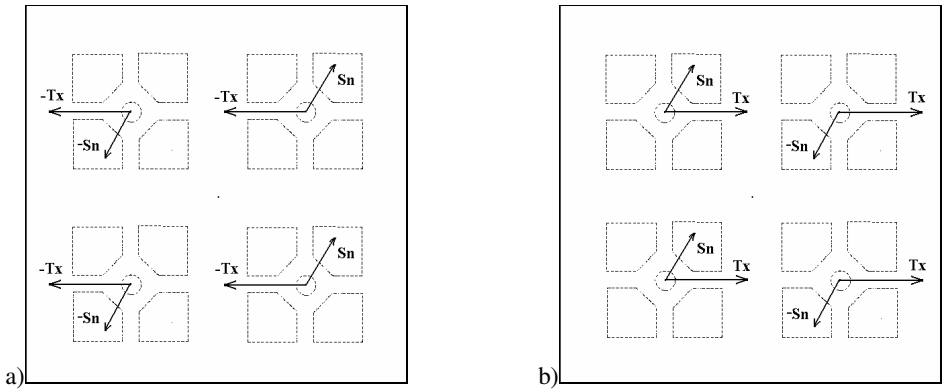

Figure 7.6.1 Direction of the forces acting during the rotation around the OY axe in positive direction a) Right finger, b) Left finger

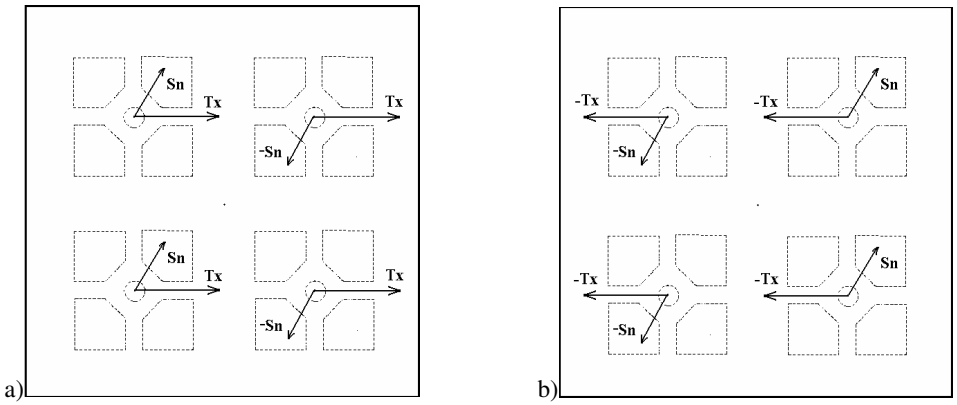

Figure 7.6.2 Direction of the forces acting during the rotation around the OY axe in negative direction a) Right finger, b) Left finger

By combining these basic events it is possible to detect compound events, i.e. the shift is along an arbitrary direction, or a shift and a twist is presented. The complex spatio-temporal tactile events can be decomposed in a linear combination of the previously presented six basic events.

7.7. Spatio-temporal tactile event detection with CNN-UM

Usually, the contacting surfaces are of large sizes; hence in this case a higher number of sensory units are required. This large pressure field has to be evaluated rapidly, and irregularities must be detected and classified real-time.

The following analogical algorithm detects and classifies the forces acting on large surfaces of the contacting objects. The algorithm recognizes twelve different basic event classes, and a combination of these classes. The first six classes are the twisting motion around the three orthogonal axes OX, OY, OZ. On each axe there are two possible directions (clock-wise and counter clock-wise twisting), hence the three by two cases. The other main class is slipping motion, which can be classified in six subclasses, corresponding to the three axes, again each with two possible directions. The overall pressure on surface can be decomposed in three separated pressure maps (Sn, Tx, and Ty), in correspondence to the three Cartesian directions. Each sensing unit is represented by four pixels. A 64*64 image can represent 32*32 sensing unit, each with 2*2 taxels. On the Sn, Tx and Ty pressure map the gray-level indicates that there is no shear stress in that region, the white indicates a negative (direction), the black a positive force. For each typical event a different set of patches appears on the Sn/Tx/Ty pressure fields, see

Figure 7.7.1. In order to identify these patches, I built a custom matching template library, containing a matching template for each event (typical pattern). The flowchart of the algorithm is presented in Figure 7.7.2.

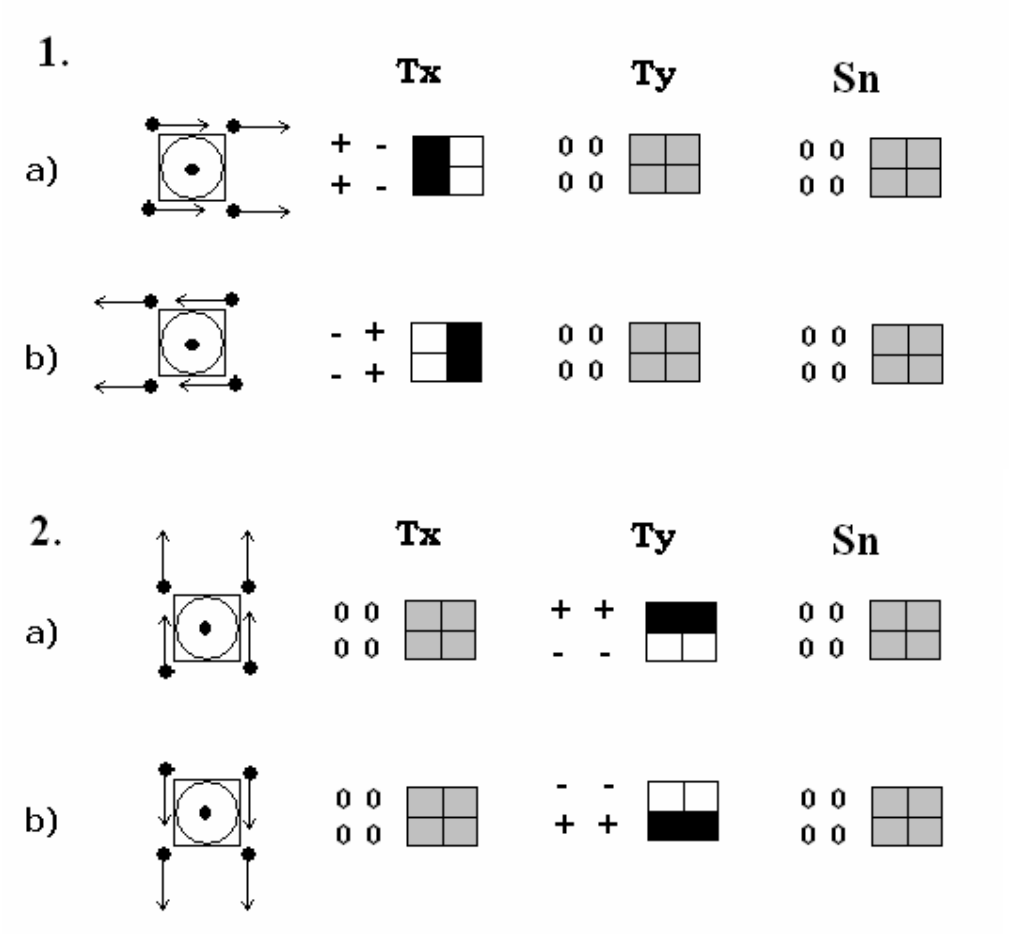

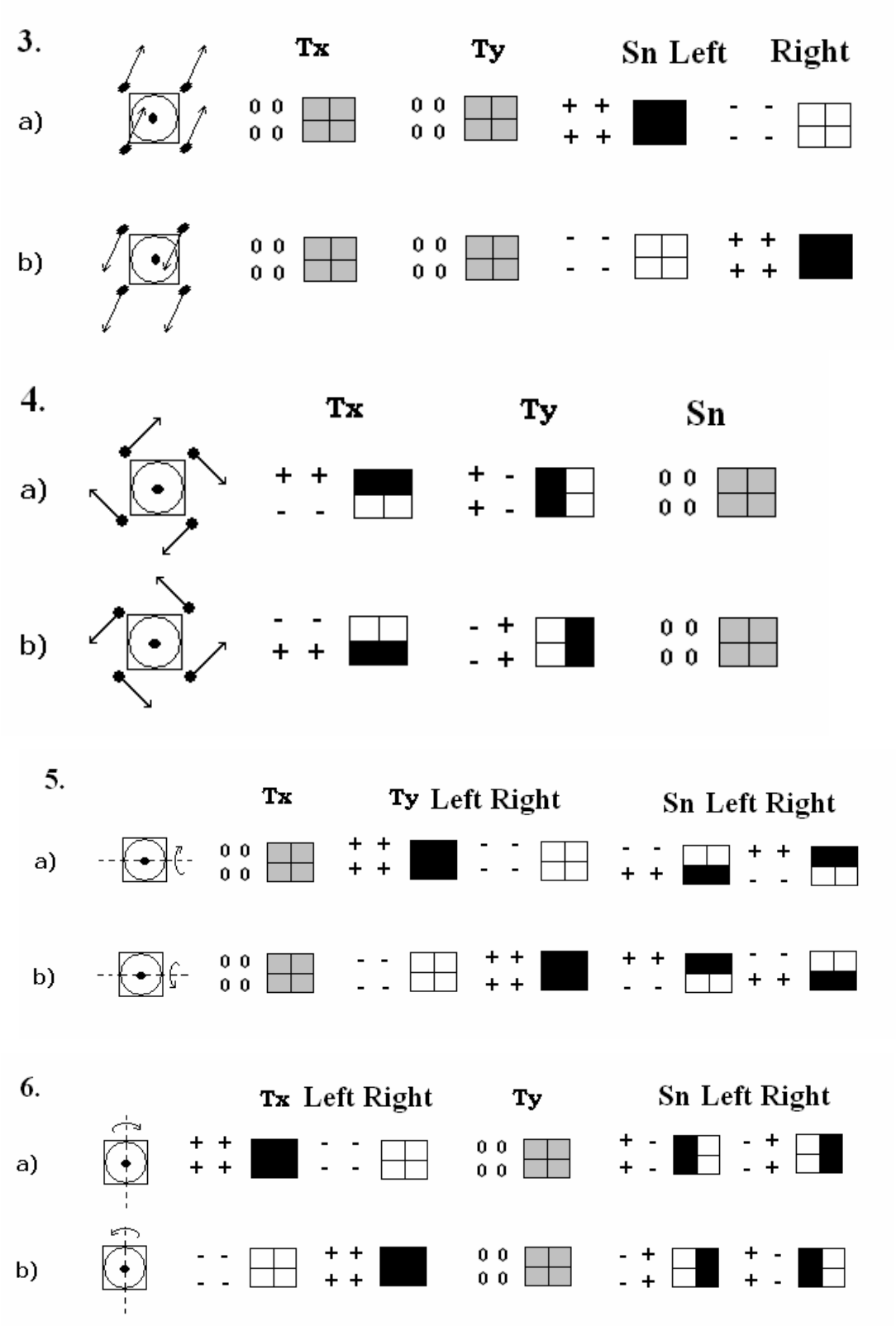

Figure 7.7.1: Shiftt: 1)OX direction, 2) OY direction, 3) OX direction,

4)Rotation around OZ axe, 5)OX axe, 6)OY axe

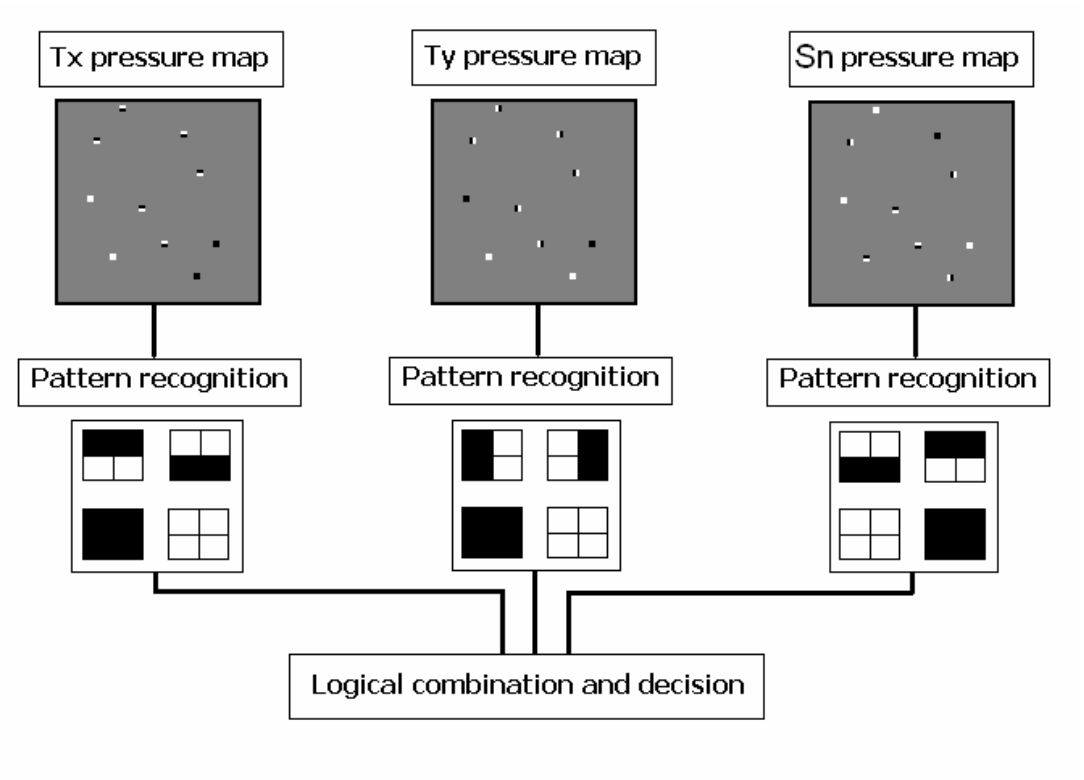

Figure 7.7.2: Detecting and recognizing typical events

8. Conclusions

In this disertation, a bio-inspired, proactive-adaptive tactile system and analogical algorithms were presented. The sensing, processing, actuating systems are strongly coupled, and they work together in order to realize an intelligent, closed-loop control of the autonomous robotic arm. I propose an efficient and fast method to detect and identify the slipping and twisting motion of the touching objects. This kind of action cannot be detected with sensors sensing only the normal (perpendicular) component of the forces acting between the surfaces. In this experimental setup the signal processing unit is a 64*64 CNN-UM analog VLSI chip; the sensing elements are Si-based tactile sensors with 500x500 µm2 taxel size. The size of the array is 2*2 taxels. Each taxel is of four piezorezisitive elements. The sensing elements are mounted on a two-fingered robot hand. Multiple 2*2 sensor elements are connected to the system. The actuator is controlled in closed loop. An integrated sensing-processing-actuating system has been developed. The analogic algorithm detects the typical events.

The motivation behind our work is the perception of the importance of comprehending and knowing the rising forces between contacting surfaces. In different areas of science (in geology for earthquake prediction, in robotics, automation etc.) and industry (motor-car-, aeronautical-, construction industry), it is essential to be able to read and process the above 3D pressure fields.

As a practical example, a method for detecting the optimal grasping force has been presented. The method has proved to be robust in practice. The maximum readout speed is 10 ms for the 32 channels, this means 100 frames/sec for the two 2*2 arrays. The running time of the analogic algorithm is 7-8 ms.

In the second part, a method to detect and identify the slipping and twisting forces acting on the contacting surfaces of large objects is presented. The overall pressure map is decomposed in three orthogonal pressure maps, all of them being processed by the topographic processing unit.

The matching templates used to detect the tactile events are presented in Appendix A

Chapter Three

SURFACE QUALITY CONTROL SYSTEM

1. Introduction

Biologically motivated automated quality control system in industrial fields: optical and tactile information processing in a way that the two modalities complement each other.

Humans use multiple sources of sensory information to estimate environmental properties. For example, the eyes and hands both provide relevant information about an object's shape. The eyes estimate shape using binocular disparity, perspective projection, etc. The hands supply haptic shape information by means of tactile and proprioceptive cues. Combining information across cues can improve estimation of object properties but may come at a cost: the loss of single-cue information. Single-cue information is lost when cues from within the same sensory modality (disparity and texture gradients in vision) are combined, but not when different modalities (vision and haptics) are combined.

Sensory estimates of an environmental property can be represented by $\hat{S}_c = f_i(S)f$ where S is the physical property being estimated, f is the operation the nervous system performs to derive the estimate, and $\hat{S}$ is the perceptual estimate. The subscripts refer to different sensory modalities (e.g., haptics and vision) or different cues within a modality (e.g., disparity and texture cues within vision). Sensory estimates are subjects to two types of error: random measurement error and bias. Thus, estimates of the same object property from different cues usually differ. To reconcile the discrepancy, the nervous system must either combine estimates or choose one, thereby ignoring the other cues. Assuming that each single-cue estimate is unbiased but corrupted by independent Gaussian noise, the statistically optimal strategy for cue combination is a weighted average [157, 158]

$$\hat{S}_c = \sum_i w_i \hat{S}_i S \qquad (14.1)$$

where:

$$w_i = \frac{1/\sigma_i^2}{\sum_j 1/\sigma_j^2}$$

w_i is the weight given to the *i*th single-cue estimate, and σ_i^2 is that estimate's variance. Combining estimates by this maximum –likelihood estimation (MLE) rule yields the least variable estimate of S and thus more precise estimates of objects properties [159].

To benefit from MLE (in the sense of reducing uncertainty), different cues to the same object property must be well correlated across objects. For example, if an object's size increases, visual and haptic signals both generally indicate the increase, so an organism would obtain the benefit of more precise estimates by using MLE. There is, however, a potential cost: Consider the situation, in which there are two cues, $\hat{S}_1$ and $\hat{S}_2$. In this case the MLE is

$$\hat{S}_c = w_1\hat{S}_1 + w_2\hat{S}_2 \qquad (14.2)$$

There are combinations of $\hat{S}_1$ and $\hat{S}_2$, producible in the laboratory, for which $\hat{S}_c$ is, on average, constant. If $S_1 = S + \Delta S_1$ and $S_2 = S + \Delta S_2$, then $\hat{S}_c$ is constant, on average, for values of ΔS_1 and ΔS_2 satisfying:

$$\Delta S_2 = -\frac{w_1}{w_2}\Delta S_1 \qquad (14.3)$$

If the combined estimate (eq.1.2) were the only one available, the nervous system would be unable to discriminate the various stimulus combinations satisfying Eq. 1.3. Such physically distinct, but perceptually indiscriminable, stimuli would be metamers [Metamers are composite stimuli that cannot be discriminated even though their constituents can be. The classic example is the inability to discriminate a yellow light consisting of one wavelength from another yellow light consisting of red added to green].

If, in contrast, the nervous system retained the single-cue estimates, $\hat{S}_1$ and $\hat{S}_2$, the various combinations satisfying Eq. 1.3 would be discriminable from one another. An inability to discriminate stimulus combinations satisfying Eq. 3 would have little practical consequence because such combinations rarely occur in the natural environment. By generating such combinations in the laboratory, it is possible to observe loss in discrimination capability predicted by MLE, which means that the nervous system combines information from different cues to form one estimate of the object property in question.

2. Textile quality inspection unit

Garment production can be divided into two distinct phases: manufacture of the textile fabric, followed by garment assembly. The two phases are often performed in different locations and by different organizations. Each phase in turn is made up of sub-phases, between which there are opportunities for inspection. My interest is in the problem of product inspection after fabric manufacturing, before final assembly.

Typically fabric is produced by looms in two-meter wide rolls at a rate of about 10mm per second. Although it might seem that product inspection could occur concurrently, the fabric is first packed into rolls and later unrolled for inspection. Reasons for this presumably include the slow speed of production, which is not sufficient to keep an inspector occupied, and the relatively hostile working environment.

This work is concerned with the replacement of manual inspection by an automatic procedure.

Two major obstacles to machine inspection of textile fabrics are the difficulty of characterizing defects, and the high data rate.

In the manual inspection process, the flaws are marked using chalk or metallic tape. At garment assembly, cutting into shapes is done on batches of approximately fifty layers. This layering is manually supervised, and the operators attempt to handle flawed regions via cutting and excising, or overlapping. In the context of automated manufacturing, there is a clearly significant scope for introducing intelligence to these phases: if location of automatically detected flaws can be supplied to an automatic cutter, an optimal cutting plan may follow, i.e. flaws avoided with minimal wastage.

For automated real-time flaw detection, where computation time for classification-detection step needs to be minimal, it is desirable to have as few template operations as possible, while still accurately classifying defective texture. On-line textile inspection of lengths 0.90–2.10 m wide fabric can occur at speeds between 1 and 60 m/min, and therefore the amount of image data which must be classified as defective or non-defective is large.

It is important to note that this application represents the first implementation of the fused optical-tactile filter to the problem of real-time automatic flaw detection in textile fabrics. Our method is very fast, requiring only a small number of CNN templates in order to detect a large variety of textile flaw types (mainly structural) in both

homogeneous and complex jacquard textiles. Further increase in the processing speed can be achieved through increased tactile array size and direct, a parallel link between the sensor arrays and processing unit (CNN-UM). The algorithm effectively reduces undesirable noise, which may be caused by the variation in textile designs or vibrations of the inspection system. This increased robustness to noise is crucial for the real-time implementation of the system. The constraints used in the design of our CNN algorithm help to eliminate the issues of the fabric stretch or rotation.

By not having to consider the colors on the textiles, only the surface geometry, our tactile CNN algorithm offers major practical advantages over commonly used pixel based visual textile inspection techniques.

Faults in textiles have traditionally been detected by vision unit inspection [160,161]. These systems are reliable, though their accuracy is not high [162]. For the characterization of the defects tactile inspection, information gathering about the physical aspects of the textile is adequate. Therefore, industrial vision units fused with tactile units are of strategic interest for the textile industry as they provide a base for a system achieving a high degree of accuracy in textile inspection.

This chapter describes the software core of a system designed for fabric inspection based on combining some simple optical and tactile image-processing operations, as well as the efficiency of the software core in detecting the usual textile defects. The prerequisites of the over all system are then discussed analytically, as well as the limitations and the restrictions due to the nature of the problem. The software algorithm and the evaluation of the first results are also presented in detail.

The design of the presented automated quality control system is guided by criteria that human experts use to inspect the surface of the fabric.

This system consists of two major parts: vision and the tactile inspection unit. In this dissertation I present the tactile fault detector and recognition system, since the visual unit does not constitute part of this dissertation. We will present snapshots recorded on the pressure field of tactile actions investigating the surface of a textile and preprocess by a CNN-UM.

In Section 3 the experimental system is described. The analysis of the tactile fault detecting process is given in Section 4, and based on the experiments, some concluding remarks are given in Section 5.

2.1. Experimental System for Detecting Faults on Textiles

On-line textile inspection of lengths 0.90–2.10 m wide fabric can occur at speeds between 1 and 60 m/min. This means that the textile rolls at a known and adjustable speed, usually about 600mm per second. The inspection system has two cooperating units. The visual unit searches the whole surface of the fabric for patches or blooms. When the visual unit finds some unusual or possible defective places it provides the coordinates of the flaws to the tactile inspection unit. The tactile unit explores the areas only indicated by the vision unit, this way the time needed for mechanical adjustments of the sensors are shortened. The main parts of the system are presented in Figure 2.1.

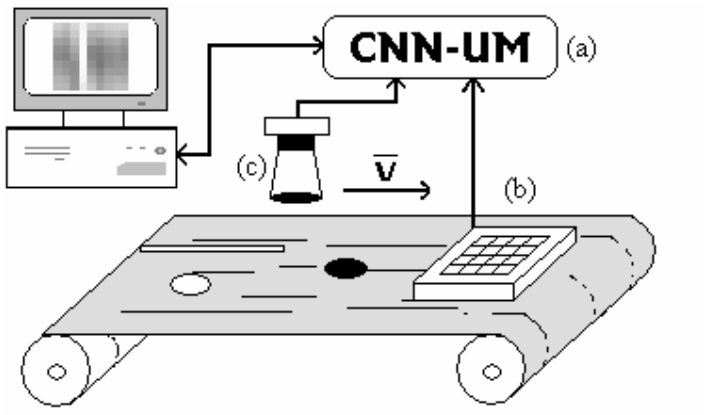

Figure 2.1: The main parts of the system: (a)AceBox 4K, (b)Tactilus®,(c) CCD camera

The analogic algorithm runs on the CNN-UM platform. The main data processing unit is the AceBox. The pressure field sensed by the tactile array is converted in to grayscale images. The scaling of the grayscale image is as follows: in those regions where the pressure is zero, which means that the surface of the tactile sensor is untouched, the image is white. Where the pressure on the sensors is the maximum they can sense, the pixels are black. Between the lowest pressure value (white) and maximum pressure value (black), the grayscale values era linearly distributed. This grayscale image-flow represents the spatio-temporal behavior of the pressure field. Converting the pressure field into grayscale image flow it is possible to process it with CNN-UM, a parallel processing architecture, designed for image processing.

Due to the system's being designed for real-time operation, we need a fast response from the processing unit, which is well accomplished by the CNN-UM. There are more reasons for this, the most important ones are:

1) the locally connected, parallel processing architecture

2) the parallel optical input of the chip.

An analogic algorithm may be especially useful when large amount of images (frames/sec) have to be processed.

For the tactile sensory array the Tactilus® tactile system is used [163], available commercially.

The PC is only used for display the events and it makes the connection between the sensor part and processing unit.

2.2. Pressure sensing through Tactilus®

Tactilus® is an electronic tactile force and pressure-indicating sensor, connected to a PC via a USB port. The reason why we use capacitor-based sensors is that they are more robust and resistant to changes in operating temperature than the two other, most common approaches, resistor-based and piezoelectric pressure sensors. In surface quality control applications it is enough to sense the normal pressure on the inspected surface, the shear forces doesn't contribute to the categorization of holes and bumps. The capacitive sensors are of linear responses, and low hysteresis. The design of the capacitive sensor array is robust and the performance is less likely to degrade over time.

Tactilus® allows precisely monitoring how force is dispersed between any two contacting or mating surfaces in real-time while the event occurs. The system includes a 50mm x 50mm palm sensor with 2.5 mm spatial resolution (21x21 tuxels) and five finger sensors, 13mm x 13mm each, 1.5 mm spatial resolution (9x9 tuxels). One tuxel is equal to one sensor point in a sensor array. The query rate of this system is up to 60,000 sensor-points/sec. The optimal range of pressure for sensor pads is 0-1 atm, accuracy $\pm 10\%$.
In order to protect the sensors, and for a better friction between the inspected surface and sensory array the tactile inspection unit is covered by a special elastic cover.

2.3. Processing the pressure fields with Aladdin Pro System

The Aladdin Professional system is a high-speed, industrial or laboratory application environment of Cellular Visual Microprocessors. The ACE16k chips and the ACE4k chips are supported as well. It is designed for developing and running analogic algorithms. Due to the extraordinarily high speed of the ACExK visual microprocessors the analogic algorithms can reach up to several thousands frames/second in some applications.

Algorithms can be coded in script language called AMC. The generated binary code (ABC) is executed on the Aladdin Professional compatible hardware. Optionally the system can be programmed in C/C++ as well as using Code Composer Studio by Texas Instruments.

Images to be processed may come from the optical input of the ACE16K chip or from the PC side (hard drives, cameras, etc.).

2.4. The Hardware

All hardware versions are composed of two main components: a DSP (digital signal processor) board and a platform containing one or two ACE chips. The DSP board together with the platform can execute the binary ABC code. The ACE chip can be considered as a co-processor of the DSP which significantly speeds up most of the image-processing steps. The DSP card and the platform are connected to each other via an internal bus (the so called platform bus).

The ACE BOX system contains an SPM6020 DSP board and either an ACE4K based platform or an ACE16K based platform. The ACE BOX follows the PC104+ standard. A PC104+ is an industrial PC standard. Its specialty is its rugged, robust quality, which can be used even in noisy industrial environment. A PC104+ machine consists of the commonly used hardware components, such as PCI motherboard with Pentium class CPU, display adapter, network module, frame grabber, etc.

The ACE BOX system can be also hosted in a desktop PC. The ACE BOX can be plugged into a normal PCI slot by using the PCIADA1 adapter card.

2.5. The Software

The Aladdin Professional software runs under Microsoft Windows NT 4.x, Microsoft Windows 2000 or Microsoft Windows XP operating systems. There are two commonly used software modules:

- CNNedit is an integrated development environment for the AMC language.

CNNedit contains a syntax coloring editor and an interactive semantic helper.

CNNedit calls the AMC compiler, and also passes the compiled binary executable (ABC) to CNNrun.

- CNNrun is the graphical environment for running analogic algorithms.

CNNrun can display images and text messages in different windows on a multi-document interface.

2.6. The core algorithm

The surface quality control system has two major units: the visual unit, and the tactile unit. The first unit inspects the whole surface of the fabric, detects the regions where there is a possible error on the surface. The tactile inspecting unit searches for errors only on regions delimited by the visual inspecting unit.

Figure 2.2: The visual input: (a) disruption, (b) hole

The algorithm classifies the errors in three major kinds of fault classes: bumps, holes and split or disruption on the textile. There are two other cases: the first is when the error is only in colors of the surface, which means that there is a colored patch on the surface (e.g. oil, ink).

The flowchart of the tactile inspecting unit is given in Figure 2.3.

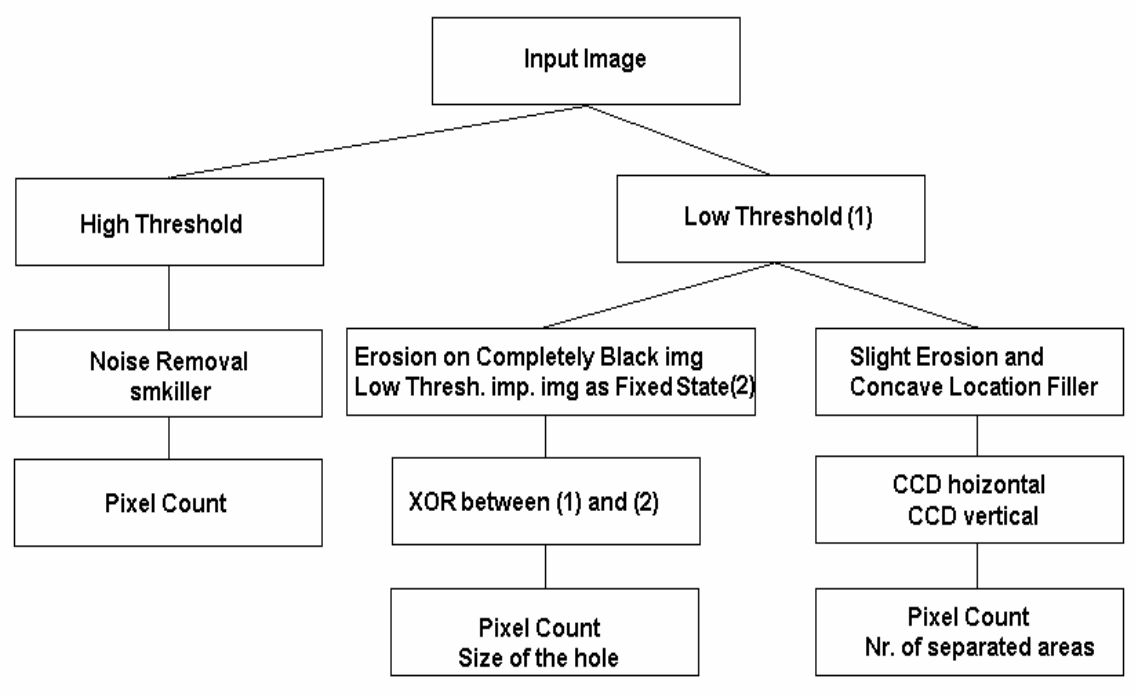

Figure 2.3: The flowchart of the algorithm

As the first step is with a less sensitive, high threshold template, we can extract the regions where the pressure is above the usual rate. In the usual-normal case it is possible to have high rate pressure. These high pressure points manifests on small, randomly occurring areas only. High pressure points are due to the noise and irregularities in the textile. If there is a compact high-pressure area exceeding the usual, it clearly shows that there is a bump on the surface (Figure 2.4).

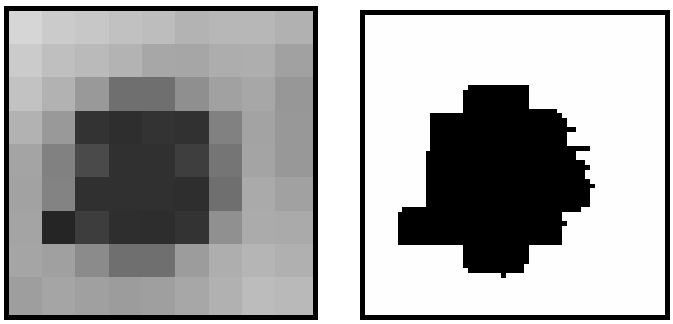

Figure 2.4: Bump on the surface

In order to detect holes and splits, we need a sensitive, low threshold, since on these regions the pressure is lower than the average. In these cases the black regions are the normal perfect points and the white regions are the points where the contact between the

two surfaces (sensor array and textile) is not firm. This could occur due to the fact that the mechanism of fitting of the sensor array and the textile is not proper. Usually on the sides of the array the pressure is lower than in the middle. The analogic algorithm should consider this as well. The significant case is when these low-pressure points produce connected large areas on the whole surface of the sensory array.

In this case the algorithm classifies the errors in two major fault classes: hole (Figure 2.5) and fiber break (Figure 2.6).

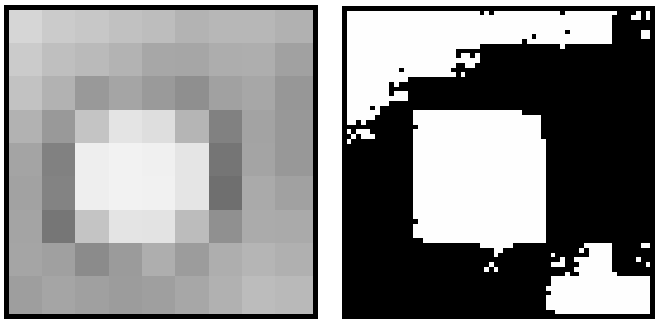

Figure 2.5: (a) The original hole, (b) threshold

Actually we want to find out if there is a hole in the middle of the pressure field. The analogic algorithm searches for places where the low pressure regions are surrounded by higher pressure regions. On the thresholded image (Figure 2.5.b.) the white patch in the middle is due to a hole and the white regions in the upper left and bottom right corner are due to the imperfect contact between the sensor array and textile surface.

The next aim is to extract the white patch from the middle. For this the algorithm uses a completely black image as input, and starts to erase from the sides by a propagating erosion template. By using this thresholded image as a fixed state the erosion will propagate only till the outer borders of the black regions on the original thresholded image. The result will be the shape of the pressured area without any hole (Fig 2.6.a). Making an XOR logical operation between the original, thresholded image and the erased black patch, the resulting image will remain only the area corresponding to the hole on the original image (Fig 2.6.b).

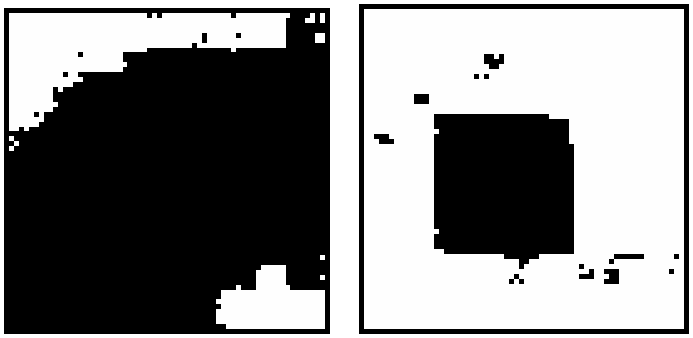

Figure 2.6: (a) contour, (b) the hole

The reason we need this algorithm, instead of simply inverting the input image, is that due to irregularities, we cannot apply a uniform pressure on the whole sensory array, especially at the borders. By counting the black pixels on the output image, we can tell the size of the hole.

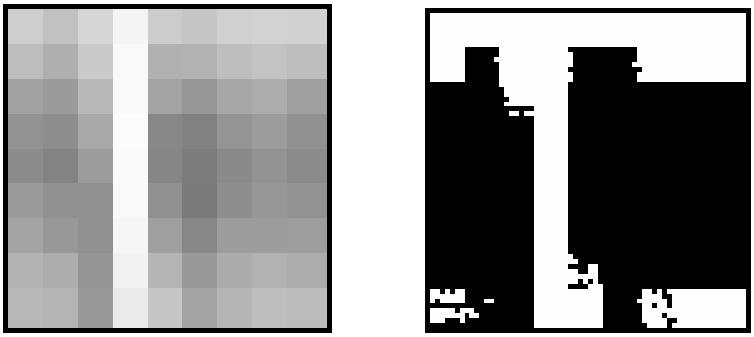

Figure 2.7: Split (a) The original tactile image, (b) threshold

The next most often occurring error is the textile break. If there is a disruption on the textile (Fig. 2.7.a), usually on the input pressure field a narrow, long undressed stripe appears. After applying the low threshold template, we get two independent areas, separated by the white stripe (Fig. 2.7.b). The next step is to count the separated areas, and if there is more than one, there must be a fiber break. First the image must be cleaned and the small patches must be removed in order not to be detected as independent areas. By applying erosion and filling the concave locations, the large compact areas will become convex as a result (Fig. 2.8.a).

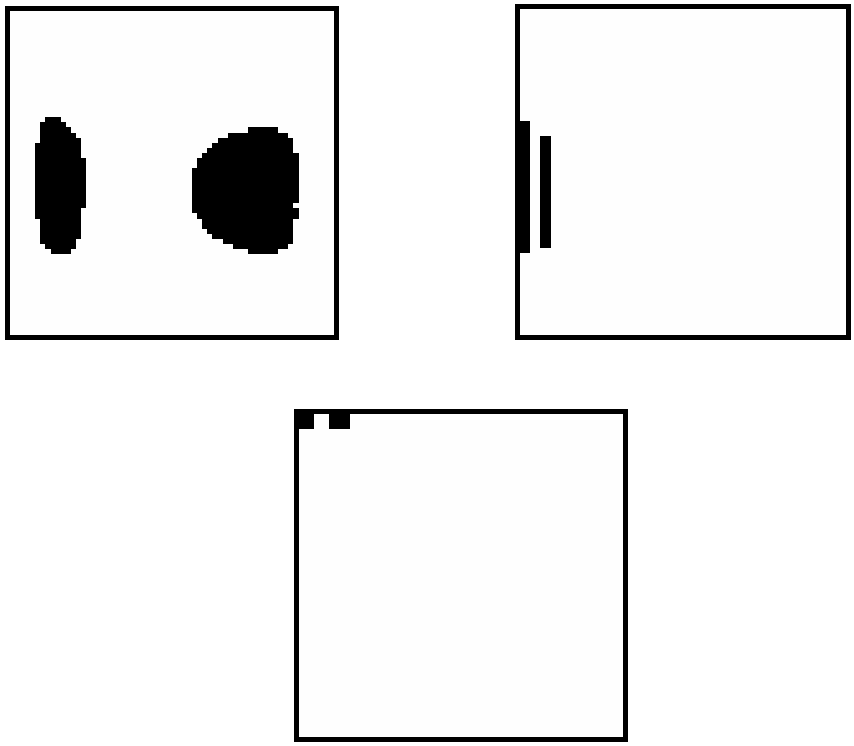

Figure 2.8: (a) erosion and concave location filer, (b) horizontal CCD, (c) vertical CCD

This is important because we can apply the horizontal CCD (Fig. 3.8.b) and the vertical CCD (Fig. 3.8.c) templates. As a result there will be only two pixels on the output image, according to the numbers of the areas.

The UMF diagram of the algorithm is given in Figure 2.9.

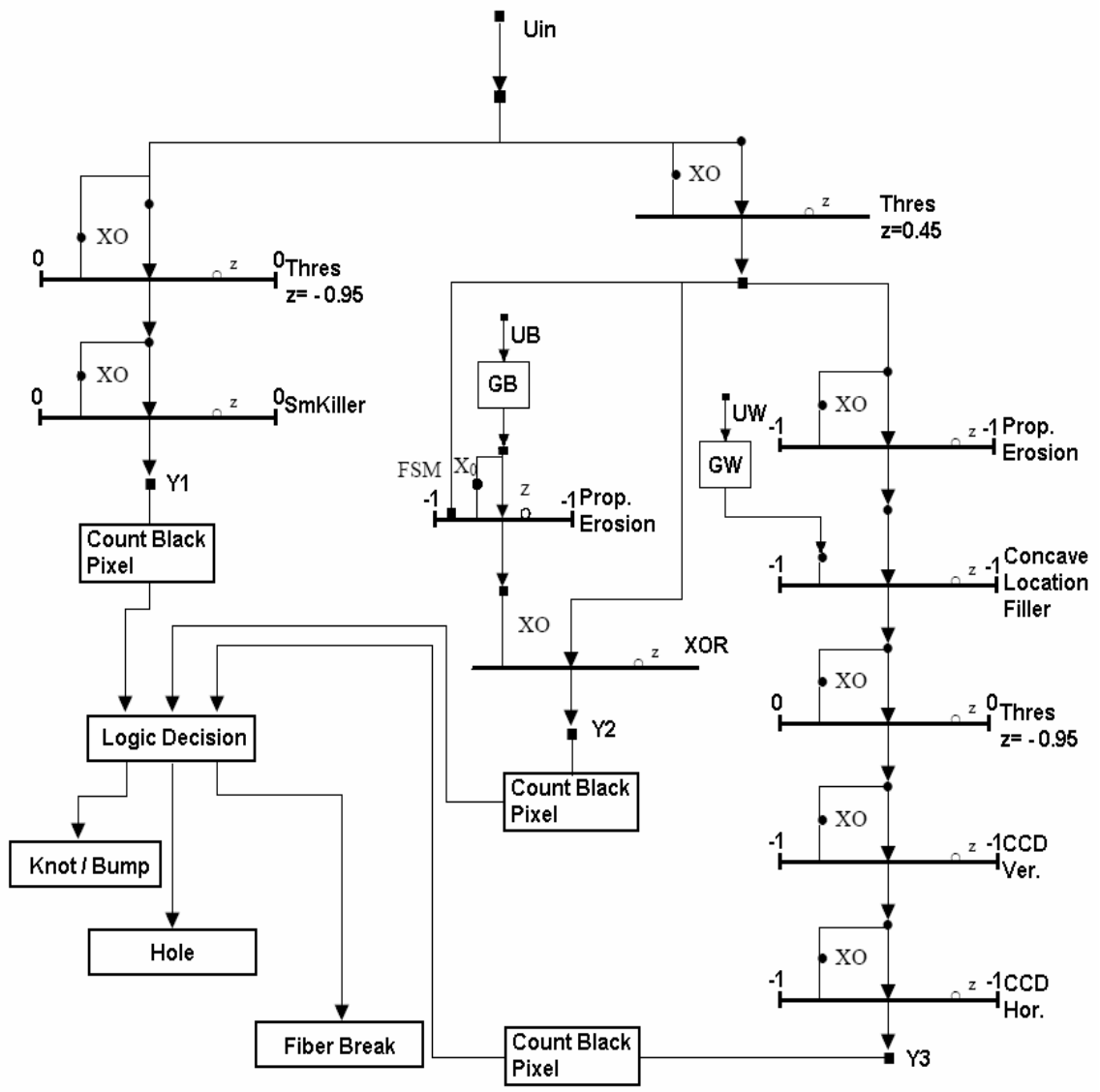

2.9 Figure UMF diagram of the textile quality inspection algorithm

3. Limitations and conclusions

A method for detecting faults on textile has been presented. It is used as a part of a whole inspection system for quality control in textile industry. The method has proved to be robust in practice, working perfectly when applied to textiles with different patterns, complexities and colors. The real-time requirements of the task have been adequately met. The operations carried out here are very fast, of the order of a 10 to 20 processed frames per second. It is important to mention that during a cycle there is only one download and one upload between the ACE4K and DSP. All the morphologic operations are done on the CNN chip. The post processing steps, like pixel counting and logical decision are done on the DSP.

The average running time of the analogic algorithm is 7ms. The largest tactile sensor array is 50mm*50mm. The width of the sensor multiplied by the running time will result the average speed of the fabric: up to 7 m per second. The sensory array inspects the adjoining images sequentially if the width of inspected surface is larger than the width of the sensor array. The average speed is decreasing proportionally with the ratio of the inspected area and sensory array.

Increasing the area of the sensor array the number of the sensor points will increase quadratic, but the running time of the algorithm will increase only linearly.

Chapter Four

SUMMARY

1. Methods of investigation

I realized an experimental system, where the tactile sensing, tactile information processing and intervention are realized in a single hardware software platform.

I used multiple, interdisciplinary knowledge along the research and experiments. For the tactile sensor, I used the literature of the capacitive and piezoresistive sensors and microelectrical and MEMS technology knowledge. The sensors are mounted on a two fingered 5 Dof robotic arm. In order to control the arm I used the direct and inverse kinematical and dynamical transformations (Denavit-Hartenberg reprezentation), methods to calculate the forces, torques.

In the biological modeling I used the results of the neuropsychology.

The CNN templates designed and used in the experiments, as well as the analogical algorithms runs on the software simulators (AladdinPro), and on the developer board containing the VLSI CNN-UM chip (AceBox – ACE4K, BII ACE16K visual CNN microprocessors).

I gave the high level, "CNN type language" description (Universal Machine on Flows, Alpha), and the low level, hardware close AMC language description of the algorithms. During designing the algorithms I paid attention to compatibility issues between different hardware and software platforms. An important aspect is the use of the locally connected linear templates in order to be able to run the algorithms on the current CNN-UM VLSI chips.

The grasping algorithms are validated in simulations and experiments, on internationally accepted tactile events.

2. New scientific results

I. Thesis: Developing a new analogical CNN algorithm class to recognize typical tactile events

I developed a proactive – adaptive, real-time robotic arm control system.

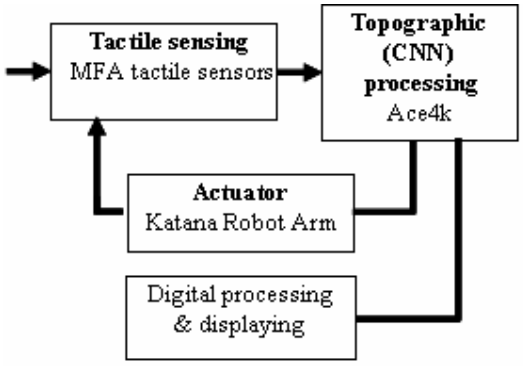

Figure 4.1 The Experimental System

I propose a new analogical algorithm class. This class gives information on the parameters of an unknown object, its surface properties, and recognizes the typical events happened to the investigated object. The information processed by this algorithm class is provided by tactile sensors. The tactile events are recognized and classified (tri-dimensional pulling and pushing, rotating, sliding, slipping). The characteristic aspects of the algorithms are the spatial and temporal precision, and the reaction time.

I.1. Gentle Grasping

I specified a proactive-adaptive algorithm, which enables a robotic arm to grasp and hold unknown objects. The algorithm consists of two parts:

1) Information gathering phase. Exploration of the surface of the object (static and kinetic friction coefficient). This is the proactive part.

2) Holding the object. Knowing the friction coefficients, the algorithm adaptively controls the robotic arm in order to maintain the smallest grasping force on the object. The system follows the forces acting between the grasper and the object real-time.

I.2. Sensing, Detecting and Analyzing Active Forces Between Contacting Surfaces

I specified a new analogical algorithm class, which recognizes and classifies the 3D forces and torques acting on the fingertip of a two fingered robotic hand. This algorithm gives a fast response to the perturbing event, in similar way to the reflex mechanism observable in nature. I gave a template class which recognizes the pulling and pushing forces along the *oxoyoz* coordinates, and the twisting torques around r, φ, θ polar coordinates. The overall pressure map is decomposed in three orthogonal pressure maps, all of them being processed by the topographic processing unit.

If the size of the sensor array is smaller than the size of the CNN-UM chip, the running-time of the algorithm is independent from the size of the sensor array. Otherwise the algorithm uses windowing, processing the signal sequentially.

II. Thesis: Biologically motivated automated quality control system in industrial fields: optical and tactile information processing in a way that the two modalities complement each other

I developed a method which investigates the surface quality of the given object. The visual information points out the suspected regions. With the fused tactile and visual information the system is able to gather more valuable and more precise information than only using these modalities separately. The running-time of the analogical algorithm is direct proportional with the linear size of the inspected surface. The algorithm detects and classifies breaks, holes and bumps on the surface.

3. Examples of application

3.1 Forces and torques on the fingertips

In this dissertation, a bio-inspired, proactive-adaptive tactile system and analogical algorithms were presented. The sensing, processing, actuating systems are strongly coupled, and they work together in order to realize an intelligent, closed-loop control of the autonomous robotic arm. I propose an efficient and fast method to detect and identify the slipping and twisting motion of the touching objects. This kind of action cannot be detected with sensors sensing only the normal (perpendicular) component of the forces acting between the surfaces. In this experimental setup the signal processing unit is a 64*64 CNN-UM analog VLSI chip; the sensing elements are Si-based tactile sensors with 500x500 μm2 taxel size. The size of the array is 2*2 taxels. Each taxel is of four piezorezisitive elements. The sensing elements are mounted on a two-fingered robot hand. Multiple 2*2 sensor elements are connected to the system. The actuator is controlled in closed loop. An integrated sensing-processing-actuating system has been developed. The analogic algorithm detects the typical events.

My work was motivated by the perception how important it is to comprehend and know the rising forces between contacting surfaces. In different areas of science (in geology for earthquake prediction, in robotics, automation etc.) and industry (motor-car-, aeronautical-, construction industry), it is essential to be able to read and process the above 3D pressure fields.

As a practical example, a method to detect the optimal grasping force has been presented. The method has proved to be robust in practice. The maximum readout speed is 10 ms for the 32 channels, this means 100 frames/sec for the two 2*2 arrays. The running time of the analogic algorithm is 7-8 ms.

A method to detect and identify the slipping and twisting forces acting on the contacting surfaces of large objects is presented as well. The overall pressure map is decomposed in three orthogonal pressure maps, all of them being processed by the topographic processing unit.

3.2 Textile quality control

The main interest is the problem of product inspection after fabric manufacturing, before final assembly.

A method to detect faults on textile has been presented. It is used as a part of a whole inspection system for quality control in textile industry. The method has proved to be robust in practice, working perfectly when applied to textiles with different patterns, complexities and colors. The real-time requirements of the task have been adequately met. The operations carried out here are very fast, of the order of a 10 to 20 processed frames per second. It is important to mention that during a cycle there is only one download and one upload between the ACE4K and DSP. All the morphologic operations are done on the CNN chip. The post processing steps, like pixel counting and logical decision are done on the DSP.

The average running time of the analogic algorithm is 7ms. The largest tactile sensor array is 50mm*50mm. The width of the sensor multiplied by the running time will result the average speed of the fabric: up to 7 m per second. The sensory array inspects the adjoining images sequentially if the width of inspected surface is larger than the width of the sensor array. The average speed is decreasing proportionally with the ratio of the inspected area and sensory array.

Increasing the area of the sensor array the number of the sensor points will increase quadratic, but the running time of the algorithm will increase only linearly.

4. Appendix A - The CNN Computer (a Cellular Wave Computer)

Cellular nonlinear/neural networks (CNNs) are regular, single or multi-layer, parallel processing structures with analog nonlinear dynamic units (cells). The state value of the individual processors is continuous in time and their connectivity is local in space. The program of these networks is completely determined by the pattern of the local interactions, the so-called template. The time-evolution of the analog transient, “driven” by the template operator and the cell dynamics, represents the elementary computation in CNN (results can be defined both in equilibrium or non-equilibrium states of the network). The standard CNN equation contains only first order cells placed on one layer of a regular grid and the interconnection pattern is linear.

A cellular wave computer architecture that includes CNN dynamics as its main instruction is the CNN Universal Machine (CNN-UM). The CNN-UM makes it possible to efficiently combine analog array operations with local logic. Since the reprogramming time is approximately equal to the settling time of a non-propagating analog operation it is capable of executing complex analogic (analog and logic) algorithms. To ensure stored programmability, a global programming unit is added to the array and for an efficient reuse of intermediate results; each computing cell is extended by local memories. In addition to local storage, every cell might be equipped with local sensors and additional circuitry to perform cell-wise analog and logical operations.

Using the CNN-UM we are able to design and run analog and logic CNN wave algorithms. It is known that CNN-UM is universal as a Turing Machine and as a nonlinear operator. Therefore many problems can be solved by this machine. Its structure suggests using it for image processing in numerous applications. Beyond the classical image processing there are a lots of new methods of solving problems based on partial differential equations which need huge computational power. Most of these kind of problems can be transformed into CNN algorithm too.

Another important scope is the biological modeling. The researchers found in early times that CNN can be used for modeling some parts of the human visual system, mainly the outer retina. Recently, a multilayer, multi-channel retina model has been developed. Because of the simple structure of CNN, it is realizable in real hardware. Nowadays implementations run 64×64 Ace4k or 128×128 Ace16k chips.

4.1. Standard CNN Dynamics

The cellular nonlinear network (CNN) is a locally connected, analog processor array which has two or more dimensions. A standard CNN architecture consists of an $M \times N$ rectangular array of cells $C(i, j)$ with Cartesian coordinate $(i, j) i = 1..M, j = 1..N$ (Figure A.1)

The sphere of influence, $S_r(i, j)$, of radius of r of cell $C(i, j)$ is defined to be the set of all neighboring cells satisfying the following property :

$$S_r(i,j) = \left\{ C(k.l) \left| \max_{1 \le k \le M, 1 \le l \le N} \{ |k-i|, |l-j| \} \le r \right. \right\} \qquad (A.1)$$

where r is a positive integer. The structure of an elementary cell can be seen on Figure A.2.

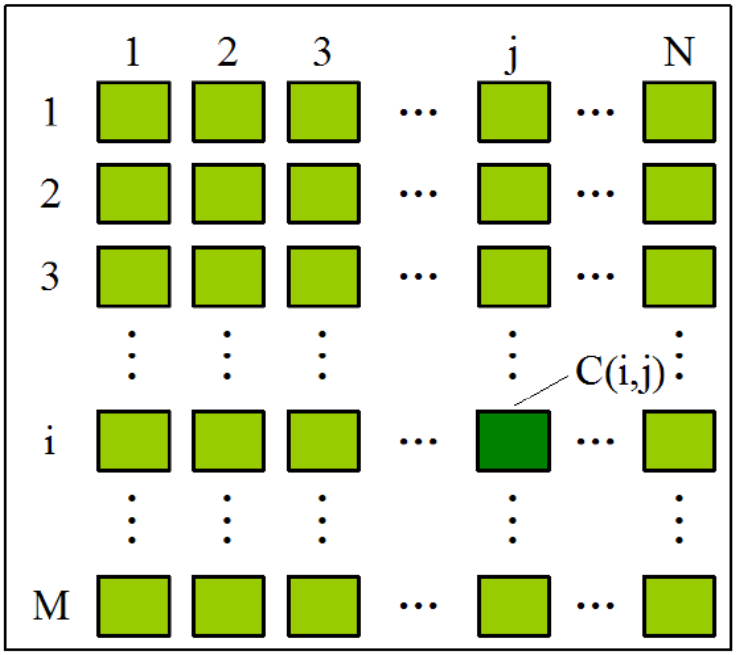

Figure A.1: MxN representation of CNN structure

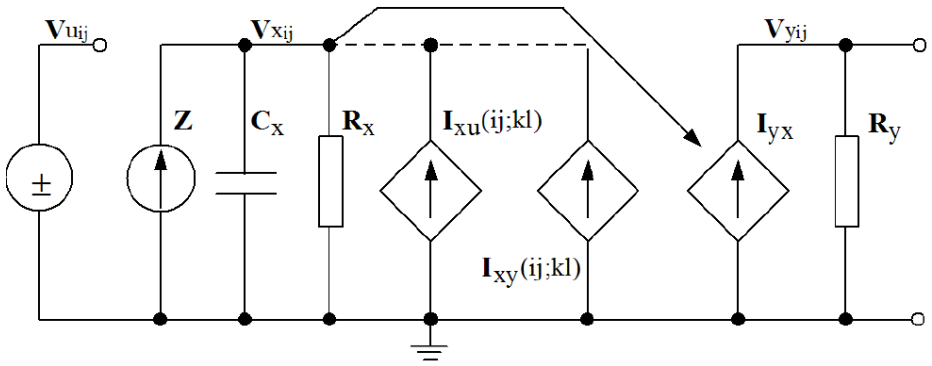

Figure A.2: The build-up of a CNN cell

$$I_{xu}(ij,kl) = B_{ij,kl}v_{u_{kl}}; \quad I_{xy}(ij,kl) = A_{ij,kl}v_{y_{kl}}; \\ I_{yx} = \frac{1}{2R_y}(\left|v_{x_{ij}}+1\right| - \left|v_{x_{ij}}-1\right|) \tag{A.2}$$

4.2. CNN Templates

The state of a cell depends on interconnection weights between the cell and its neighbors. These parameters are expressed in the form of the template:

$$A = \begin{bmatrix} a_{i-1j-1} & a_{i-1j} & a_{i-1j+1} \\ a_{ij-1} & a_{i1j} & a_{ij+1} \\ a_{i+1j-1} & a_{i+1j} & a_{i+1j+1} \end{bmatrix} B = \begin{bmatrix} b_{i-1j-1} & b_{i-1j} & b_{i-1j+1} \\ b_{ij-1} & b_{i1j} & b_{ij+1} \\ b_{i+1j-1} & b_{i+1j} & b_{i+1j+1} \end{bmatrix} z = z_{ij} \tag{A.3}$$

A template has two main parts, a feed-forward and feedback matrixes. These parts are called *A* and *B* templates. The *z* on Equation (A.3) is the offset (bias) term. In the simplest case the template is given by 19 numbers, 9 feedback, 9 feed-forward and one bias terms. This 19 number template is an elementary operation of CNN-UM and codes a complex spatial-temporal dynamics. An analogical algorithm might contain some templates and logical operations. The following differential equation system describes the dynamics of the network:

$$C_x \frac{dv_{x_{ij}}(t)}{dt} = -\frac{1}{R_x} v_{x_{ij}}(t) + \sum_{C(k,l)\in S_r(i,j)} A_{ij;kl} v_{y_{kl}}(t) + \sum_{C(k,l)\in S_r(i,j)} B_{ij;kl} v_{u_{kl}}(t) + z_{ij} \qquad (A.4)$$

$$v_{y_{ij}}(t) = f(v_{x_{ij}}(t)) = 1/2(\left|v_{x_{ij}}(t)+1\right| - \left|v_{x_{ij}}(t)-1\right|),$$

$$i = \overline{1,M}; j = \overline{1,N}$$

The figure of the given function can be seen on Figure A.3. This is called standard non-linearity.

In the case where the values of $A_{ij;kl}$; $B_{ij;kl}$ do not depend on i and j, the template is space invariant. In most cases the value of the offset current does not depends on space $z_{ij} = z$. Because of the regular **2D** shape of the CNN, the value of a cell can be represent by a pixel of a picture. This gray-scale value can be between white (-1) to black (1).

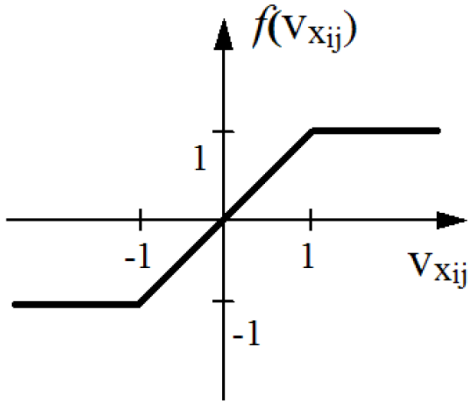

Figure A.3: The output characteristic function of a CNN cell.

Sometimes we use fixed state mask whose values allow or permit the change of the values of their cells. 3D CNN networks can connect like layers and this gives multi-layer CNN networks. Its differential equation is similar to Eq. (A.4):

$$C_{xm} \frac{dv_{x_{mij}}(t)}{dt} = -\frac{1}{R_{xm}} v_{x_{mij}}(t) + \sum_{n=1}^{P} \left(\sum_{C(k,l)\in S_r(i,j)} A_{mn;ij;kl} v_{y_{nkl}}(t) + \sum_{C(k,l)\in S_r(i,j)} B_{mn;ij;kl} v_{u_{nkl}}(t) \right) + z_{mij} \qquad (A.5)$$

where p is the number of layers, m is the current layer, and A_{mn} and B_{mn} give the connection between n and m layers. For the solution of a given example, we have to give the input U, $x(0)$ initial state and the templates with the algorithm.

The result is Y after running the transient. In most cases we can work with predefined templates that can be found in the software library.

4.3. CNN Universal Machine

The CNN Universal Machine (CNN-UM) is based on a CNN (Figure A.4). This is the first programmable analog processor array computer with own language and operation system whose VLSI implementation has same computing power as a supercomputer in image processing applications. The extended universal cells of CNN-UM are controlled by global analogic programming unit (GAPU), which has analog and logic parts: global analog program register, global logic program register, switch configuration register and global analogic control unit. Every cell has analog and logical memory.

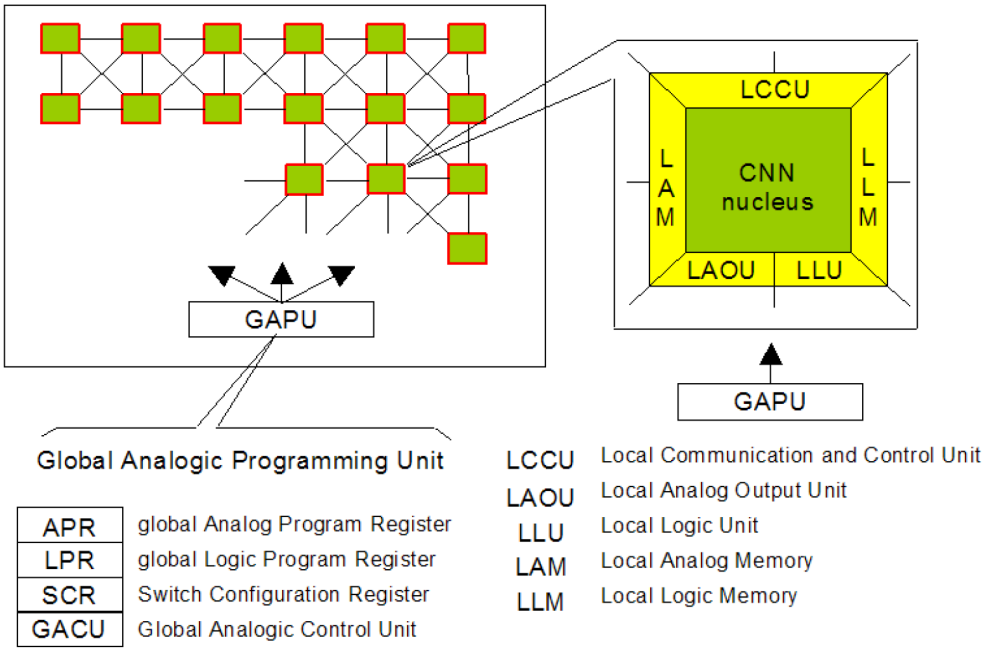

Figure A.4: The architecture of CNN Universal Machine

5. APPENDIX B – Universal Machine on Flows

This appendix introduces a new computational model for exploring the algorithmic and computational complexity of the CNN-UM operating on image flows. The continuous nature of the computations performed on the CNN-UM is captured by a subset of the recently defined Universal Machine on Flows (UMF). The new, purely continuous computational model can imitate the complete CNN-UM processing. Hopefully, using this model, new insights can be gained into the computational capabilities of the CNN-UM and the algorithms developed for the CNN-UM can be more easily described from a computational complexity standpoint.

The first section describes the Continuous Machine on Flows (CMF) model with mathematical precision, specifying its mode of computation, inputs, outputs and other details. Furthermore, constructive algorithm is given, which prove that the CNN-UM can be translated into a CMF.

5.1. The Continuous Machine on Flows

The formal definition of the new computational model provides the basis on which to build the computational complexity analysis in later sections. Let us first start with the definition of a **flow**. Φ is a flow iif:

$\phi(t) \in [-B, B] \in \Re; t \in [0, T] \in \Re$ and differentiable except in countable number of points and $\phi(0) \in \Re$ is a well-defined known value; notation: $<\phi> = T$, i.e. the length of the flow

You can intuitively think of a flow as a continuously changing function in the time interval $t \in [0, T]$. Our proposed computing model operates exclusively on such flows.

The **continuous machine on flows** (CMF) as a mathematical object is given by an 8-tuple,

$CMF(\Phi, A, B, \Gamma, \blacklozenge, {}^{i}\Phi, {}^{o}\Phi, {}^{o}\phi)$, where:

- The $\blacklozenge$ is a special symbol that signals the non-existence of a flow, all functions on $\blacklozenge = \blacklozenge$
- $\Phi = \{\phi_i, i \in [1, I] \in Z\}$ is a set of a countable number of flows defined in a finite time-window. Outside of the time-window: $\phi_i(t) = \blacklozenge$, notation: $|\Phi| = I$ i.e. number of flows
- ${}^{i}\Phi$ is the set of explicit input flows: ${}^{i}\Phi \subset \Phi$. These flows have predefined dynamics in a time-window or as a default: ${}^{i}\Phi(t) = {}^{i}\Phi(0)$, if $t > 0$
- ${}^{o}\Phi$ is the set of result (or output) flows ${}^{o}\Phi \subset \Phi$ and ${}^{o}\phi \notin {}^{o}\Phi$

- ${}^{o}\phi$ is a specially designated single output flow, serving as an indicator showing when the machine has stopped. This is analogous to the acceptance state of a Turing machine.
- $A = \{\alpha_i\}$, $\alpha_i(\phi_k(t))$ is a special function: $\Re \cup \{\blacklozenge\} \rightarrow \Re \cup \{\blacklozenge\}$
  otherwise if $\alpha(\blacklozenge)$ is undefined then $\alpha(\blacklozenge) = \blacklozenge$
- $B = \{\beta_i\}$, β_i is a multi-variable function of ${}^{\gamma\beta}\Phi_i \subseteq \Phi$: $\Re^{|{}^{\gamma\beta}\Phi_i|} \rightarrow [-K, +K] \in \Re$. It is bounded, continuous except in countable number of points.
- $\Gamma = \{\gamma_i\}$, γ_i is a multi-variable function of ${}^{\gamma\beta}\Phi_i \subseteq \Phi$: $\Re^{|{}^{\gamma\beta}\Phi_i|} \rightarrow [-L, +L] \in \Re$. It is bounded, differentiable and not continuous only in countable number of points.
- ${}^{\gamma\beta}\Phi_i$ is the set of input variables in the β_i or γ_i functions of ϕ_i, thus ϕ_i is an $|{}^{\gamma\beta}\Phi_i|$-port [9]
- to ensure locality: $\frac{3}{4}\,|{}^{\gamma\beta}\Phi_i|^2 + \frac{1}{4}\,|{}^{\gamma\beta}\Phi_i| > \sum_j |{}^{\gamma\beta}\Phi_j \cap {}^{\gamma\beta}\Phi_i|$ should be satisfied

This 8-tuple completely specifies the machine for computation. The dynamics of the i^{th} flow: $\phi_i(t) \in \Phi \setminus {}^{i}\Phi$ is governed by these rules using the flows $\{{}^{\gamma\beta}\Phi_i \cup \phi_k\}$; i, k < $|\Phi|$:

$$\begin{aligned}
&\text{if } \alpha_i(\phi_k(t)) = \blacklozenge \text{ or } \exists \phi \in {}^{\gamma\beta}\Phi_i(t), \phi = \blacklozenge \text{ then } \phi_i(t) = \blacklozenge \\
&\text{else if } \alpha_i(\phi_k(t)) = 0 \text{ then } \phi_i(t) = \gamma_i({}^{\gamma\beta}\Phi_i(t)) \\
&\text{else } \frac{d\phi_i(t)}{dt} = \beta_i({}^{\gamma\beta}\Phi_i(t))
\end{aligned}$$

From the above equations, it follows that the CMF defines a map: $\Re^{|{}^{i}\Phi|}(t) \rightarrow \Re^{|{}^{o}\Phi|}(t)$.

The operation of the CMF can be described as follows: it starts at t = 0, setting $\Phi(0) = 0$ and executing the dynamics specified by A, B and Γ. It stops if ${}^{o}\phi(t) = \blacklozenge$ and ${}^{o}\Phi(t)$ is the output. Note that this stopping condition is similar to the way the end of computation is defined on a Turing machine.

Remarks:

The CMF can be used as a **decision machine**:

- Accept: if ${}^{o}\phi(t) = \blacklozenge \;\forall\, \phi_i(t) \in {}^{o}\Phi_i : \phi_i(t) \neq \blacklozenge$
- Decline: if ${}^{o}\phi(t) = \blacklozenge \;\exists\, \phi_i(t) \in {}^{o}\Phi_i : \phi_i(t) = \blacklozenge$
- The partial recursive functions are equivalent to $\exists\, {}^{i}\Phi$ or $\Phi(0)$ input: $\forall t > 0 \;\; {}^{o}\phi(t) \neq \blacklozenge$

Simplification: $\phi(0) = 0$ can be pre-defined for all $\phi \in \Phi \setminus {}^{i}\Phi$ ${}^{i}\Phi_2 = {}^{i}\Phi \cup \Phi_0$, $|\Phi_0| = |\Phi \setminus {}^{i}\Phi|$ to specify the initial states and $\Phi = \Phi \cup \{s_0\}$ for s_0: $\alpha = 1$, $\beta = 1$ for all other ϕ_i : $\alpha' = s_0\,\alpha$ and $\gamma' = \delta(s_0)\,\Phi_0^{(i)} + (1-\delta(s_0))\,\gamma$, where $\delta(x) =$ if (x=0) 1 else 0

5.2. The flow graph of CMF

Let us define the *flow graph* of CMF, which tries to capture the internal interdependencies of the computation. Let the nodes be the flows, with the directed links representing the connections; formally: $G_{CMF}(\Phi, \{\forall i\ ^{\gamma\beta}\Phi_i \rightarrow \phi_i\})$. The processing structure of the CMF at a given time-instant can be described by a sub-graph, which contains only those links, where the source node is in the actual/valid function of the destination flow. This sub-graph can be decomposed to α_0 and α_1 sub-graphs. The **α_0 sub-graph** contains only those nodes, whose α value is equal to zero and only those links, where the source node is a flow in its γ function. Similarly, the **α_1 sub-graph** contains only those nodes, whose $\alpha \neq 0$ and only those links, where the source node is a flow in its β function.

The locality of the CMF network is guaranteed if the clustering coefficient is less than 3/4. The clustering coefficient is the division of the total number of sub-graph edges of the nodes in the immediate neighborhood of the central node by all the possible edges in this sub-graph.

Consider the following simple flow-structure:

$\phi_1(0) = 1, \alpha = 0, \gamma = \phi_2$ $\qquad\qquad$ $\phi_2(0) = 2, \alpha = 0, \gamma = \phi_1$

We will call this situation **state-anomaly**. This anomaly means that the computation can be in a deadlock, whence the algorithm is unusable. Keeping any of the following constraints (which are not necessary but enough), the CMF avoids the state-anomaly.

(1) All α functions must have only a countable number of zero crossings.

(2) The α_0 sub-graph at each time-instance must not contain a directed circle.

5.3. Implementing the CNN-UM on the CMF

Consider the following CNN template {A, B, z} execution on an *MxN* grid running until T

$$\dot{x} = -x + A * y + B * u + z, \quad y = f(x)$$

The CMF equivalent:

- $^{i}\Phi = \{ u_{11} \ldots u_{MN}, z_{11} \ldots z_{MN}\}$; $^{o}\Phi = \{y_1, \ldots, y_{MN}\}$; $\Phi = {}^{i}\Phi \cup {}^{o}\Phi \cup \{ x_{11}, \ldots, x_{MN}, {}^{o}\phi\}$
- for $\forall ij$, $x_{ij}(0)$ is given; $\alpha_{ij} = 1$, $\gamma_{ij} = x_{ij}$, $\beta_{ij} = A*y + B*u + z - x$
- for $\forall ij$, $y_i(0) := f(x_i)$; $\alpha_{ij} = 0$, $\gamma_{ij} = f(x_{ij})$, $\beta_{ij} = 0$
- $^{o}\phi(t) :=$ if $(0 < t < T) : 1$ else ♦

Boundary conditions can be handled in the following way:

- fixed: coded into flow with $\alpha = 0$
- periodic or zeroflux: modifying the function β of the boundary cells/flows

Extension for using a **fixed state mask**:

- ${}^{i}\Phi_2 = {}^{i}\Phi \cup \{ m_{11}, \ldots, m_{MN} \}$;
- change x_{ij}: $\alpha'_{ij} = m_{ij}$; if $m_{ij} = 0$ freezes else activate the cell

A **timer** or clock can be established with the following construction:

- $\phi(0) = 0$, $\alpha = \phi - T$, $\beta = 1$, where T is the period/trigger-time
  - to stop computation: $\gamma = \blacklozenge$
  - to restart computation: $\gamma = 0$

Time-constant of a layer defined by the layer's state resistance and capacity: R and C

- change x_{ij}: $\beta'_{ij} = (RC)^{-1} \beta_{ij}$; the RC is the time-constant: τ

Arithmetic operation, e.g. x ***ADD*** *y*: $\alpha = 0$; $\gamma(x,y) = x + y$

Logic operation, e.g. x ***NAND*** *y*:

- if 0 = false, 1 = true: $\alpha = 0$; $\gamma(x,y) = 1 - x\ y$
- if -1 = false, 1 = true: $\alpha = 0$; $\gamma(x,y) = (1 - x - y - x\ y) / 2$

GW: Global white (white defined as -1) $\alpha = 0$, $\gamma = \Sigma\ (\phi_i + 1)$

Higher-order cells: connect flows in β-functions

Memory to store one time-instant of a flow: ϕ_{memory}: $\beta = 0$, $\gamma = \phi_{input}$, $\alpha = 0$ (write), 1 (read)

6. APPENDIX C - Template Derivation

In the appendix, the templates involved in the gentle grasping and the pressure field algorithms are listed. The templates are expressed in a vector format:

$$\begin{bmatrix} k_0 & k_1 & k_2 \\ k_3 & k_4 & k_5 \\ k_6 & k_7 & k_8 \end{bmatrix} \Rightarrow [k_0, k_1, k_2, k_3, k_4, k_5, k_6, k_7, k_8] \quad \text{(A1)}$$

SOBEL: A=[0,0,0,0,-1,0,0,0,0]; B=[-1,-2,-1,0,0,0,1,2,1]; I=0.1

THRES: A=[0,0,0,0,3,0,0,0,0]; B=[0,0,0,0,0,0,0,0,0]; I=1.6

CCD: A=[0,0,0,-2.3,3,2.3,0,0,0]; B=[0,0,0,0,0,0,0,0,0]; I=0

Matching templates:

Tx_CW: A=[0,0,0,0,1,0,0,0,0]; B=[0,0,0,0,1,1,0,-1,-1]; I=-3.5

Tx_CCW: A=[0,0,0,0,1,0,0,0,0]; B=[0,-1,-1,0,1,1,0,0,0]; I=-3.5

Ty_CW: A=[0,0,0,0,1,0,0,0,0]; B=[0,0,0,0,1,-1,0,1,-1]; I=-3.5

Ty_CCW: A=[0,0,0,0,1,0,0,0,0]; B=[-1,1,0,-1,1,0,0,0,0]; I=-3.5

Txy_Black: A=[0,0,0,0,1,0,0,0,0]; B=[0,1,1,0,1,1,0,0,0]; I=-3.5

Txy_White: A=[0,0,0,0,-1,0,0,0,0]; B=[0,-1,-1,0,-1,-1,0,0,0]; I=-3.5

BIBLIOGRAPHY

[1] E. Ono, N. Kita, S. Sakane: Strategy for unfolding a fabric piece by cooperative sensing of touch and vision. *Proceedings of the International Conference on Intelligent Robots and Systems* (IROS '95)

[2] T. Wösch, W. Feiten: Reactive Motion Control for Human–Robot Tactile Interaction. *Proceedings of the 2002 IEEE, International Conference on Robotics & Automation Washington, DC* . May 2002

[3] A. Kis, F. Kovács and P. Szolgay: Analogic CNN Algorithms for Textile Quality Control Based on Optical and Tactile Sensory Inputs. *Proc. of The 8th IEEE International Biannual Workshop on Cellular Neural Networks and their Applications, Budapes, 2004.*

[4] M. H. Lee: Tactile Sensing: New Directions, New Challenges. *The International Journal of Robotics Research Vol. 19, No. 7, pp. 636-643, July 2000.*

[5] R. D. Howe: Tactile Sensing and Control of Robotic Manipulation. *Journal of Advanced Robotics. 8(3):245-26, 1994.*

[6] W.D. Hills: Active Touch Sensing. *International Journal of Robotics Research, 1(2):33-44, 1982.*

[7] T. Speeter A Tactile Sensing System for Robotic Manipulation. *International Journal of Robotics Research, 9(6):25-36, December 1990.*

[8] R. S. Fearing: Tactile Sensing Mechanisms. *Int. Journal of Robotics Research, 9(3):3-23, 1990.*

[9] J. Rebman and K. A. Morris: A Tactile Sensor with Electrooptic Transduction. *In A. Pugh, editor, Robot Sensors, Vol. 2: Tactile and Non-Vision, pages 145-155. IFS Publications/Springer-Verlag, 1986*

[10] S. Begej: Planar and Finger-Shaped Optical Tactile Sensors for Robotic Applications. *IEEE Journal of Robotics and Automation, 4(5):472-484, October 1988.*

[11] A. R. Grahn and L. Astle: Robotic Ultrasonic Force Sensor Arrays. *In Alan Pugh, editor, Robot sensors, Vol. 2: Tactile and Non-Vision, pages 297-315. IFS Publications/Springer-Verlag, 1986*

[12] J. Biggs, and M. A. Srinivasan: Tangential Versus Normal Displacements of Skin: Relative Effectiveness for Producing Tactile Sensations. *10th Int. Symposium on Haptic Interfaces for Virtual Environment and Teleoperator Systems, Orlando, FL,pp. 121-128, IEEE Computer Society, 2002.*

[13] G. Moy, U. Singh, E. Tan, R. S. Fearing: Human Psychophysics for Teletaction System Design. *The Electronic Journal of Haptics Research Vol. 1, No. 3, February, 18, 2000.*

[14] B. J. Kane, M. R. Cutkosky, and G. T. A. Kovacs: A Traction Stress Sensor Array for Use in High-Resolution Robotic Tactile Imaging. *Journal of microelectromechanical systems, vol. 9(4), 2000*

[15] A. Kis, N. Bottka, F. Kovács, and P. Szolgay: Elementary CNN Algorithms and an Experimental System for Typical Tactile Actions. *Proc. of IEEE ECCTD03, pp I-413- I-416, Krakow, 2003*

[16] L. O. Chua, L. Yang: Cellular Neural Networks: Theory. *IEEE Transactions on Circuits and Systems*, Vol. 35, pp. 1257–1272., 1988

[17] T. Roska, L. O. Chua: The CNN Universal Machine – an Analogic Array Computer. *IEEE Trans. on Circuits and Systems II: Analog and Digital Signal Processing* Vol. 40, No. 3, pp. 163-173, 1993

[18] E. R. Kandel, J. H. Schwartz and T. M. Jessell: Principles of Neural Science. *Publisher: McGraw-Hill/Appleton & Lange; 4th edition* (Jan. 5, 2000)

[19] Schlesinger G: The mechanical structure of artificial limbs. *Berlin: Springer* (1919).

[20] J. Napier: Hands. *Princeton University Press*, Princeton, New Jersey (1992)

[21] Trinkle J, Abel J, Paul R.: Enveloping, frictionless, planar grasping. *In: Robotics and Automation. Proceedings. 1987 IEEE International Conference on*, vol 4, pp 246-251

[22] M.R. Cutkosky and R.D. Howe, *Dextrous Robot Hands* (Springer Verlag. New York, 1990).

[23] Jacobson C, Sperling L (1976) Classifiction of the hand-grip: A preliminary study. *Journal of occupational medicine* 18: 295-298

[24] Kamakura N, Matsuo M, Ishii H, Mitsuboshi F, Miura Y (1980) Patterns of static prehension in normal hands. *The American Journal Of Occupational Therapy.: Official Publication Of The American Occupational Therapy Association* 34: 437-445

[25] Mamassian P (1997) Prehension of objects oriented in three-dimensional space. *Exp Brain Res* 114: 235-245.

[26] Paulignan Y, Frak VG, Toni I, Jeannerod M (1997) Influence of object position and size on human prehension movements. *Exp Brain Res* 114: 226-234

[27] Churchill A, Hopkins B, Ronnqvist L, Vogt S (2000) Vision of the hand and environmental context in human prehension. In, vol 134, pp 81-89

[28] Marotta JJ, Goodale MA (2001) Role of familiar size in the control of grasping. *J Cogn Neurosci* 13: 8-17.

[29] Cooney WP, III, Chao EY (1977) Biomechanical analysis of static forces in the thumb during hand function. *J Bone Joint Surg Am* 59: 27-36.

[30] Cutkosky MR (1989) On grasp choice, grasp models, and the design of hands for manufacturing tasks. *Robotics and Automation, IEEE Transactions on* 5: 269-279

[31] Iberall T (1986) The representation of objects for grasping. *Proceedings of the Eighth cognitive Society Conference*: 547-561

[32] Jacobson C, Sperling L (1976) Classifiction of the hand-grip: A preliminary study. *Journal of occupational medicine* 18: 295-298

[33] Kroemer KHE (1986) Coupling the hand with the handle: An improved notation of touch, grip, and grasp. *Human factors* 28: 337-340

[34] Landsmeer JMF (1962) Power grip and precision handling. *Annals of the rheumatic diseases* 21: 164-170

[35] Lister G (1977) The hand: Diagnosis and indications. *Edinburgh: Churchill Livingston*

[36] Napier JR (1956) The prehensile movements of the human hand. *Journal of bone and joint surgery* 38B: 902-913

[37] Skerick S, Weiss M, Flatt AE (1971) Functional evaluation of congential hand anomalies. *American jounral of occupational therapy* 25: 98-104

[38] Arbib MA, Iberall T, Lyons D (1985) Coordinated control programs for movements of the hand. *Exp Brain Res Suppl* 10: 111-129

[39] Iberall T, MacKenzie C (1990) Opposition space and human prehension. *In: Venkataraman ST, Iberall T (eds) Dextrous robot hands. Springer-Verlag*., New York, pp 32-54

[40] Iberall T (1986) The representation of objects for grasping. *Proceedings of the Eighth cognitive Society Conference*: 547-561

[41] Baud-Bovy G, Soechting JF (2001) Two virtual fingers in the control of the tripod grasp. *J Neurophysiol* 86:604–615

[42] Cutkosky MR, Howe RD (1990) Human grasp choice and robotic grasp analysis. In: *Venkataraman T, Iberall T, (eds) Dextrous robot hands, Springer, Berlin, Heidelberg, New York*, pp5–31

[43] Flanagan JR, Burstedt MK, Johansson RS (1999) Control of fingertip forces in multidigit manipulation. *J Neurophysiol 81*: 1706-1717

[44] Santello M, Soechting JF (2000) Force synergies for multifingered grasping. *Exp Brain Res* 133:457–467

[45] V.M. Zatsiorsky, R.W. Gregory and M.L. Latash, "Force and torque production in static multifinger prehension: Biomechanics and control. I. Biomechanics", *Biol. Cybern.*, **87**, 50–57 (2002).

[46] Zatsiorsky VM, Gao F, Latash ML (2003) Finger force vectors in multi-finger prehension. *J Biomech* 36: 1745-1749

[47] Shim J, Latash M, Zatsiorsky V (2003) Prehension synergies: trial-to-trial variability and hierarchical organization of stable performance. *Exp Brain Res* 152: 173-184

[48] Zatsiorsky VM, Latash M, Gao F, Shim JH (2004) The principle of superposition in human prehension. *Robotica 22*:231–234

[49] Long C, Conrad PW, Hall EA, Furler SL (1970) Intrinsic-extrinsic muscle control of the hand in power grip and precision handling. *An electromyographic study. J Bone Joint Surg* Am 52: 853-867.

[50] Jacobson MD, Raab R, Fazeli BM, Abrams RA, Botte MJ, Lieber RL (1992) Architectural design of the human intrinsic hand muscles. *J Hand Surg [Am]* 17:804-809

[51] Darling WG, Cole KJ, Miller GF (1994) Coordination of index finger movements. *J Biomech* 27: 479-491.

[52] Maier MA, Hepp-Reymond MC (1995a) EMG activation patterns during force production in precision grip. I. Contribution of 15 finger muscles to isometric force. *Exp Brain Res* 103: 108-122

[53] Mahaffey P (1999) The contribution of the intrinsic muscles to grip and pinch strength. *J Hand Surg [Am]* 24: 870-871.

[54] Kozin SH, Porter S, Clark P, Thoder JJ (1999) The contribution of the intrinsic muscles to grip and pinch strength. *J Hand Surg [Am]* 24: 64-72.

[55] Huesler EJ, Maier MA, Hepp-Reymond MC (2000) EMG activation patterns during force production in precision grip. III. Synchronisation of single motor units. *Exp Brain Res* 134: 441-455.

[56] Milner TE, Dhaliwal SS (2002) Activation of intrinsic and extrinsic finger muscles in relation to the fingertip force vector. *Exp Brain Res* 146:197-204

[57] Basmajian JV, Luca CJD (1978) Muscles Alive: Their Functions Revealed by Electromyography. *Williams & Wilkins, Baltimore, MD*

[58] Backdahl M, Carlsoo S (1961) Distribution of activity in muscles acting on the wrist (an electroyographic study). *Acta Morph Neerl-Scand* 4: 136-144

[59] Chao EY, Opgrande JD, Axmear FE (1976) Three dimensional force analysis of finger joints in selected isometric hand function. *Journal of Biomechanics* 19: 387-396

[60] Li ZM, Zatsiorsky VM, Latash ML (2001a) The effect of finger extensor mechanism on the flexor force during isometric tasks. *J Biomech 34*: 1097-1102.

[61] Valero-Cuevas FJ (2000) Predictive modulation of muscle coordination pattern magnitude scales fingertip force magnitude over the voluntary range. *J Neurophysiol* 83:1469–1479

[62] Pearlman JL, Roach SS, Valero-Cuevas FJ (2004) The fundamental thumb-tip force vectors produced by the muscles of the thumb. *Journal of Orthopaedic Research* 22: 306-312

[63] Vallbo AB, Johansson RS (1984) Properties of cutaneous mechanoreceptors in the human hand related to touch sensation. *Human Neurobiology* 3: 3-14

[64] Johansson RS, Vallbo AB (1983) Tactile sensory coding in the glabrous skin of the human hand. *Trends in Neuroscience* 6: 27-32

[65] Cutkosky MR, Howe RD (1990) Human grasp choice and robotic grasp analysis. In: Venkataraman T, Iberall T (eds) Dextrous robot hands. *Springer, Berlin Heidelberg New York,* pp 5–31

[66] Jindrich DL, Zhou Y, Becker T, Dennerlein JT (2003) Non-linear viscoelastic models predict fingertip pulp force-displacement characteristics during voluntary tapping. *Journal of Biomechanics* 36: 497-503.

[67] Pataky T (2004) Investigation into tangential force coordination. In: Kinesiology. *The Pennsylvania State University, State College, PA*

[68] Jenmalm P, Dahlstedt S, Johansson RS (2000) Visual and tactile information about object-curvature control fingertip forces and grasp kinematics in human dexterous manipulation. *J Neurophysiol 84*: 2984-2997.

[69] Johansson RS (2002) Dynamic use of tactile afferent signals in control of dexterous manipulation. *Adv Exp Med Biol* 508: 397-410

[70] Johnson K (2001) The roles and functions of cutaneous mechanoreceptors. *Curr Opin Neurobiol* 11: 455-461

[71] Johansson RS, Westling G (1984) Roles of glabrous skin receptors and sensorimotor memory in automatic control of precision grip when lifting rougher or more slippery objects. *Exp Brain Res* 56: 550-564

[72] Cole KJ, Johansson RS (1993) Friction at the digit-object interface scales the sensorimotor transformation for grip responses to pulling loads. *Exp Brain Res* 95:523–532

[73] Forssberg H, Eliasson AC, Kinoshita H, Westling G, Johansson RS (1995) Development of human precision grip. IV. Tactile adaptation of isometric finger forces to the frictional condition. *Exp Brain Res* 104: 323-330

[74] Cadoret G, Smith AM (1996) Friction, not texture, dictates grip forces used during object manipulation. *J Neurophysiol* 75:1963–1969

[75] Stoeckel MC, Weder B, Binkofski F, Choi H-J, Amunts K, Pieperhoff P, Shah NJ, Seitz RJ (2004) Left and right superior parietal lobule in tactile object discrimination. *Eur J Neurosci* 19: 1067-1072

[76] Gordon AM, Duff SV (1999) Fingertip forces during object manipulation in children with hemiplegic cerebral palsy. I: anticipatory scaling. *Dev Med Child Neurol* 41: 166-175.

[77] Schwarz M, Fellows SJ, Schaffrath C, Noth J (2001) Deficits in sensorimotor control during precise hand movements in Huntington's disease. *Clin Neurophysiol* 112: 95-106.

[78] Nowak DA, Hermsdorfer J (2003) Digit cooling influences grasp efficiency during manipulative tasks. *Eur J Appl Physiol* 89:127–133

[79] Augurelle A-S, Smith AM, Lejeune T, Thonnard J-L (2003) Importance of Cutaneous Feedback in Maintaining a Secure Grip During Manipulation of Hand-Held Objects. *J Neurophysiol* 89: 665-671

[80] Burstedt MK, Flanagan JR, Johansson RS (1999) Control of grasp stability in humans under different frictional conditions during multidigit manipulation. *J Neurophysiology* 82:2393–2405

[81] Kinoshita H, Kawai S, Ikuta K (1995) Contributions and coordination of individual fingers in multiple finger prehension. *Ergonomics* 38:1212–1230

[82] Leijnse JNAL (1997) The controllability of the unloaded human finger with superficial or deep flexor. *Journal of Biomechanics* 30: 1087-1093

[83] Huijing P (1999a) Muscular force transmission: a unified, dual or multiple system? A review and some explorative experimental results. *Archives Of Physiology And Biochemistry* 107: 292-311

[84] Kilbreath SL, Gandevia SC (1994) Limited independent flexion of the thumb and fingers in human subjects. *J Physiol* 479: 487-497

[85] Schieber MH, Poliakov AV (1998) Partial inactivation of the primary motor cortex hand area: effects on individuated finger movements. *J Neurosci* 18: 9038-9054.

[86] Cochran DJ, Riley MW (1986) The effects of handle shape and size on exerted forces. *Human Factors* 28: 253-265

[87] Lamoreaux L, Hoffer MM (1995) The effect of wrist deviation on grip and pinch strength. *Clin Orthop*: 152-155.

[88] Bernstein NA (1967) The co-ordination and regulation of movement. *Pergamon, Oxford*

[89] Macpherson JM (1991) How flexible are muscle synergies? In: Humphrey DR, Freund HJ (eds) Motor control: concepts and issues. *John Wiley & Sons, Berlin, Germany,* pp 33-48

[90] Scholz JP, Schoner G (1999) The uncontrolled manifold concept: identifying control variables for a functional task. *Exp Brain Res* 126: 289-306.

[91] Todorov E, Jordan MI (2002) Optimal feedback control as a theory of motor coordination. *Nature neuroscience* 5: 1226-1235

[92] S. Arimoto, K. Tahara, M. Yamaguchi, P.T.A. Nguyen and H.Y. Han, "Principles of superposition for controlling pinch motions by means of robot fingers with soft tips", *Robotica*, **19**, 21–28 (2001).

[93] Johansson RS, Westling G (1984) Roles of glabrous skin receptors and sensorimotor memory in automatic control of precision grip when lifting rougher or more slippery objects. *Exp Brain Res* 56:550–564

[94] McIntyre J, Berthoz A, Lacquaniti F (1998) Reference frames and internal models for visuo-manual coordination: what can we learn from microgravity experiments? *Brain Research Reviews* 28: 143-154

[95] Gysin P, Kaminski TR, Gordon AM (2003) Coordination of fingertip forces in object transport during locomotion. *Exp Brain Res* 149:371–379

[96] Mason MT, Salisbury JK (1985) Robot Hands and the Mechanics of Manipulation. *MIT Press, Cambridge, Massachusetts*

[97] Murray RM, Li Z, Sastry SS (1994) A mathematical introduction to robotic manipulation. *CRC Press, Boca Raton*

[98] Kao I, Cutkosky MR, Johansson RS (1997) Robotic stiffness control and calibration as applied to human grasping tasks. *Robotics and Automation, IEEE Transactions on* 13: 557-566

[99] Cutkosky MR, Kao I (1989) Computing and controlling compliance of a robotic hand. *Robotics and Automation, IEEE Transactions on* 5: 151-165

[100] Hanafusa H, Asada H (1977) Stable prehension by a robot hand with elastic fingers. *In: Proc. 7th ISIR*, pp 361-368

[101] Nguyen V-D (1989) Constructing stable graps. *The International Journal of Robotics Research 8*: 26-37

[102] Milner TE, Franklin DW (1998) Characterization of multijoint finger stiffness: dependence on finger posture and force direction. *Biomedical Engineering, IEEE Transactions on* 45: 1363-1375

[103] Van Doren CL (1998) Grasp stiffness as a function of grasp force and finger span. *Motor Control* 2: 352-378.

[104] Shimoga KB (1996) Robot Grasp Synthesis Algorithms: A Survey. *The International Journal of Robotics Research* 15: 230-266

[105] P. Dario, Contact sensing for robot active touch, in *Robotic Science*, M. Brady (ed.), Cambridge, MA: MIT Press, 1989, chap. 3, 138-163.

[106] P. P. L. Regtien, Tactile imaging, *Sensors and Actuators, A,* 31, 83-89, 1992.

[107] R. A. Russell, *Robot Tactile Sensing*, Brunswick, Australia: Prentice-Hall, 1990.

[108] A. D. Berger and P. K. Khosla, Using tactile data for real-time feedback, *Int. J. Robotics Res.*, 10(2), 88-102, 1991.

[109] S. Begej, Planar and finger-shaped optical tactile sensors for robotic applications, *IEEE J. Robotics Automation*, 4, 472-484, 1988.

[110] R. A. Russell and S. Parkinson, Sensing surface shape by touch, *IEEE Int. Conf. Robotics Automation,* Atlanta, GA, 1993, 423-428.

[111] R. D. Howe, A tactile stress rate sensor for perception of fine surface features, *IEEE Int. Conf. Solid-State Sensors Actuators,* San Francisco, CA, 1991, 864-867.

[112] S. Sugiyama, K. Kawahata, H. Funabashi, M. Takigawa, and I. Igarashi, A 32 □32 (1K)-element silicon pressure-sensor array with CMOS processing circuits, *Electron. Commun. Japan*, 75(1), 64-76, 1992.

[113] J. S. Son, E. A. Monteverde, and R. D. Howe, A tactile sensor for localizing transient events in manipulation, *IEEE Int. Conf. Robotics Automation,* San Diego, CA, 1994, 471-476.

[114] M. R. Tremblay and M. R. Cutkosky, Estimating friction using incipient slip sensing during manipulation task, *IEEE Int. Conf. Robotics Automation,* Atlanta, GA, 1993, 429-434.

[115] S. Omata and Y. Terubuna, New tactile sensor like the human hand and its applications, *Sensors and Actuators, A,* 35, 9-15, 1992.

[116] R. Bayrleithner and K. Komoriya, Static friction coefficient determination by force sensing and its applications, *IROS'94*, Munich, Germany, 1994, 1639-1646.

[117] M. A. Abidi and R. C. Gonzales, The use of multisensor data for robotic applications, *IEEE Trans. Robotics Automation*, 6, 159-177, 1990.

[118] A. A. Cole, P. Hsu, and S. S. Sastry, Dynamic control of sliding by robot hands for regrasping, *IEEE Trans. Robotics Automation*, 8, 42-52, 1992.

[119] P. K. Allen and P. Michelman, Acquisition and interpretation of 3-D sensor data from touch, *IEEE Trans. Robotics Automation*, 6, 397-404, 1990.

[120] H. R. Nicholls (ed.), *Advanced Tactile Sensing for Robotics*, Singapore: World Scientific Publishing, 1992. © 1999 by CRC Press LLC

[121] J. G. Webster (ed.), *Tactile Sensors for Robotics and Medicine*, New York: John Wiley & Sons, 1988.

[122] L. D. Harmon, Automated tactile sensing, *Int. J. Robotics Res.*, 1(2), 3-32, 1982.

[123] W. D. Hillis, A high resolution imaging touch sensor, *Int. J. Robotic Res.*, 1(2), 33-44, 1982.

[124] Y. Yamada and M. R. Cutkosky, Tactile sensor with 3-axis force and vibration sensing functions and its applications to detect rotational slip, *IEEE Int. Conf. Robotics Automation,* San Diego, CA, 1994, 3550-3557.

[125] B. J. Kane, M. R. Cutkosky, and G. T. A. Kovacs: A Traction Stress Sensor Array for Use in High-Resolution Robotic Tactile Imaging. *Journal of microelectromechanical systems, vol. 9(4), 2000*

[126] F. Zhu and J. W. Spronck: A capacitive tactile sensor for shear and normal force measurements, *Sensors and Actuators, A,* 31, 115-120, 1992.

[127] K. Suzuki, K. Najafi, and K. D. Wise, A 1024-element high-performance silicon tactile imager, *IEEE Trans. Electron Devices*, 17(8), 1852-1860, 1990.

[128] M. R. Wolffenbuttel and P. L. Regtien, The accurate measurement of a micromechanical force using force-sensitive capacitances, *Conf. Precision Electromagnetic Meas.,* Boulder, CO, 1994, 180-181.

[129] R. S. Fearing, Tactile sensing mechanism, *Int. J. Robotics Res.,* 9(3), 3-23, 1990.

[130] J. Rebman and K. A. Morris, A tactile sensor with electro-optical transduction, in *Robots Sensors, Tactile and Non-Vision,* Vol. 2, A. Pugh (ed.), EFS Publications, 1986, 145-155.

[131] R. E. Saad, A. Bonen, K. C. Smith, and B. Benhabib, Distributed-force recovery for a planar photoelastic tactile sensor, *IEEE Trans. Instrum. Meas.*, 45, 541-546, 1996.

[149] G. T. A. Kovacs: Micromachined Transducers Sourcebook. *McGraw-Hill*, 1998

[150] Katana Robot – K-Team S.A., www.neuronics.ch

[151] Pressure Profile Systems, TactArray, www.pressureprofile.com

[152] M. Ádám, É. Vázsonyi, I. Bársony, G. Vásárhelyi, Cs. Dücso: Three Dimensional Single Crystalline Force Sensor by Porous Si Micromachining. *Proceedings of IEEE Sensors* 2004, Vienna.

[153] E. R. Kandel, J. H. Schwartz and T. M. Jessell: Principles of Neural Science. *Publisher: McGraw-Hill/Appleton & Lange; 4th edition* (Jan. 5, 2000)

[154] Analogic Computers Ltd.: Aladdin Pro R3.2. Budapest, 2004, www.analogic-computers.com

[155] S. Espejo, R. Dominguez-Castro, G. Linan, A. Rodriguez-Vázquez: A 64x64 CNN Universal Chip with Analog and Digital I/O. *Proc. of 5th IEEE International Conference on Electronics, Circuits and Systems, (ICECS'98)*; pp. 203-206, Lisboa, 1998.

[156] T. Roska: Computational and Computer Complexity of Analogic Cellular Wave Computers. *Jurnal of Circuits, Systems and Computers*, Vol. 12(4), pp. 539-562, 2003.

[157] J.J. Clark, A. L. Yuille, Data fusion for Sensory Information Systems (Kluwer Academic, Boston, MA, 1990)

[158] M. S. Landy, L. T. Maloney, E.B. Johnston, M. J. Young, Vision Res. 35, 389 1995

[159] Z. Gharhramani et al., Self-Organization, Computational Maps, And Motor Control*, Elsevier, Amsterdam,* 1997 pp. 117-147.

[160] A. Bodnarova: “Textile Flaw Detection Using Optimal Gabor Filters”. *Proceedings of the International Conference on Pattern Recognition (ICPR'00)-Volume 4*, p.4799, September 03-08, 2000

[161] C. Bahlmann, G. Heidemann, H. Ritter: “Artificial Neural Networks for Automated Quality Control of Textile Seams”. *Pattern Recognition*, volume 32, number 6, pp. 1049–1060, June 1999

[162] R. Franke: "Scattered Data Interpolation: Tests of Some Methods", *Mathematics of Computation*, Vol.38, No. 157, pp. 181−200, 1982

[163] Sensor Products, XSENSOR Real-Time Tactile Pressure Measurement, East Hanover, 2002, www.xsensor.com

[164] S. Espejo, R. Dominguez-Castro, G. Linan, A. Rodriguez-Vázquez: "A 64x64 CNN Universal Chip with Analog and Digital I/O", *Proceedings of 5th IEEE International Conference on Electronics, Circuits and Systems, (ICECS'98)*, pp. 203-206, Lisboa, 1998

[165] A. Kis, N. Bottka, F. Kovács, and P. Szolgay: ”Elementary CNN Algorithms and an Experimental System for Typical Tactile Actions”, Proc. of IEEE ECCTD03, pp I-413- I-416, Krakow, 2003

THE AUTHOR'S PUBLICATIONS

Journal papers

[1] **Attila Kis**, Ferenc Kovács & Péter Szolgay: "3D Tactile Sensor Array Processed by CNN-UM: A Fast Method for Detecting and Identifying Slippage and Twisting Motion", *International Journal on Circuit Theory and Application (CTA),* 2006; 34: pp. 517-531

[2] Gábor Vásárhelyi, Mária Ádám, Éva Vázsonyi, Zsolt Vízváry, **Attila Kis**, István Bársony & Csaba Dücső "Characterization of an Integrable Single - Crystalline 3D Tactile Sensor", *IEEE Sensors Journal,* 2006, vol.6, nr.4, pp. 928-934

Conference papers

[1] **Attila Kis**, Ferenc Kovács & Péter Szolgay: „Grasp Planning Based on Fingertip Contact Forces and Torques", *Proceedings of the Eurohaptics International Conference EH 06, July 3-6, 2006*, Paris, France, pp. 455-459

[2] **Attila Kis**, Ferenc Kovács & Péter Szolgay: "Hardware and Software Environment for a Tactile Sensor Array", *Eurosensors XIX*, Barcelona September, 2005

[3] **Attila Kis**, Ferenc Kovács & Péter Szolgay: "*Analogic CNN Algorithms for Textile Quality Control Based on Optical and Tactile Sensory Inputs* ", Budapest July, CNNA, 2004

[4] **Attila Kis**, Nicholas Bottka, Ferenc Kovács & Péter Szolgay: "Elementary CNN Algorithms and an Experimental System for Typical Tactile Actions", *IEEE European Conference on Circuit Theory and Design ECCTD03*, Krakow September, 2003

[5] **Attila Kis**, Gábor Vásárhelyi, Antalné Ádám, Péter Szolgay: "Tactile sensing: sensors and algorithms", *Hungarian Neuroscientists Society MITT05*, Pécs January, 2005; pp. 129

[6] Bársony István, Dücső Csaba, **Kis Attila**, Négyessy László, Kovács Ferenc, Szolgay Péter: "Taktilis érzékelők, érzékelés és processzálás", *A Magyar Infobionikai Kutatóközpont Bemutatkozása, Magyar Tudományos Akadémia,* Budapest Május, 2005